University of California
Santa Barbara

Thermalization and its breakdown in isolated quantum systems

A dissertation submitted in partial satisfaction
of the requirements for the degree

Doctor of Philosophy
in
Physics

by

James Robert Garrison

Committee in charge:

Professor Matthew P. A. Fisher, Chair
Professor Chetan Nayak
Professor David M. Weld

June 2016

The Dissertation of James Robert Garrison is approved.

Professor Chetan Nayak

Professor David M. Weld

Professor Matthew P. A. Fisher, Committee Chair

May 2016

Thermalization and its breakdown in isolated quantum systems

by

James Robert Garrison

To my family, old and new.

Acknowledgements

First and foremost, I would like to thank Matthew Fisher, my Ph.D. advisor and perhaps the most creative and insightful person I have known. I will forever be in awe of Matthew's broad knowledge and deep physical intuition, his enthusiasm and determination, and his passion for physics. Matthew has provided incredible support during my time at UCSB, and he has always had my long-term interest at heart. He has nurtured my independent thinking as a scientist, while also convincing me that physics is at its best when it is a collaborative endeavor. He has never hesitated to challenge me. Working with Matthew has been a pleasure, and I look forward to continuing our friendship and physics discussions for years to come.

I am deeply grateful to the other members of my Ph.D. committee, each of whom has served as an influential mentor throughout graduate school. I deeply admire Chetan Nayak's work, and I value his opinion on all things. David Weld has helped me better understand the experimental implications of my own work, and my discussions with him have made me a better physicist. I would also like to thank John Martinis for serving on my advancement committee and for holding me to a high standard.

Tarun Grover has in many ways acted as a second advisor to me. From our early conversations about measuring entanglement entropy in variational Monte Carlo to our studies of the F-theorem, my discussions with Tarun have always expanded my knowledge. I am grateful for our research together on the eigenstate thermalization hypothesis, which resulted in Chapter 2 of this dissertation. Tarun's great enthusiasm for physics is

contagious, and I praise his desire to fully recognize and deeply understand the broad unifying themes in physics. Tarun has been an incredibly supportive mentor, and I know I will look to him as an inspiration throughout my career.

During my time at UCSB, I have benefitted enormously from collaborations led by other senior researchers as well. Cenke Xu introduced me to Kitaev's toric code and honeycomb models, and I am grateful for the opportunity to do research together on spin liquids. Bela Bauer has taught me a great deal about physics and numerics, and I have enjoyed working with him to study many-body localization. He has also demonstrated to me how to finish projects in a timely fashion.

I would also like to thank the graduate students with whom I have worked most closely and become good friends. Ryan Mishmash played an essential role in helping me get started with research, and I have learned much by following in his footsteps. Katie Hyatt has always impressed me with her broad knowledge, especially when it comes to scientific computing. And although I have not yet *officially* collaborated with Jen Cano, I have counted her as an important colleague and friend since we met on our first day of graduate school.

I credit many of the more senior graduate students at UCSB for inspiring me to study condensed matter physics. Mark Howard first mentioned to me the connections between quantum information and condensed matter theory. Miles Stoudenmire explained these connections in depth, much to my amazement. Matt Block graciously let me listen in while he taught Ryan Mishmash variational Monte Carlo, and this knowledge formed the

basis of my early research endeavors.

Lesik Motrunich has served as an important mentor and collaborator, and he has graciously hosted my visits to Caltech over the years. When I strive for excellence, I am reminded of Lesik's careful thinking and high standards. Additionally, I would like to thank all collaborators on papers I co-authored during my time at UCSB, including Samuel Bieri, Hong-Chen Jiang, Andrew Potter, and Donna Sheng.

I want to thank broadly all of the physics faculty at UCSB, especially those in condensed matter theory. In particular, Leon Balents has served as an essential mentor, and I am grateful to Andreas Ludwig for his patience and encouragement during office hours my first year of graduate school. Mark Srednicki introduced me to the eigenstate thermalization hypothesis when I was visiting as a prospective student; my many enjoyable conversations that day led to my decision to attend UCSB.

One of the great benefits of attending graduate school in Santa Barbara is the large number of postdoctoral researchers around. I am particularly grateful to Bryan Clark for guiding my numerical development during my early years of graduate school. I have also learned a great deal by talking with Maissam Barkeshli, Tim Hsieh, Max Metlitski, Eun-Gook Moon, Louk Rademaker, and Yi-Zhuang You, among others.

I recognize David Huse for an important conceptual contribution to the work in Chapter 2, as well as Fabian Essler and Thomas Veness, with whom I have corresponded at length on work related to Chapter 3. I would also like to thank everybody listed in the acknowledgements to the papers I have co-authored during graduate school. In addition to

those mentioned in the conclusions of Chapters 2 and 3, this includes Sankar Das Sarma, Sarang Gopalakrishnan, Ribhu Kaul, Chris Laumann, Patrick Lee, Sid Parameswaran, Subir Sachdev, Senthil Todadri, and Ashvin Vishwanath.

I have been fortunate to attend a number of physics schools, including a winter school at the Magnet Lab in Tallahassee, summer schools in Sherbrooke and Trieste, and the Boulder Summer School. The Aspen Center for Physics has provided a serene environment where I have been able to think deeply and to interact with many of the greatest minds in physics. I am very fortunate to have attended three Aspen winter conferences during my time at UCSB. I am grateful to all the organizers, lecturers, and funders of these programs

I am indebted to Federico Becca for inviting Ryan Mishmash and me to present a "simple" DMRG tutorial at a SISSA summer school on quantum spin liquids in Trieste, Italy. I would also like to thank Edward Rezayi for inviting me to give my first colloquium talk at California State University, Los Angeles. In addition, I would like to thank Xiaoliang Qi, Eun-Ah Kim, Roger Melko, and Arun Paramekanti for hosting my visits to Stanford, Cornell, Perimeter Institute, and the University of Toronto, respectively. I have also benefitted enormously from conversations with Dima Abanin, Iván González, Alexey Gorshkov, and Robert Konik, and I would like to thank everybody who provided advice and guidance during my postdoc decision making process.

I have had the great pleasure of many stimulating physics conversations with a number of graduate students whose time overlapped mine at UCSB, including Ahmed Almheiri,

Yoni BenTov, Zhen Bi, Lucas Brady, Ru Chen, Dominic Else, Keith Fratus, Kurt Fujiwara, Christine Hartmann, Gavin Hartnett, Ann Hermundstad, Jason Iaconis, Daniel Ish, Hyejin Ju, Brendan Keller, Younghyun Kim, Christina Knapp, SungBin Lee, Yonah Lemonik, Eric Mefford, Alexandra Miller, Chaitanya Murthy, Peter O'Malley, Teddy Parker, Kaushal Patel, Kelly Pawlak, Erik Perkins, Eugeniu Plamadeala, Alex Rasmussen, Justin Rofeh, Lucile Savary, Kevin Slagle, James Sully, Michael Swift, Alan Tran, Farzan Vafa, Amit Vainsencher, Brayden Ware, and Ted White. I have also become friends and colleagues with countless graduate students from other institutions, and among them I would especially like to thank Clare Abreu and Lauren Sierens.

Omer Blaes and Fyl Pincus both served as Chair of the UCSB Physics Department during my time here, and I commend each of them for a job well done. I also appreciate Don Marolf for his role as the department's graduate advisor during my first few years of graduate school. I am grateful to the staff of the department, including Jennifer Farrar and Jean Dill, as well as others whose work has been less visible (but no less important) to me.

The physics experience at UCSB would not be the same without the presence of the Kavli Institute for Theoretical Physics on this campus. I am grateful to the UCSB faculty members whose work decades ago led to the establishment of the institute here. I have also benefitted enormously by the presence of Microsoft Station Q. The supercomputing clusters at the Center for Scientific Computing at UCSB have been an essential ingredient of my research, and I am very lucky to have attended a campus where such access is

provided free of charge. I appreciate the work of Paul Weakliem and his staff for keeping these machines available and running.

I would also like to thank the National Science Foundation. In addition to being the ultimate source of funding for much of my graduate degree and research, it has provided essential support to many of the schools and institutes I have mentioned previously. Fundamental research on physics and other sciences is possible in this country largely due to support from the United States government.

I had a number of important mentors during my undergraduate years, including Robert Brown, Jeffry Madura, John Ruhl, and Mano Singham. I am especially grateful to my senior project advisor, Tanmay Vachaspati, from whom I learned that there are indeed open scientific questions regarding the foundations of quantum mechanics. More generally, I wish to thank all teachers I have had since preschool.

I want to recognize and thank all developers of free and open source software. The existence of free software, combined with the internet, provided endless intellectual stimulation which complemented my education in precisely the ways in which the public school system fell short. Without it, I simply cannot imagine what trajectory my life would have taken. Upon graduating college, I experienced the extreme good fortune of being hired into the job I dreamed of having throughout adolescence; for this I am forever grateful to Eben Moglen. During my two years at the Software Freedom Law Center, I fulfilled a passion and learned so much about the workings of the world. I am grateful to all of my colleagues during that time of immense personal and professional growth,

especially Cathy Cook, Richard Fontana, Bradley Kuhn, Dan Ravicher, Karen Sandler, Ian Sullivan, James Vasile, and Aaron Williamson. In my travels during this time I met several former graduate students, many of whom regretted leaving school. As a result, once I ultimately decided to embark on a Ph.D. I was determined not to be distracted until reaching the finish line.

I also want to thank the creators and developers of the Julia programming language, which has in recent years revolutionized my own personal numerical work in physics. It is incredibly liberating to be able to write my code in a *single* high level, high speed programming language. Furthermore, the Julia community includes many of the brightest computational scientists in the world, and I have learned much from interacting with other Julia developers and users.

I thank Randy Sargent and Illah Nourbakhsh, my supervisors at Carnegie Mellon University, for their consistent support and encouragement throughout graduate school. My voice instructor, Paul Sahuc, played a similar role as well. I have been very fortunate to have had many good friends during my time at UCSB. Rather than attempt to list everybody (few of whom will ever read this), I will mention my Santa Barbara roommates: Nick, Jeff, Vince, and Howard.

My family has been wonderfully, consistently supportive throughout my education and throughout my life. Nearly everything that I am or will become I owe in large part to my parents. My sister, Teresa, has consistently been somebody I can trust and rely on. My grandparents and the remainder of my extended family deserve recognition as well.

I want specifically to thank my grandfather for buying me my first electronics kit, my parents for having the insight to purchase a family computer before that was considered normal, and my uncle for showing me where to type the programs into the computer so that they would run, and for mentoring my early programming projects.

My life forever changed in January 2012 when my partner, Misha, entered my life. I admire our shared core values, and our marriage nearly a year ago fulfilled every dream I could have imagined. It also resulted in effectively doubling the number of people I consider family; this, of course, is the "new" family to which I refer in the dedication.

Curriculum vitae

James Robert Garrison

Education

2016	Ph.D. in Physics (expected), University of California, Santa Barbara.
2012	M.A. in Physics, University of California, Santa Barbara.
2006	B.A. in History and Psychology, Case Western Reserve University.
2006	B.S. in Mathematics and Physics, Case Western Reserve University.

Publications

"Many-body localization in the presence of a small bath," Katharine Hyatt, James R. Garrison, Andrew C. Potter, and Bela Bauer [arXiv:1601.07184].

"Does a single eigenstate encode the full Hamiltonian?" James R. Garrison and Tarun Grover [arXiv:1503.00729].

"Theory of a Competitive Spin Liquid State for Weak Mott Insulators on the Triangular Lattice," Ryan V. Mishmash, James R. Garrison, Samuel Bieri, and Cenke Xu, *Phys. Rev. Lett.* **111**, 157203 (2013) [arXiv:1307.0829].

"Non-Fermi-liquid d-wave metal phase of strongly interacting electrons," H.-C. Jiang, M. S. Block, R. V. Mishmash, J. R. Garrison, D. N. Sheng, O. I. Motrunich, and M. P. A. Fisher, *Nature* **493**, 39–44 (2013) [arXiv:1207.6608].

"A novel hybrid simulation for study of multiscale phenomena," P. E. Krouskop, J. Garrison, P. C. Gedeon, and J. D. Madura, *Molecular Simulation* **32**, 825–830, (2006).

Abstract

Thermalization and its breakdown in isolated quantum systems

by

James Robert Garrison

A very fundamental problem in quantum statistical mechanics involves whether—and how—an isolated quantum system will reach thermal equilibrium after waiting a long time. In quantum systems that *do* thermalize, the long-time expectation value of any "reasonable" operator will match its predicted value in the canonical ensemble. The Eigenstate Thermalization Hypothesis (ETH) posits that this thermalization occurs at the level of each individual energy eigenstate; in fact, any single eigenstate in a micro-canonical energy window will predict the expectation values of such operators exactly. In the first part of this dissertation, we identify, for a generic model system, precisely which operators satisfy ETH, as well as limits to the information contained in a single eigenstate. Remarkably, our results strongly suggest that a single eigenstate can contain information about energy densities—and therefore temperatures—far away from the energy density of the eigenstate.

Additionally, we study the possible breakdown of quantum thermalization in a model of itinerant electrons on a one-dimensional chain, with both spin and charge degrees of freedom. This model exhibits peculiar properties in the entanglement entropy, the apparent scaling of which is modified from a "volume law" to an "area law" after performing a

partial, site-wise measurement on the system. These properties and others suggest that this model realizes a new, non-thermal phase of matter, known as a Quantum Disentangled Liquid (QDL). The putative existence of this phase has striking implications for the foundations of quantum statistical mechanics.

Contents

List of figures

Chapter 1

Introduction

Condensed matter physics involves the study of macroscopic systems composed of a very large number of interacting, microscopic particles[1]. With so many degrees of freedom, understanding the behavior of such a system can at first appear to be a daunting task. Remarkably, it is often possible to simplify a problem, identifying the most important degrees of freedom as well as their excitations (such as the collective modes of vibration in a solid). With this, one can understand emergent, *macroscopic* properties, including the speed of sound in a metal, or its electrical conductivity and color.

At its core, the study of condensed matter physics involves understanding phases of matter, as well as transitions between those phases as one varies macroscopic parameters (such as temperature, pressure, or an applied magnetic field). One of the most familiar phase transitions is the transformation of liquid water to solid ice as its temperature is

[1] In theory, we typically assume the number of particles is infinite ($N \to \infty$, otherwise known as the "thermodynamic limit"), even though any physically realistic system will have a finite particle count (say, of order 10^{23}).

decreased below 0°C. While the molecules of a liquid are arranged without pattern, the H_2O molecules of ice spontaneously arrange themselves into a hexagonal crystal lattice structure. This phenomenon is known as *spontaneous symmetry breaking*—in this case, the breaking of translational symmetry. Symmetry breaking is what distinguishes phases from one another in the traditional paradigm of condensed matter physics, due primarily to the remarkable insight of the late Russian physicist Lev Landau.

While gas, liquid, and solid are the most commonly discussed phases in everyday life, the concept of phases and phase transitions is actually far more general. A less familiar phase transition, perhaps, is one exhibited by iron. At room temperature, iron is a ferromagnet: microscopically, nearby electron spins align with one other to point in the same direction (thus spontaneously breaking *rotational symmetry*). If the domains of aligned spins are large enough, a sample of iron will act as a permanent magnet. As the existence of broken symmetry suggests, ferromagnetism itself is a phase of matter. If heated far above room temperature to its "Curie temperature" of 1043 K, iron will transition to become a paramagnet. In this phase, rotational symmetry is restored, and the properties we associate with a permanent magnet will be lost due to thermal fluctuations.

Overall, there are two main branches of condensed matter physics. *Quantum* condensed matter physics is the study of condensed matter systems where quantum effects are important—that is, the system cannot be accurately described by classical physics. Typically these will be materials with structural rigidity (such as metals), hence the al-

ternative term, "hard" condensed matter physics. By contrast, *soft* condensed matter physics studies systems in which quantum effects are unimportant, including polymers and many biological materials.

Typically, quantum effects are relevant at low temperatures; however, what is a "low" temperature depends upon the relevant energy scales. For copper, the relevant energy scale (the Fermi energy) is 7.00 eV $\approx$ 80000 K, which is an order of magnitude hotter than the surface of the sun! Hence, room temperature (300 K) is by comparison quite low, and the properties of metals are governed by quantum mechanics.

Quantum condensed matter physics is a wide field, accounting for a variety of phenomena, including superfluid helium-3 and -4 [1,2], the band theory of metals (explained by Landau's Fermi liquid theory [3]), semiconductors, magnetism (which can in fact *only* be explained within quantum mechanics [4, 5]), and conventional superconductivity [6]. Active areas of research include frustrated magnetism [7], unconventional superconductivity (such as the "high temperature" superconductors made of cuprates [8] and iron pnictides [9]), strange metals and non-Fermi liquids [10], topological phases of matter (such as the fractional quantum Hall effect) [11], and symmetry protected topological phases (e.g. topological insulators) [12, 13]. Each of these are low temperature phenomena, and understanding each one involves identifying the nature of the quantum ground state and its low-lying excitations[2].

In explaining each of the above phenomena—as well as many in soft condensed matter

[2]One of the most basic questions about a phase is whether there exists an energy gap between the ground state and its excitations. A superconductor, for instance, has a gap, while a normal metal does not.

physics—we generally assume the validity of canonical statistical mechanics; that is, we consider a system to be in (or near) thermal equilibrium, its state described by the canonical ensemble

$$\rho = \frac{e^{-\beta H}}{\mathrm{Tr}\left(e^{-\beta H}\right)}, \tag{1.1}$$

where H is the Hamiltonian describing the system and $\beta \equiv 1/k_B T$ is its inverse temperature. Of course, it is also possible to consider high-energy or non-equilibrium phenomena, but doing so is generally much more challenging.

Unlike much of the historical research on condensed matter physics, we will not use Eq. 1.1 as a starting point. Instead, we will primarily focus on how and under what conditions Eq. 1.1 (and thus the concept of temperature) *results* from the evolution of an isolated quantum system with finite energy density. The Schrödinger equation is thought to accurately describe the universe, and if it is to be consistent with observation, it ought to be possible to understand equilibration and thermalization (i.e. the relaxing of a system to a uniform temperature) within this framework. Because the Schrödinger equation is linear, the typical classical explanations of the validity of statistical mechanics are not valid, as they rely on the dynamical chaos of non-linear systems. As we will soon detail, not only can the evolution of an isolated quantum system result in the thermal behavior exhibited in Eq. 1.1, but there also exist *non-thermalizing* phases of matter in which quantum statistical mechanics breaks down.

Before diving into quantum thermalization, we will first take two brief detours. First, we will give a brief introduction to some simple model systems studied in condensed

matter physics and within this dissertation. Second, we will provide background on the importance of quantum entanglement in condensed matter, as it is key to understanding quantum thermalization.

1.1 Model systems

Generally, the goal in constructing a model system is to identify the microscopic degrees of freedom of a system that are relevant to the phenomenon of interest. The atomic nuclei of a metal are arranged in a crystal lattice, and for electronic properties we can typically take the positions of the nuclei to be fixed (since neutrons and protons are much heavier than electrons). We can generally ignore the motion of all but the valence electrons. Thus, a simple model of a metal will consist of electrons hopping on a lattice from site to site, and to simplify things further we will allow at most one spin-up and one spin-down electron per site. The remaining ingredient is the electrostatic repulsion between the negatively-charged electrons. If we consider only an on-site interaction (assuming screening effects at larger distances), we get the simplest possible model of interacting, itinerant electrons, known as the Hubbard model [14],

$$H_{\text{Hubbard}} = -t \sum_{\langle ij \rangle \, \sigma} \left(c^{\dagger}_{i\sigma} c_{j\sigma} + \text{H.c.} \right) + U \sum_{i} n_{i\uparrow} n_{i\downarrow}, \tag{1.2}$$

where $\sum_{\langle ij \rangle}$ denotes a sum over neighboring sites i and j of the lattice, $n_{i\sigma} = c^{\dagger}_{i\sigma} c_{i\sigma}$, $n_i = n_{i\uparrow} + n_{i\downarrow}$, and σ represents the two possible values of spin, $\uparrow$ and $\downarrow$. The first

term represents kinetic energy due to hopping, and the second term adds an energy penalty U when two electrons occupy the same site. This model can account for a great deal of physical behavior, and it is possible to construct variations (for instance, further-neighbor couplings, anisotropic hopping, or even ring-exchange terms). Despite its apparent simplicity, the 2D Hubbard model may even contain the essential physics relevant to understanding high-temperature superconductivity in the cuprates [15]. In this dissertation, the 1D Hubbard model, supplemented with a nearest-neighbor repulsion term, will form the basis of Chapter 3.

Let us now consider two limits of the Hubbard model. When $U \ll t$, interactions are weak, and the model is in a conducting, Fermi liquid phase (assuming dimension greater than one), representative of a normal metal and qualitatively similar to non-interacting electrons [3]. In the strong-coupling limit ($U \gg t$), let us for simplicity assume that the system is at half-filling—that is, there is an equal number of spin-up and spin-down electrons, the sum of which equals the number of sites on the lattice. In this limit, charge fluctuations are greatly suppressed, and the most important low-energy degrees of freedom involve spin fluctuations, leading to the spin-1/2 Heisenberg model,

$$H_{\text{Heisenberg}} = J \sum_{\langle ij \rangle} \mathbf{S}_i \cdot \mathbf{S}_j, \tag{1.3}$$

where $J = 4t^2/U + \mathcal{O}(t^3/U^2)$ and $\mathbf{S}_i$ represents the spin on site i [16].

The Heisenberg model is an important model of quantum magnetism. Another model

of quantum magnetism is given by the spin-1/2 transverse-field Ising model,

$$H_{\text{Ising}} = J \sum_{\langle ij \rangle} \sigma_i^z \sigma_j^z + h \sum_i \sigma_i^x. \tag{1.4}$$

The one-dimensional version of this model is well understood, and in fact describes the physics of the material $CoNb_2O_6$ [17]. This model, supplemented with a longitudinal field, will be used extensively in this dissertation for demonstrations of thermalization in Chapter 2.

Simple models such as these can be used to realize many different phases. In fact, the relevant physics often does not depend on the precise details of the model. This concept of *universality* is fundamental to condensed matter physics. One notable example of this is the universal quantitative behavior of many models near a second order phase transition, which can be understood in terms of Wilson's *renormalization group* [18].

Historically, condensed matter physicists have been interested in simple model systems because they represent the low-energy properties of real materials. However, quite recently it has become possible to implement these models nearly exactly in experiments on cold atomic gases [19, 20]. In fact, even the aforementioned lattice models can be realized by constructing an optical lattice from laser beams, and interactions between atoms can be controlled by tuning a Feshbach resonance [21, 22]. With this, experimentalists are now able to construct *synthetic* quantum matter and simulate the dynamics of certain classes of Hamiltonians. These systems evolve according to the Schrödinger equation, as they are nearly isolated from the remainder of the universe.

One of the most notable uses of cold atomic gases in an optical lattice is to simulate the Bose Hubbard model [23–25], which is similar to the Hubbard model but with bosonic particles instead of fermions. In these experiments it is possible to witness the transition between a superfluid and Mott insulator by changing the depth of the optical lattice, which results in precise tuning of U/t. It is also possible to implement the standard, fermionic Hubbard model in experiment [20, 26], and in principle it is even possible to include additional terms, such as ring exchange [27].

Although models of quantum magnetism were historically of interest because they represent the low-energy (i.e. low-temperature) microscopic models of certain materials, they also provide a simple context in which to understand quantum thermalization. However, it is important to wonder whether simple models with only one species are rich enough to exhibit the full range of possible thermalization behaviors. In Chapter 3 we will revisit this question, finding evidence for the partial breakdown of thermalization in a two-component, Hubbard-like model.

1.2 Entanglement

One of the most fascinating aspects of quantum mechanics is entanglement, a phenomenon in which spatially separated portions of a quantum system must be described by a shared state. Because the only complete description is one of the full system, an entangled system cannot accurately be described as a sum of its parts. Entanglement is a distinctly quantum effect, arguably the essential ingredient of quantum mechanics.

In 1935, Einstein, Podolsky, and Rosen (EPR) proposed that quantum mechanics is an incomplete theory, and that our perception of entanglement is actually the result of local, "hidden" variables which completely describe the state of a system [28]. Nearly three decades later, John S. Bell published a landmark theorem which demonstrated that EPR's assumption of local hidden variables leads to probabilistic predictions that are in contradiction with quantum mechanics [29]. Since then, Bell test experiments have consistently demonstrated that quantum mechanics prevails, entanglement truly exists, and any theory of "local realism" cannot describe our physical world [30–32]. Further research, including into so-called Greenberger-Horne-Zeilinger (GHZ) states, has provided a non-probabilistic demonstration of quantum entanglement [33, 34]. Recently, three groups have demonstrated the first loophole-free violations of Bell's theorem, thus putting entanglement on an incredibly firm foundation [35–37].

The theoretical study of entanglement has had implications in many fields of physics. Over the past two decades, our growing understanding of entanglement has in many ways *revolutionized* quantum condensed matter physics [38]. Given a many-body ground state $|\psi\rangle$, a basic quantification of its entanglement structure is given by the entanglement

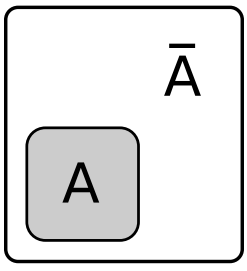

Figure 1.1: An entanglement cut between subregion A and its complement $\overline{A}$.

entropy of a spatial subregion A. Given such an entanglement cut (see Figure 1.1), the von Neumann entanglement entropy is given by

$$S(\rho_A) = -\operatorname{Tr}(\rho_A \ln \rho_A), \tag{1.5}$$

where $\rho_A \equiv \operatorname{Tr}_{\overline{A}} |\psi\rangle \langle\psi|$ is the reduced density matrix describing the system in subregion A and $\overline{A}$ is the complement of A. Remarkably, the entanglement entropy of a gapped ground state typically satisfies an "area law," meaning it scales as the area of the boundary (L_A^{d-1}), where L_A is the linear dimension of subregion A and d is the number of dimensions [38–40]. (This is in contrast with a typical or random state in Hilbert space which satisfies a "volume law," $S(\rho_A) \sim L_A^d$ [41, 42].) Gapless systems can exhibit a multiplicative logarithmic correction to the area law, including 1D gapless systems described by a conformal field theory [43], as well as systems which contain a Fermi surface [44]. Subleading corrections to the entanglement scaling can provide additional insights into the state (for instance, in the case of topological phases [45–47]). Even more can be learned by considering the full entanglement spectrum (i.e. the eigenvalues of ρ_A) [48], which remarkably provides deep insights even when the subsystem A is non-contiguous [49].

An alternative method for quantifying the entanglement of a subregion is in terms of the Rényi entropies, given by

$$S_\alpha(\rho_A) = \frac{1}{1-\alpha} \ln \left[\operatorname{Tr}(\rho_A^\alpha)\right], \tag{1.6}$$

which reduces to the von Neumann entropy (Eq. 1.5) in the limit $\alpha \to 1$. In many cases, the Rényi entropy for integer $\alpha \geq 2$ is easier to compute or measure than the von Neumann entropy. The Rényi entropies are related by the inequality $S_n \geq S_m$ when $n < m$. In particular, S_2 serves as a lower bound on the von Neumann entropy S_1. In fact, given multiple Rényi entropies it is possible to derive more stringent bounds, including $S_1 \geq 2S_2 - S_3$ [50].

Calculation of Rényi entropies for integer $\alpha \geq 2$ typically involves what is known as a "replica trick," in which α copies of the system are considered on an α-sheeted Riemann surface, with branch cuts placed at the boundary of subregion A. This trick can be implemented analytically, for instance in conformal field theory [43, 51–53], where often it is possible to find an analytic continuation of $S(\alpha)$ and use it to determine the von Neumann entropy. It is also possible to measure Rényi entropies numerically in quantum Monte Carlo, where one considers α copies of the system and measures the expectation value of a "swap" operator, which permutes the configurations of the copies within subregion A [54]. The swap operator can also be measured in variational Monte Carlo [55], and similar tricks exist for measuring Rényi entropies of interacting fermions in determinantal Monte Carlo [56, 57].

There are a variety of ways to experimentally detect entanglement in many-body systems. One is through the use of special observables called entanglement witnesses, which can be constructed to experimentally detect a specific entangled state [58–61]. Experimentally measuring entanglement entropies, the holy grail of which would be to measure

the von Neumann entropy, is unfortunately much more difficult than entanglement detection. Currently, the only known method for measuring the von Neumann entropy is to first perform full tomography on a subregion A to determine the density matrix ρ_A, but this is costly and works only for the smallest of systems. However, if one has access to a coherent quantum network of controlled-SWAP gates (e.g. on a universal quantum computer), it is in principle possible to estimate non-linear functionals of a quantum state, including the von Neumann entropy [62].

Although direct measurement of the von Neumann entropy is experimentally out of reach, it is now possible to measure Rényi entropies S_α for integer $\alpha \geq 2$ by physically implementing a version of the "swap" operator mentioned above [63, 64]. A recent experiment measured the Rényi entropy S_2 by performing controlled interference between two identical copies of a bosonic quantum state [65] and measuring the resulting particle number parity on each site using a quantum gas microscope [66]. In principle, the experimental tools exist for measuring Rényi entropies in fermionic systems as well [67–70]. Sadly, whether one is measuring bosons or fermions, the protocol for measuring Rényi entropy has a "sign problem" in that the number of measurements needed scales exponentially with S_α. This is because the protocol involves estimating a quantity exponentially close to zero ($\langle \mathrm{Tr}\,(\rho_A^\alpha)\rangle = e^{-(\alpha-1)S_\alpha}$) from repeated measurement outcomes of $+1$ or -1, similar to a quantum Monte Carlo program which measures the swap operator. Nevertheless, it should be possible to measure Rényi entropies for arbitrarily large 1D systems which exhibit an area law. The scaling of entanglement entropy, long considered to be a

purely theoretical notion, has now entered the experimental realm.

Having provided background about entanglement, we now turn to the central topic of this dissertation, quantum thermalization.

1.3 Quantum thermalization and its breakdown

An isolated quantum system exhibits unitary time evolution according to the Schrödinger equation,

$$H\left|\Psi\right\rangle = i\hbar\frac{d}{dt}\left|\Psi\right\rangle. \tag{1.7}$$

The main question in studying quantum thermalization is whether (and under what conditions) such an isolated system will eventually reach thermal equilibrium, without assuming contact with any external "bath" or measuring apparatus. In other words, can a system's interactions with *itself* be sufficient for thermalization to occur?

At first, the answer appears to be no, for a simple reason. If an isolated system is prepared in (or near) a pure state, it will remain so at all times[3]. However, a "thermal" system is described by a highly mixed state, given above by Eq. 1.1. Since a pure state can never evolve to a mixed state, an arbitrary initial state cannot reach the canonical ensemble in the long-time limit.

However, there is a simple escape from this apparent paradox. Given a full system in a pure state $\left|\Psi\right\rangle$, the reduced density matrix $\rho_A \equiv \mathrm{Tr}_{\overline{A}}\left|\Psi\right\rangle\left\langle\Psi\right|$ of a subregion A will generally be in a mixed state. Thus, it is possible a system to be appear *locally thermal*

[3]In particular, unitary time evolution implies information must be conserved.

within subregion A, even if the full system is in a pure state.

The mention of subsystems is reminiscent of the discussion of entanglement in the previous section. In fact, it has been realized that the spreading of entanglement is itself the mechanism for thermalization in an isolated quantum system [71]. As a thermalizing system evolves, information that was once local to a region of the system becomes encoded into global operators. The quantum system itself acts as its *own* reservoir, and over time each subsystem becomes increasingly entangled with the remainder of the system. Once thermal equilibrium is reached, essentially no information about the initial state remains within a subsystem, other than the system's initial energy density (which determines its equilibrium temperature). A sufficiently small subsystem is then in a mixed state described by the canonical ensemble, and its entanglement entropy is equal to its thermal entropy. This equality implies that the entanglement entropy scales as a volume law with subsystem size, just as thermal entropy is an extensive quantity. We will discuss thermalization from the perspective of entanglement in detail in Chapter 2.

1.3.1 The Eigenstate Thermalization Hypothesis

A breakthrough in understanding quantum thermalization occurred in the early 1990s, as a result of work done independently by Josh Deutsch and Mark Srednicki. Their result, now known as the "Eigenstate Thermalization Hypothesis" (ETH), postulates that the ultimate fate of a quantum system rests on whether (or not) the eigenstates of the system themselves predict the correct thermal equilibrium values for simple operators [72–

75]. Within this framework, thermalization is not a property of the detailed quantum dynamics of a system, but rather a property of its eigenstates—particularly those of finite energy density. Over time, numerical studies have continued to provide support for the validity of ETH in several non-integrable quantum systems [76–80].

In previous literature, it has often been claimed that ETH holds only for simple or "few body" operators [76, 81, 82]. In Chapter 2, we introduce and provide evidence for a strong form of ETH in which a single eigenstate correctly predicts thermal values for *all* operators within a subregion A, as long as the volume of region A is a vanishing fraction of the total system size in the thermodynamic limit. Remarkably, this result allows one to predict properties of a system at all temperatures given knowledge of just a single eigenstate.

There also exist systems for which ETH does not hold—that is, the finite energy density eigenstates do not appear thermal, and as such these systems fail to thermalize. Let us now turn to consider the breakdown of thermalization.

1.3.2 Integrable systems

One notable class of systems which fail to thermalize to the canonical ensemble are those which are integrable. Integrable systems have an infinite sequence of extensive conserved quantities, given by sums of local operators. These conserved quantities often allow such systems to be solvable (e.g. in the case of the 1D nearest-neighbor Heisenberg and Hubbard chains); however, they also prevent these systems from thermalizing. It

has been conjectured that integrable systems relax to a "generalized Gibbs ensemble," meaning that they thermalize to the extent consistent with all conserved quantities [83–86].

In Ref. [87], Kinoshita et al. performed an experiment on a trapped 1D gas of ^{87}Rb bosons with a point-like collisional interaction. The physics of this system is described by the Lieb-Liniger model, which is itself integrable [88]. Kinoshita et al. found that, even after thousands of collisions, the bosons do not move toward thermal equilibrium. This provides an interesting counterpoint to quantum thermalization, as well as a testament to the extent to which cold atomic systems are almost completely isolated from the remainder of the universe.

Interestingly, a version of ETH is typically satisfied even in integrable systems [81]. Although there exist eigenstates that are non-thermal, the fraction of non-thermal eigenstates vanishes in the thermodynamic limit. These non-thermal eigenstates are both infinite in quantity yet very rare.

1.3.3 Many-body localization

Another class of systems which fail to thermalize are those which are localized. In a 1958 paper, Philip Anderson considered localization in the context of non-interacting models, demonstrating that the eigenstates of certain strongly disordered systems fall off exponentially outside a region of localization [89]. In 2006, Basko et al. argued perturbatively that localization can persist even in the context of weak interactions [90].

Since then, numerical work has provided mounting evidence for the existence of a localized phase in systems with strong disorder [91–94], a phenomenon that now goes by the name "many-body localization" (MBL). These systems are characterized by vanishing DC conductivity, and they retain some local memory of the initial state at all times. The MBL phase has recently been realized in experiments on cold atomic gases [95–97] and trapped ions [98].

The lack of thermalization in MBL systems can also be understood in terms of entanglement. Over time, entanglement grows only logarithmically in these systems, unlike in thermal systems [99]. Additionally, eigenstates in the MBL phase typically exhibit an area law scaling of the entanglement entropy [93]. This is reminiscent of a quantum ground state, and is in dramatic contrast with highly-excited thermal states (which exhibit volume law scaling).

Let us briefly consider systems in which the entire many-body spectrum is localized. It has been demonstrated that these "fully-MBL" (fMBL) systems themselves contain infinitely many quasi-local integrals of motion [100–104]. Thus, the breakdown of thermalization can be understood in terms of an integrability which emerges in the presence of strong disorder.

1.3.4 Quantum Disentangled Liquids

Is a strong, classical disorder potential the only way for thermalization to fail in a non-integrable quantum system? In Ref. [105], Grover and Fisher considered multi-component

quantum liquids with both heavy and light particles, and conjectured that there can exist a phase of matter in which the light particles are bound to the heavy particles and fail to thermalize independently of them. This phase, named a "Quantum Disentangled Liquid" (QDL), breaks ergodicity and is not thermal. In Chapter 3 we will investigate the QDL phase in the context of a Hubbard-like model. We provide a qualitative diagnostic—phrased in terms of entanglement entropy after partial measurement—that can identify eigenstates in this phase.

1.4 Numerical methods

In this dissertation, we will study the thermalization properties of exact, finite energy density eigenstates. Because the systems we study are non-integrable, the eigenstates cannot be constructed analytically and instead must be determined numerically.

The most straightforward way to determine exact eigenstates is to diagonalize the full Hamiltonian matrix on a computer. Sadly, full exact diagonalization is limited to small lattice systems, as the Hilbert space size M scales exponentially with system size, and the Hamiltonian is an $M \times M$ matrix. Still, there are a few tricks we can use to help scale to slightly larger system sizes. In a translationally invariant system, one can represent the Hamiltonian such that it is block diagonal in the momentum basis, which reduces the Hilbert space size by a factor of the system size L. It is also simple to take advantage of other abelian symmetries to further reduce the size of the Hilbert space. We detail these methods in Appendix A.

Additionally, it is possible to diagonalize not the full spectrum, but only a portion of it. Specifically, shift-invert and Krylov space methods allow one to obtain highly excited eigenstates of a Hamiltonian without diagonalizing it in full [94, 106, 107]. However, even with symmetries and Krylov space methods, the known algorithms for finding eigenstates still scale exponentially with system size.

Let us briefly consider an important class of states that can easily be represented on a computer. The density matrix renormalization group (DMRG), introduced in 1992, has become an incredibly powerful computational tool for low-energy, one-dimensional quantum physics problems [108, 109]. A few years after its introduction, it was realized that DMRG is effective because it represents quantum states as matrix product states (MPS) [110, 111], which are a special class of states with low entanglement. Because MBL states have area law entanglement scaling, there has been progress in studying MBL systems with matrix product states [112–115]. In principle, this should allow physicists to study MBL at much larger system sizes. On the other hand, non-localized states exhibit a volume law scaling of entanglement entropy, and thus cannot be efficiently represented as matrix product states. As such, the thermalization studies in this dissertation are beyond the reach of matrix product states, and we rely on numerical exact diagonalization to determine eigenstates in Chapters 2 and 3.

1.5 Outline

This dissertation is organized as follows. In Chapter 2, we introduce and provide numerical evidence for a strong form of ETH in which the reduced density matrix of a subsystem corresponding to a single eigenstate approaches the thermal density matrix as long as the subsystem size is much less than the total system size. This work is under review, and a preprint is available at Ref. [78]. In Chapter 3, we provide numerical evidence for the breakdown of ETH in a translationally invariant, two component system with both spin and charge degrees of freedom. Chapter 4 concludes this dissertation and provides an outlook for the future. Finally, Appendix A contains a brief introduction to performing numerical exact diagonalization calculations on systems with abelian symmetries.

Chapter 2

Which operators satisfy the Eigenstate Thermalization Hypothesis?

The Eigenstate Thermalization Hypothesis (ETH) posits that the reduced density matrix for a subsystem corresponding to an excited eigenstate is "thermal." In this chapter, we expound on this hypothesis by asking: for which class of operators, local or non-local, is ETH satisfied? We show that this question is directly related to a seemingly unrelated question: is the Hamiltonian of a system encoded within a single eigenstate? We formulate a strong form of ETH where in the thermodynamic limit, the reduced density matrix of a subsystem corresponding to a pure, finite energy density eigenstate asymptotically becomes equal to the thermal reduced density matrix, as long as the subsystem size is

much less than the total system size, irrespective of how large the subsystem is compared to any intrinsic length scale of the system. This allows one to access the properties of the underlying Hamiltonian at arbitrary energy densities/temperatures using just a *single* eigenstate. We provide support for our conjecture by performing an exact diagonalization study of a non-integrable 1D lattice quantum model with only energy conservation. In addition, we examine the case in which the subsystem size is a finite fraction of the total system size, and find that even in this case, a large class of operators continue to match their canonical expectation values. Specifically, the von Neumann entanglement entropy equals the thermal entropy as long as the subsystem is less than half the total system. We also study, both analytically and numerically, a particle number conserving model at infinite temperature which substantiates our conjectures.

2.1 Introduction

Given a local Hamiltonian, what information about the system is encoded in a single eigenstate? If the eigenstate happens to be a ground state of the Hamiltonian, tremendous amount of progress can be made on this question for Lorentz invariant systems [116–118], especially conformal field theories (CFTs) [43, 51, 52, 119], and for topological phases [45, 46, 48]. For example, one can read off the central charge of a CFT from the ground state entanglement [43, 51, 52], while for topological phases, essentially all 'topological data' such as braiding statistics of anyons can be extracted from the degenerate ground states [45, 47, 48]. In this chapter we argue that a single finite energy density eigenstate

of an ergodic quantum many-body Hamiltonian is sufficient to determine the properties of the system at all temperatures.

It is not very surprising that the *ground states* of quantum many-body systems contain some information about their excitations. This is because an entanglement cut often mimics an actual physical cut through the system, thus exposing the underlying excitations along the entangling boundary [48]. The same intuition is tied to the fact that the ground state entanglement satisfies a "boundary law" of entanglement entropy [39, 120], that is, the von Neumann entanglement entropy $S_1 = -\operatorname{Tr}_A(\rho_A \ln(\rho_A))$ of the ground state corresponding to a subsystem A scales with the size of the boundary of subsystem A.

How does the nature of information encoded evolve as one goes from the ground state to an excited eigenstate? Typically, there always exist eigenstates with energy E just above the ground state which continue to satisfy an area law of entanglement. These are the eigenstates which have zero energy density, i.e. $\lim_{V\to\infty} \frac{E-E_0}{V} = 0$ where E_0 is the ground state energy and V is the total volume of the system. These eigenstates can often be interpreted as the action of a sum of local operators acting on the ground state; for example, in a system with spontaneous symmetry breaking one can construct an eigenstate consisting of a few magnons by a superposition of spin-flips acting on the ground state. Furthermore, the level spacing between two contiguous low-lying excitations scales as $\delta E \sim 1/L^\alpha$ where $\alpha > 0$ depends on dimensionality and the phase of matter under consideration. In this chapter, we will instead be concerned with excited eigenstates that

have a *finite energy density*, i.e. $\lim_{V\to\infty} \frac{E-E_0}{V} \neq 0$. For notational convenience, we will set $E_0 = 0$ for the remainder of this chapter.

As argued by Srednicki [73–75], a typical finite energy density state (i.e. a typical state in the Hilbert space that satisfies $\langle\psi|H|\psi\rangle = Ve$ where e is the energy density) when time-evolved with the Hamiltonian H for sufficient time is expected to lead to predictions dictated by the basic tenets of equilibrium statistical mechanics, *if* the system thermalizes. Such an expectation leads to the "Eigenstate Thermalization Hypothesis" (ETH) [72–75], which stipulates that the thermalization occurs at the level of each individual eigenstate. An alternative approach by Deutsch [72], which is based on perturbing an integrable system by a small integrability breaking term, leads to the same suggestion. If ETH holds true, then in the thermodynamic limit the equal-time correlators of an operator with respect to a finite energy density eigenstate $|\psi\rangle$ are precisely equal to those derived from a thermal ensemble, i.e.

$$\langle\psi|O|\psi\rangle = \frac{\mathrm{Tr}\left(Oe^{-\beta H}\right)}{\mathrm{Tr}\left(e^{-\beta H}\right)} \tag{2.1}$$

where β is chosen such that the Eq. 2.1 holds true when $O = H$, the Hamiltonian. Henceforth we will use the notation $|\psi\rangle_\beta$ to denote an eigenstate whose energy density corresponds to temperature β^{-1}. A notable exception to ETH is a many-body localized system in the context of strongly disordered interacting quantum systems, [71, 90, 91, 93, 102, 121, 122] which fails to thermalize and does not satisfy Eq. 2.1. The possibility [105, 123–128], or impossibility [129–132], of the violation of ETH without disorder has

also been discussed recently.

In this chapter, we restrict ourselves to systems where ETH, as defined by Eq. 2.1, holds. However, Eq. 2.1 alone is incomplete unless one also specifies the class of operators for which it holds. For example, one simple non-local operator for which Eq. 2.1 breaks down is the projection operator $|\psi\rangle\langle\psi|$ onto the eigenstate $|\psi\rangle$ that enters Eq. 2.1; the left hand side of Eq. 2.1 yields unity for this operator, while the right hand side is exponentially small in the volume, a clear disagreement. On that note, it is often mentioned that in systems where Eq. 2.1 does hold, it does so only for "few body" operators [76, 81, 82] where, to our knowledge, the precise meaning of few-body operator has not been clarified (see Ref. [133] for related discussion). In this chapter, we conjecture and provide numerical evidence that Eq. 2.1 holds for *all* operators within a subsystem A when the volume V_A of subsystem A satisfies $V_A \ll V$ (or, more precisely, when $V_A/V \to 0$ as $V \to \infty$). We also explore the more general case where subsystem A spans a finite fraction $f \equiv V_A/V > 0$ of the total system size. We provide some evidence that when the fraction is less than a critical $O(1)$ number f^*, then all operators *not* explicitly involving energy conservation take their thermal values. We also explore the more general condition $V_A < V/2$ and show that even in this case, Eq. 2.1 holds for a large class of operators. On that note, we should mention that the questions such as which Hamiltonians (and which operators) satisfy ETH is now entering the realm of experimental physics (see e.g. Ref. [96]) due to advances in high resolution imaging techniques [66].

The satisfaction of Eq. 2.1 for all operators in a subsystem A is equivalent to the

statement that the reduced density matrix $\rho_A(|\psi\rangle_\beta) = \mathrm{Tr}_{\overline{A}} |\psi\rangle_{\beta\beta}\langle\psi|$ corresponding to an eigenstate $|\psi\rangle_\beta$ is given by

$$\rho_A(|\psi\rangle_\beta) = \rho_{A,\mathrm{th}}(\beta) \tag{2a}$$

where

$$\rho_{A,\mathrm{th}}(\beta) = \frac{\mathrm{Tr}_{\overline{A}}\left(e^{-\beta H}\right)}{\mathrm{Tr}\left(e^{-\beta H}\right)},$$

$\overline{A}$ being the complement of A. Note that the trace in the denominator is over the whole Hilbert space. When V_A is held constant, the equality in Eq. 2a means the density matrices become elementwise equal in any basis as $V \to \infty$.

One immediate consequence of Eq. 2a is that the thermodynamical properties of a system at arbitrary temperatures can be calculated using a *single* eigenstate. For example, Eq. 2a implies that to the leading order, the Rényi entropies S_α $(= -\frac{1}{\alpha-1}\ln\left[\mathrm{Tr}_A(\rho_A^\alpha)\right])$ for an eigenstate $|\psi\rangle_\beta$ corresponding to a subsystem A with $V_A \ll V$ are given by

$$S_\alpha = \frac{\alpha}{\alpha-1} V_A \beta \left(f(\alpha\beta) - f(\beta)\right), \tag{2.3}$$

where $f(\beta)$ is the free energy density at temperature β^{-1}. The above equation allows one to access the free energy density f at an arbitrary temperature by varying α. Note that Eq. 2.3 holds only to the leading order because Rényi entropies S_α receive additional subleading contributions due to the conical singularity induced at the boundary of subsystem A [43, 51, 52]. In the limit $\alpha \to 1$, one recovers the equality between the

von Neumann entanglement entropy S_1 and the thermal entropy $S_{\rm th} = V_A s_{\rm th}(\beta)$, where $s_{\rm th}(\beta)$ is the thermal entropy density at temperature β^{-1}, a result which was argued to hold in Ref. [134] for the special case of two weakly coupled ergodic systems. We emphasize that these results cannot be derived from Eq. 2.1 alone were it to hold only for local operators, since entanglement entropies do not correspond to the expectation value of any local operator. We also note that Refs. [135, 136] simulated the thermal Rényi entropy S_α (starting with the expression on the right hand side of Eq. 2a) using Quantum Monte Carlo to access the properties of the system at temperature $(\alpha\beta)^{-1}$. Of course, Quantum Monte Carlo methods are not well suited to verifying ETH since they cannot access properties of a *single* eigenstate (the left hand side of Eq. 2a).

We will also discuss an approximate, but more intuitive form of ETH, given by

$$\rho_A(|\psi\rangle_\beta) \approx \frac{e^{-\beta H_A}}{\mathrm{Tr}_A\left(e^{-\beta H_A}\right)} \tag{2b}$$

where H_A is the projection of the original Hamiltonian onto subsystem A. This form is approximate compared to Eq. 2a because generically, it does not capture the correlations near the boundary correctly due to the somewhat arbitrary truncation scheme used to obtain H_A. Nevertheless, equations 2a and 2b both yield the same results for all bulk quantities such as the Rényi entropy densities, as well as correlation functions of operators that have support only far from the boundary.

A central task of this chapter is to check the validity of Eqs. 2a and 2b and their consequences for model non-integrable systems. As already mentioned, we will argue

that ETH allows one to calculate thermodynamical quantities as well as correlators *at all temperatures/energy densities using only a single eigenstate*. We will demonstrate this explicitly by studying a quantum 1D model numerically.

As mentioned above, we find evidence that Eq. 2.1 holds for many operators even when V_A/V is held constant with V_A/V less than some number $f^* > 0$. In particular, as we discuss later, our results strongly indicate that $f < 1/2$ is sufficient to guarantee equivalence between the von Neumann entropy density of a pure eigenstate, and the thermal entropy density at the corresponding temperature. This is in contrast to Ref. [137] where it was argued that such an equivalence holds only in the limit $f^* \to 0$. Recently [138,139], the requirement $f^* \to 0$ was substantiated using analytical and large scale numerical calculations for *free* fermions, an integrable system. Our results indicate that the $f^* \to 0$ requirement is likely a consequence of the integrable nature of the models in Refs. [138, 139].

The chapter is organized as follows. Section 2.2 discusses general considerations for the validity of ETH, and introduces a division of all operators in a given subsystem into two distinct classes, which have different requirements for ETH to hold. Section 2.3 illustrates some general features of ETH by studying properties of a hardcore boson model with global particle number conservation for infinite temperature eigenstates. Section 2.4 introduces the model we study in the remainder of the chapter, the transverse field Ising model with longitudinal field. Section 2.5 focuses on the entanglement entropies at finite temperature. Section 2.6 studies the validity of ETH when $V_A \ll V$ by providing a close

look into the entanglement Hamiltonian, focusing on its spectrum and Schmidt vectors. This section also demonstrates the validity of Eq. 2a when $V_A \ll V$ by considering the trace norm distance between both sides. Section 2.7 explores the validity of ETH when V_A/V is taken to be finite as $V \to \infty$. Section 2.8 provides an application, by using the reduced density matrix from a single eigenstate to predict correlators at all (finite) temperatures. Section 2.9 summarizes our results and provides thoughts for future discussion.

2.2 General considerations

2.2.1 Determining the Hamiltonian from microstates in classical statistical mechanics

Suppose, for an isolated system described by classical statistical mechanics in a total volume V, we are given access to all classical microstates in a small energy window $[E, E + \Delta E]$, where $\Delta E \sim \sqrt{V}$ is on the order of the energy fluctuations in the total system were the system coupled to a thermal bath, and thus all microstates correspond to the same *energy density*. We pose the question: does this information suffice to determine the underlying Hamiltonian, assuming that the Hamiltonian is local? The answer is indeed yes, following the standard procedure of obtaining the canonical ensemble from a microcanonical ensemble. In particular, let us make a fictitious division of the system into A and $\overline{A}$ such that $V_A \ll V_{\overline{A}}$, and count the number of times a particular configuration

C_A appears in subsystem A. This determines the probability distribution for finding a given configuration, $P(C_A)$. If all microstates are equally likely, then [140]

$$P(C_A) = \frac{e^{-\beta E(C_A)}}{\sum_{\{C_A\}} e^{-\beta E(C_A)}} \tag{2.4}$$

where $E(C_A)$ is the energy in subsystem A. One may now invert this equation to obtain the energy $E(C_A) = -\frac{1}{\beta}\ln(P(C_A))$, up to an irrelevant constant shift of energy. In a classical statistical mechanical system $E(C_A)$ *is* the Hamiltonian for subsystem A. In particular, knowing $E(C_A)$, one may now calculate any thermodynamic property at *any* temperature. Here it is crucial to note that Eq. 2.4 does not assume that the energy density $E(C_A)/V_A$ equals the energy density E/V of the microstates being sampled.

As discussed in the introduction, we will provide evidence that the quantum mechanical analog of Eq. 2.4 is given by Eqs. 2a, 2b. We now proceed to discuss the conditions under which Eqs. 2a, 2b are valid.

2.2.2 Two classes of operators

For reasons soon to be discussed, we find it useful to separate operators in a given Hilbert space into two classes:

Class I ("Equithermal Operators"): If the reduced density matrix takes the thermal form (i.e. the right hand side of Eq. 2b), then in the limit $V_A \to \infty$, the expectation value of equithermal operators receives contribution only from the eigenstates of H_A at an energy density corresponding to the temperature β^{-1}. One might have thought that

this is true for all operators, however, there exist operators such as $e^{-n\beta H_A}$, whose expectation value includes contribution from eigenstates of H_A at temperature $[(n+1)\beta]^{-1}$ in addition to the temperature β^{-1}. Clearly, local operators fall into this class, as do sums of local operators. Several non-local operators, including the von Neumann entropy S_1, also fall into this class.

Class II ("Non-equithermal Operators"): We dub all operators not in Class I as "non-equithermal operators", or Class II operators. All Rényi entropies S_α (for $\alpha \neq 1$) fall into this class [141].

2.2.3 ETH: Class I vs. Class II operators

Let us first consider the relationship between Eq. 2.1 and Eqs. 2a, 2b. Eq. 1 may be rewritten as,

$$\mathrm{Tr}_A\left(\rho_A O\right) = \frac{\mathrm{Tr}_A\left(O\ \mathrm{Tr}_{\overline{A}}\left(e^{-\beta H}\right)\right)}{\mathrm{Tr}\left(e^{-\beta H}\right)} \tag{2.5}$$

If this equation holds for *all* operators in a subsystem A, hermitian as well as non-hermitian, then one obtains Eq. 2a, $\rho_A(|\psi\rangle_\beta) = \rho_{A,\mathrm{th}}(\beta)$. This is because one may expand both the ρ_A and $\rho_{A,\mathrm{th}}$ in terms of the complete set of operators in subsystem A, and by choosing appropriate O prove that they are equal to each other element-by-element. One of the most important consequences of this equality is that it allows one to extract properties of the Hamiltonian at arbitrary temperatures using a single eigenstate, which is one of the central points of this chapter.

We will now discuss ETH for both Class I and Class II operators. For each class, we consider separately two cases: (i) when $V_A \ll V$; and (ii) when the ratio $f \equiv V_A/V$ is taken to be fixed and finite as $V_A, V \to \infty$.

ETH for Class I operators

Let us first briefly discuss ETH for Class I operators when $V_A \ll V$. This includes both the case where V_A is held fixed as $V \to \infty$, as well as the case where the limits $V_A, V \to \infty$ are taken such that $V_A/V \to 0$. In fact, this is the traditional definition of ETH—that all local, "few-body" operators match their values in the canonical ensemble in this case.

Let us now consider the validity of ETH for Class I operators in the fixed-ratio limit where $0 < f < \frac{1}{2}$ is finite. In contrast to classical statistical mechanics, we expect that quantum mechanically, one does not require the constraint $V_A \ll V_{\overline{A}}$ for ETH to hold for a large class of Class I operators. Indeed, as discussed below, several known results already point to the conclusion that Eq. 2.1 holds for at least some operators in Class I, as long as $V_A < V_{\overline{A}}$ with both $V_A, V_{\overline{A}} \to \infty$.

One piece of evidence that suggests that Eq. 2.1 might hold for Class I operators as long as $V_A < V_{\overline{A}}$ comes from the study of quantum quenches in conformal field theories (CFTs). As shown in Ref. [142], the time-dependent reduced density matrix $\rho_A(t)$ of a system initially prepared in a low-entanglement state, and evolved with a CFT Hamiltonian, approaches the thermal density matrix, as long as $V_A < V/2$, with $V_A, V \to \infty$. Ref. [142]

characterized the closeness between $\rho_A(t)$ and the thermal density matrix $\rho_{A,\text{th}}$ (Eq. 2a) in terms of the operator overlap $I(t) = \frac{\text{Tr}(\rho_A(t)\rho_{A,\text{th}})}{\left(\text{Tr}(\rho_A^2(t))\,\text{Tr}(\rho_{A,\text{th}}^2)\right)^{1/2}}$, which is exponentially close to unity for $V_A/2 < t < V_{\overline{A}}/2$. It is important to note that in the thermodynamic limit, I only receives contribution from eigenstates at temperature β^{-1}, so this only guarantees that operators in Class I will satisfy Eq. 2.1.

Another piece of evidence comes from the recent studies of large central charge conformal field theories [143–145]. In particular, Refs. [143, 145] studied the entanglement entropy of pure eigenstates in finite temperature conformal field theories with large central charge. In the limit $V_A, V \gg 1/T$, while keeping V_A/V fixed, it was found that the entanglement entropy becomes equal to the thermal entropy at all non-zero temperatures as long as $V_A < V_{\overline{A}}$.

Lastly, the entanglement entropy for a random pure state is given by [42, 146–150]:

$$S = -\ln\left(|\mathcal{H}_A|^{-1} + |\mathcal{H}_{\overline{A}}|^{-1} - |\mathcal{H}|^{-1}\right) \tag{2.6}$$

where $|\mathcal{H}_A|, |\mathcal{H}_{\overline{A}}|, |\mathcal{H}|$ are the sizes of the Hilbert spaces of subsystems A, $\overline{A}$ and the total system ($= A \cup \overline{A}$) respectively. Thus, as soon as $V_A < V_{\overline{A}}$, one obtains $S = -\ln(|\mathcal{H}_A|)$, which is indeed the thermal entropy for subsystem A at infinite temperature. Since random pure states mimic eigenstates at infinite temperature (i.e. $|\psi\rangle_{\beta=0}$), this again suggests that the condition $V_A < V_{\overline{A}}$ is perhaps sufficient, at least for some operators.

On the other hand, there is a well-known Class I operator for which ETH fails when

the ratio of subsystem to total system size $f = V_A/V$ is finite [1]. When f is finite, the energy variance of the reduced density matrix $\rho_A(|\psi\rangle_\beta)$ will be suppressed by a factor of $(1-f)$ compared with the value the variance would have taken in the canonical ensemble. Ultimately, this is due to the fact that a single eigenstate has precisely zero energy variance $\langle(H-\langle H\rangle)^2\rangle$ in the full system, unlike the canonical ensemble, where the variance scales proportionally with system size. This relationship can be expressed as

$$\mathrm{Tr}[\rho_A(|\psi\rangle_\beta)\mathcal{O}_{A,\beta}] = \frac{V_A}{V}\ \mathrm{Tr}[\rho_{A,\mathrm{th}}(\beta)\mathcal{O}_{A,\beta}], \tag{2.7}$$

where $\mathcal{O}_{A,\beta} = (H_A - \langle H_A\rangle_\beta)^2$ is the energy variance operator. We will explore implications of the subsystem energy variance mismatch more carefully in Section 2.7.

It is worth noting that for the case of time-evolved states, the full system variance is independent of time. For a given initial state, this variance may indeed be different from the energy variance expected in the canonical ensemble, which implies that the energy variance for any subsystem that is a finite fraction of the total system will disagree, even at long times [151]. However, we expect that for "typical" initial states (which are typically inaccessible from an experimental point of view), the overall energy variance will match its result in the canonical ensemble, and so the energy variance for any subsystem will also match after thermalization ("canonical typicality" [41, 152, 153]).

Overall, while we expect that ETH is obeyed by many Class I operators when $f > 0$ is finite, it cannot be satisfied by all such operators, since the subsystem energy variance

[1] We are grateful to David Huse to pointing this out to us.

provides an important counterexample. Nonetheless, we expect that all Class I operators *not* related to energy conservation (or another conserved quantity) should satisfy ETH as given in Eq. 2.1. A more precise conjecture along these lines is that the set of operators spanned by H_A^n where n ranges between unity and the size of the Hilbert space do not satisfy ETH in the sense of Eq. 2.7 above. The number of such operators is still exponentially smaller than the total number of independent operators in a subsystem (e.g. in a spin-1/2 spin system, the total number of operators in a region A is 4^{V_A}, while the number of operators of the form H_A^n is 2^{V_A}, the size of the Hilbert space in region A).

ETH for Class II operators

The extra ingredient introduced by Class II operators is that if ETH holds for them, then taking such an operator's expectation value with respect to a state $|\psi\rangle_\beta$ allows one to access the properties of the Hamiltonian at a temperature different than β^{-1}. For example, the Rényi entropy S_α corresponding to $\rho_A(|\psi\rangle_\beta)$ satisfies $S_\alpha = \frac{\alpha}{\alpha-1} V_A \beta \left(f(\alpha\beta) - f(\beta)\right)$, thus allowing one to access the free energy density at temperature $(\alpha\beta)^{-1}$.

Let us first consider the validity of ETH for Class II operators when $V_A \ll V$. Remarkably, the results presented in the remainder of this chapter demonstrate that ETH is valid for all Class II operators in this limit. Thus, a single eigenstate of finite energy density contains knowledge of the properties of the system at all temperatures.

Now let us turn to the case in which V_A/V is finite, which turns out to be much

more subtle. As mentioned in the previous subsection, there is already a Class I operator for which ETH fails in this limit, namely the subsystem energy variance. Thus, we do not expect that ETH will hold for all Class II operators either when f is finite. In addition, for a given ratio V_A/V with both $V_A, V \to \infty$, there is a physical constraint on the range of energy densities for which the spectrum of $|\psi\rangle_\beta$ in principle can match that of $\rho_{A,\mathrm{th}}(\beta)$. To appreciate this, let us consider a slightly different problem—an arbitrary Hamiltonian of hardcore bosons with particle number conservation, at *infinite temperature*. We will consider an explicit example of such a system in the next section. Since the total particle number operator $\hat{N}$ commutes with the Hamiltonian and satisfies the equation $\hat{N} = \hat{N}_A + \hat{N}_{\overline{A}}$, the reduced density matrix ρ_A for a wavefunction $|\psi\rangle_{\beta=0}$ is block diagonal in the number of particles N_A in subsystem A. Furthermore, if ETH holds (as given by a generalization of Eqs. 2a and 2b), then the Schmidt decomposition is given by

$$|\psi\rangle_{\beta=0} = \sum_{N_A=0}^{N} \sqrt{\lambda_{N_A}} \sum_i |u_i\rangle_{N_A} \otimes |v_i\rangle_{N-N_A} \tag{2.8}$$

where λ_{N_A} are the Schmidt coefficients in the sector N_A, and $|u_i\rangle_{N_A}$, $|v_i\rangle_{N-N_A}$ are the corresponding eigenvectors. The label i captures fluctuations of particles within a fixed sector N_A. Note that there is no index i on λ_{N_A} because we are at infinite temperature and all Schmidt states within a sector N_A are equally likely.

The decomposition in Eq. 2.8 allows one to calculate properties of subsystem A at infinite temperature even *away* from filling N/V since the reduced density matrix ρ_A will

contain sectors with various densities N_A/V_A. However, there is both an upper limit and a lower limit on the density in subsystem A, since

$$\max\left[N-(V-V_A),0\right] \leq N_A \leq \min\left[N,V_A\right] \tag{2.9}$$

And thus the particle density N_A/V_A in subsystem A satisfies

$$\max\left[1-(1-n)/f,0\right] \leq \frac{N_A}{V_A} \leq \min\left[n/f,1\right] \tag{2.10}$$

where $n \equiv N/V$ is the overall particle density and $f \equiv V_A/V$. Thus, a necessary condition for the wavefunction in Eq. 2.8 to encode properties of the system at *all* fillings is

$$f \leq \min\left[n,1-n\right] \tag{2.11}$$

The above discussion, with some modifications, carries to systems with (only) energy conservation, at an arbitrary temperature. The Schmidt decomposition of an eigenstate $|\psi\rangle_\beta$ with eigenvalue E may now be written as:

$$|\psi\rangle_\beta = \sum_i \sqrt{\lambda_i}|u_i\rangle \otimes |v_i\rangle \tag{2.12}$$

The physical content of ETH, as approximated in Eq. 2b, is that $\lambda_i \propto e^{-\beta E_{A,i}}$ where $E_{A,i}$ is the i'th energy eigenvalue of H_A (the projection of the Hamiltonian to subsystem A) while $|u_i\rangle$ is the corresponding eigenstate of H_A. Denoting the ground state energy

to be zero, one naively expects that $\langle u_i|H_A|u_i\rangle \leq E \; \forall \; |u_i\rangle$ since the energy density in the subsystem $\overline{A}$ cannot be less than the ground state energy density. However, this argument has a loophole since in contrast to the particle number operator $\hat{N}$, the total Hamiltonian is *not* separable into subsystems A and $\overline{A}$: $H = H_A + H_{\overline{A}} + H_{A\overline{A}}$, which actually allows $\langle u_i|H_A|u_i\rangle$ to exceed E as we will see in Section 2.7 in the context of the model Hamiltonian in Eq. 2.30 below. To understand the constraint on $\langle u_i|H_A|u_i\rangle$ precisely, let us derive an expression which encapsulates the classical notion that the sum of energies in subsystem A and $\overline{A}$ equals E.

We first note:

$$\langle u_{i0}| \otimes \langle v_{i0}|H|\psi\rangle_\beta = E \langle u_{i0}| \otimes \langle v_{i0}|\psi\rangle_\beta \tag{2.13}$$

$$= E\sqrt{\lambda_{i0}} \tag{2.14}$$

The above expression can be re-evaluated using the decomposition $H = H_A + H_{\overline{A}} + H_{A\overline{A}}$:

$$\langle u_{i0}| \otimes \langle v_{i0}|H|\psi\rangle_\beta \tag{2.15}$$

$$= \langle u_{i0}| \otimes \langle v_{i0}|H_A + H_{\overline{A}} + H_{A\overline{A}}|\psi\rangle_\beta$$

$$= \sqrt{\lambda_{i0}}\langle u_{i0}|H_A|u_{i0}\rangle + \sqrt{\lambda_{i0}}\langle v_{i0}|H_{\overline{A}}|v_{i0}\rangle + \sum_j \sqrt{\lambda_j}\langle u_{i0}| \otimes \langle v_{i0}|H_{A\overline{A}}|u_j\rangle \otimes |v_j\rangle \tag{2.16}$$

Equating the two ways to calculate the same expression, one finds:

$$\begin{aligned}&\langle v_{i0}|H_{\overline{A}}|v_{i0}\rangle + \sum_j \sqrt{\frac{\lambda_j}{\lambda_{i0}}}\langle u_{i0}| \otimes \langle v_{i0}|H_{A\overline{A}}|u_j\rangle \otimes |v_j\rangle \\ &= E - \langle u_{i0}|H_A|u_{i0}\rangle \end{aligned} \tag{2.17}$$

Due to the variational principle for the ground state, $\langle v_{i0}|H_{\overline{A}}|v_{i0}\rangle \geq -cL^{d-1}$ where c is a constant (recall that in our convention, the ground state energy for the full Hamiltonian is set to zero). Since both E and $\langle u_{i0}|H_A|u_{i0}\rangle$ scale as L^d, the only way for $\langle u_{i0}|H_A|u_{i0}\rangle$ to exceed E is that the second term on the left hand side of Eq. 2.17, viz. $E_{\text{boundary}} \stackrel{\text{def}}{=} \sum_j \sqrt{\frac{\lambda_j}{\lambda_{i0}}}\langle u_{i0}| \otimes \langle v_{i0}|H_{A\overline{A}}|u_j\rangle \otimes |v_j\rangle$, is negative and scales as L^d. When that happens, ETH no longer holds, as we now argue on general grounds, and will also demonstrate numerically for a lattice Hamiltonian in Section 2.7. To see this, we reiterate that ETH requires that (i) $|u_i\rangle$'s are approximate eigenstates of H_A, and (ii) $\lambda_i \propto e^{-\beta\langle u_i|H_A|u_i\rangle} = e^{-\beta E_{A,i}}$. Firstly, when $\langle u_{i0}|H_A|u_{i0}\rangle < E$ so that ETH could in principle hold, the E_{boundary} term can be neglected because the 'diagonal term' in E_{boundary} (i.e. the term corresponding to $j = i0$) scales as the boundary ($\propto L^{d-1}$) and is thus subleading, while the off diagonal terms scale as e^{-L^d} and thus vanish in the thermodynamic limit (recall that $V_{\overline{A}} > V_A$). On the other hand, when $\langle u_{i0}|H_A|u_{i0}\rangle > E$, the $|v_{i0}\rangle$'s now correspond to states of zero energy density, and the aforementioned argument for neglecting off-diagonal terms is no longer valid. So, let us assume that $\langle u_{i0}|H_A|u_{i0}\rangle > E$ and each $|u_{i0}\rangle$ continues to be an

eigenstate of H_A. Thus, one requires that

$$\int de' \sqrt{\frac{\lambda(e')}{\lambda(e)}} M(e,e') e^{S(e')} \propto g(e)/L^{d-1}, \tag{2.18}$$

where we have taken the continuum limit and $\lambda(e)$ denotes the Schmidt eigenvalue corresponding to an eigenvector $|u\rangle$ at energy density e, while $M(e,e') = \langle u(e)| \otimes \langle v(e)|H_{A\overline{A}}|u(e')\rangle \otimes |v(e')\rangle$ and $g(e) = e - \langle u(e)|H_A|u(e)\rangle/L^d$. It is obvious from Eq. 2.18 that $\lambda(e) \propto e^{-\beta E_A} = e^{-\beta e f L^d}$ is no longer the solution. In fact, the only way for the integral on the left hand side of Eq. 2.18 not to have any exponential dependence on L (as required by the right hand side) is that the integrand itself does not have such dependence, i.e. $\sqrt{\frac{\lambda(e')}{\lambda(e)}} \propto \frac{1}{M(e,e')} e^{-S(e')}$. This implies a breakdown of ETH when $\langle u_{i0}|H_A|u_{i0}\rangle > E$.

The above discussion implies that for a given wavefunction and bipartition, the maximum energy density that is potentially accessible in a subsystem A, such that the corresponding Schmidt weight satisfies ETH is,

$$e^* = \min(E/V_A, e_{\max}) = \min(e/f, e_{\max}) \tag{2.19}$$

where $e = E/V$ is the energy density corresponding to the wavefunction and $e_{\max}$ is the maximum energy density for the Hamiltonian H (recall that $e_{\max}$ can be finite for lattice-regularized quantum systems, e.g. for models of fermions or spins/hardcore bosons). Above, we have assumed that $e < e_{\max}/2$. In the case when $e > e_{\max}/2$, the range of

available energies is instead bounded from below by $\max[0, e_{\max}(1-1/f) - e/f]$. If our goal is to capture the fluctuations in the system for all energy densities so that *all* Class II operators not related to energy conservation satisfy ETH, we obtain an analog of Eq. 2.11 for the energy: $E/V_A \geq e_{\max}$, and, $(e_{\max}V - E)/V_A \geq e_{\max}$. Expressed in terms of the fraction V_A/V, and the energy density of the eigenstate $e = E/V$, this constraint is

$$f \leq f^* \equiv \min\left[\frac{e}{e_{\max}}, 1 - \frac{e}{e_{\max}}\right]. \tag{2.20}$$

Let us emphasize that the above constraint is a *necessary* condition for ETH to hold for all Class II operators, not a sufficient one. Just as some Class I operators cannot satisfy ETH when f is finite, we expect that there also exist Class II operators for which ETH fails when f is finite, even when the above condition holds. Even so, significant deviation in the eigenvalue spectrum begins where this constraint breaks down, as our numerical results will demonstrate in Section 2.7.

2.2.4 Summary

Let us summarize the discussion in this section.

1. We conjecture that ETH holds for all local and non-local Class I operators as long as $V_A \ll V$. This implies that ETH is *not* restricted only to few-body operators (as can be seen in the limit $V_A/V \to 0$ as $V_A, V \to \infty$). When the subsystem is taken to be a finite fraction $f < \frac{1}{2}$ of the total system size, we provide some evidence in Section 2.7 that all operators not involving energy conservation satisfy ETH as well.

2. We conjecture that ETH also holds for all Class II operators when $V_A \ll V$. It follows that a single eigenstate contains information about all energy densities available to the system. When f is finite, we suspect that ETH also holds for all operators that probe the system below an energy density e^* (given by Eq. 2.19) and that do not involve energy conservation; however, we leave this as an open question.

3. Determining the full Hamiltonian from a single eigenstate is equivalent to the satisfaction of Eq. 2.1 for both Class I and Class II operators. Our results provide strong evidence that this is true when $V_A \ll V$. Therefore, one should be able to extract information about the full Hamiltonian at arbitrary energy densities/temperatures using a single eigenstate.

2.3 A warmup: eigenstates at infinite T

2.3.1 Von Neumann and Rényi entropy

By definition, the thermal entropy reaches a maximum at infinite temperature. Together with Eq. 2.35, this implies that when ETH holds, eigenstates at "infinite temperature" are ones where the entanglement entropy is at its maximum. Consider a 1D transverse field Ising model with longitudinal field, $H = \sum_{i=1}^{L} \left(\sigma_i^z \sigma_{i+1}^z + h_x \sigma_i^x + h_z \sigma_i^z\right)$. Here the von Neumann entropy S_1 takes its maximum possible value when the eigenvalues of the reduced density matrix are all equivalent to one another. Thus, from counting the basis size of the reduced Hilbert space, we expect for infinite temperature eigenstates

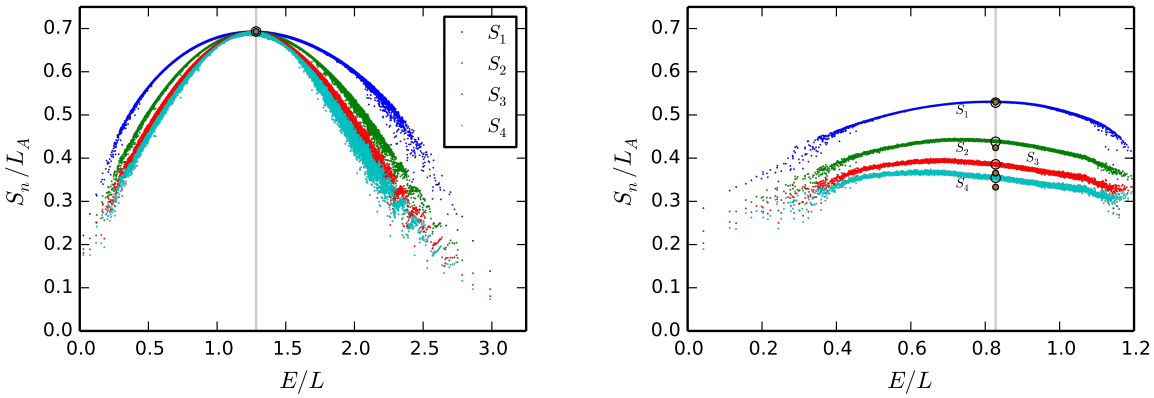

Figure 2.1: Entanglement entropies S_1 through S_4 for a model with no conservation law (left panel, given by Eq. 2.30 at $L = 21$), and a model with particle number conservation (right panel, given by Eq. 2.22 at $L = 27$ with filling $N = 6$). We use the parameters mentioned in the text to place each model at a nonintegrable point. In each case we consider eigenstates in the $k = 1$ sector, with subsystem size $L_A = 4$. The grey vertical line denotes infinite temperature (point of maximum S_1), and the black circles mark the theoretical predictions for the entanglement entropies there. The brown markers denote the theoretical values of the entropies in the limit $L_A, L \to \infty$ while $L_A/L \to 0$, as given by Eqs. 2.26 and 2.27. Notice that the Rényi entropies all match at infinite temperature if and only if there are no additional conservation laws besides energy.

that each eigenvalue of the reduced density matrix will approach 2^{-L_A} in the thermodynamic limit when $f = L_A/L < \frac{1}{2}$. From this, it follows that the Rényi entropies at infinite temperature satisfy

$$S_\alpha = L_A \ln 2, \tag{2.21}$$

that is, they are independent of Rényi index α. The left panel of Figure 2.1 shows how the entropies S_1 through S_4 together match this predicted value at the infinite temperature point for a $L = 21$ system with periodic boundary conditions and subsystem size $L_A = 4$. In general, as $L \to \infty$ the $T = \infty$ entropy density is given by $S_\alpha/L_A = \ln 2$.

Now let us instead consider a model with an additional conservation law, namely particle number conservation. Consider a 1D chain of hardcore bosons

$$\begin{aligned} H = &- \sum_i \left(t b_i^\dagger b_{i+1} + t' b_i^\dagger b_{i+2} + \text{H.c.} \right) \\ &+ \sum_i \left(V n_i n_{i+1} + V' n_i n_{i+2} \right) \end{aligned} \tag{2.22}$$

where $n_i \equiv b_i^\dagger b_i$. We focus on this system with periodic boundary conditions at the non-integrable point $t = V = 1$ and $t' = V' = 0.96$. This model was previously studied and shown to exhibit ETH in Refs. [154, 155].

Due to particle number conservation, the reduced density matrix from any pure state is block diagonal, with each block corresponding to some filling number N_A of the subsystem A. The block of the reduced density matrix $\rho_A^{(N_A)}$ corresponding to filling N_A is a $d_{N_A} \times d_{N_A}$ matrix, where $d_{N_A} \equiv \binom{L_A}{N_A}$. At infinite temperature and for $L_A/L < \frac{1}{2}$, the

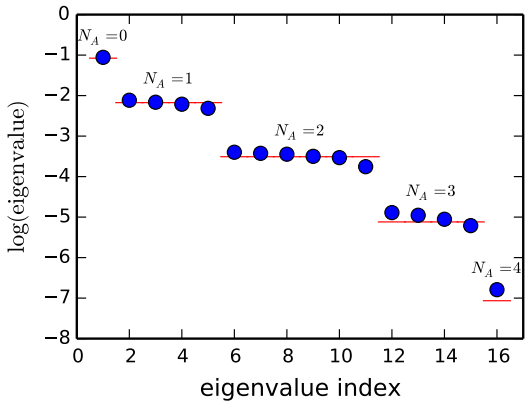

Figure 2.2: Eigenvalue spectrum of the reduced density matrix of an infinite temperature eigenstate, $\rho_A(|\psi\rangle_{\beta=0})$ for the hardcore boson model Eq. 2.22 with $L = 27$, $L_A = 4$, and filling $N = 6$. The red lines plot the theoretical value of each eigenvalue in the thermodynamic limit, determined from the filling N_A of the sector in which it lies.

eigenvalues of ρ_A must be equal to one another within a given block, but the eigenvalues in different blocks will be different: they are in fact proportional to $\binom{L-L_A}{N-N_A}$, the number of microstates consistent with such a configuration in subsystem A. Taking into account that $\mathrm{Tr}(\rho_A) = 1$, one finds that each of the $d_{N_A} = \binom{L_A}{N_A}$ eigenvalues of $\rho_A^{(N_A)}$ are given by $\lambda_{N_A} \equiv \binom{L-L_A}{N-N_A}/\binom{L}{N}$. The spectrum of ρ_A we find for a single eigenstate (as shown in Figure 2.2) is in agreement with that of the thermal reduced density matrix $\rho_{A,\mathrm{th}}(\beta = 0)$ studied in Ref. [135], consistent with ETH.

With this, the von Neumann entropy at infinite temperature becomes

$$S_1 = -\sum_{N_A} d_{N_A} \lambda_{N_A} \ln \lambda_{N_A} \tag{2.23}$$

and the Rényi entropies are given by

$$S_\alpha = -\frac{1}{\alpha - 1} \ln \left(\sum_{N_A} d_{N_A} \lambda_{N_A}^\alpha \right), \tag{2.24}$$

where the sums over N_A are restricted to subsystem particle fillings N_A that satisfy the constraint in Eq. 2.9. The above expressions are valid when $L_A/L < \frac{1}{2}$.

Because the eigenvalues are non-uniform, the Rényi entropies S_α at infinite temperature depend on the Rényi index α, in contrast to an energy-only conserving model. The right panel of Figure 2.1 shows how the actual values of S_1 through S_4 match those predicted by the above counting argument.

For comparison, we also calculate S_α analytically in the thermodynamic limit. For simplicity, we consider the limits, $L, N, L_A \to \infty$ such that $n = N/L$ is held constant, while $L_A/L \to 0$. In these limits, one can evaluate the expressions in Eq. 2.24 using Stirling's approximation $\ln(x!) \approx x \ln(x) - x$. One finds that in the limits considered, S_α receives contribution only from N_A given by

$$N_A^* = \frac{L_A}{1 + \left(\frac{1}{n} - 1\right)^\alpha} \tag{2.25}$$

Thus, S_α probes the system at filling $N_A^*/L_A = \frac{1}{1+\left(\frac{1}{n}-1\right)^\alpha}$, which is different than the actual filling n, unless $\alpha = 1$ (which corresponds to the von Neumann entanglement entropy). This also immediately leads to expressions for Rényi and von Neumann entan-

glement entropies in the thermodynamic limit:

$$S_\alpha/L_A = -\frac{1}{\alpha-1}\ln\left[n^\alpha + (1-n)^\alpha\right] \tag{2.26}$$

and

$$S_1/L_A = -\left[n\ln(n) + (1-n)\ln(1-n)\right]. \tag{2.27}$$

We plot these values in Figure 2.1 for comparison. Remarkably, even with the small system sizes we can access, the difference between the exact finite size result (obtained by counting over all sectors) and the result valid in the thermodynamic limit is quite small.

In the above derivation, it is also possible to relax the restriction $L_A/L \to 0$ as $L_A, L \to \infty$. We then find that N_A^* is given by the solution to

$$N_A^* = \frac{L_A}{1 + \left(\frac{1-f}{n - fN_A^*/L_A} - 1\right)^\alpha}, \tag{2.28}$$

which reduces to Eq. 2.25 when $f \to 0$.

Let us note a few things about this equation:

1. When $\alpha = 1$, the solution is $N_A^* = nL_A$, regardless of f. Thus, the von Neumann entropy always probes the system at its given filling, even when f is finite. Further analysis shows that Eq. 2.27 holds generally when $f < \frac{1}{2}$.

2. When the system is at half filling ($n = \frac{1}{2}$), the solution is $N_A^* = \frac{1}{2}L_A$, regardless of f or α.

3. When $\alpha > 1$, $0 < f < \frac{1}{2}$, and $n \neq \frac{1}{2}$, the filling fraction N_A^*/L_A probed by the Rényi entropy S_α actually depends on f. As a result, the Rényi entropies for a given L_A depend on f. This can be contrasted with the von Neumann entropy, which is independent of f as long as $f < \frac{1}{2}$. The right panel of Figure 2.1 illustrates this nicely: the analytical $f \to 0$ prediction for the von Neumann entropy (Eq. 2.27) matches the corresponding numerical result quite well, but the Rényi entropies differ significantly because $f = 4/27$ is finite.

We expect that analogous features hold true also for the model that conserves only energy, which we will discuss in the later sections.

2.3.2 Subsystem energy variance

Let us also consider the average subsystem filling variance of the particle-number conserving system given by Eq. 2.22 at infinite temperature. While the average subsystem filling is given by $\langle N_A \rangle = nL_A = Nf$, the variance in this quantity for a single eigenstate with $f \equiv L_A/L < \frac{1}{2}$ is given by

$$\left\langle (N_A - \langle N_A \rangle)^2 \right\rangle = L_A(1-f)(1-n)\frac{L}{L-1}. \tag{2.29}$$

Although both the filling and its variance are proportional to L_A as expected, the variance includes an additional factor $(1-f)$, which causes it to be suppressed compared with the grand canonical ensemble when f is finite. In Section 2.7 we will witness a similar suppression of the subsystem energy variance when the condition $L_A/L \to 0$ is relaxed.

2.4 Model Hamiltonian with only energy conservation

To develop some understanding of the questions posed in the introduction, we study a finite 1D quantum spin-1/2 chain with the following Hamiltonian:

$$H = \sum_{i=1}^{L} \left(\sigma_i^z \sigma_{i+1}^z + h_x \sigma_i^x + h_z \sigma_i^z \right) \tag{2.30}$$

We set $h_x = 0.9045$ and $h_z = 0.8090$ such that the model is far away from any integrable point, and is expected to satisfy ETH in the sense of Eq. 2.1 as shown in Ref. [77]. We use periodic boundary conditions throughout.

We diagonalized the Hamiltonian in Eq. 2.30 for system sizes up to $L = 21$, obtaining all eigenvalues and eigenstates. As hinted earlier, to each eigenstate we assigned a temperature β^{-1} by finding the value β for which the energy expectation value in the canonical ensemble matches the energy of the eigenstate:

$$\frac{\langle \psi | H | \psi \rangle}{\langle \psi | \psi \rangle} = \frac{\mathrm{Tr}\left(H e^{-\beta H} \right)}{\mathrm{Tr}\left(e^{-\beta H} \right)}. \tag{2.31}$$

By definition, $\beta = +\infty$ for the ground state and $\beta = -\infty$ for the highest excited state. In practice, the range of available β values on a finite size system is much smaller. With $L = 21$, for instance, the first excited state has $\beta \approx 4.0$, and the second-to-highest excited state has $\beta \approx -0.6$ (as determined from Eq. 2.31). It follows that eigenstates outside the range $4.0 \gtrsim \beta \gtrsim -0.6$ will not appear fully thermal due to the large thermal correlation length expected at low temperatures. (This can be seen for instance in Figure 2.3, where the finite size corrections to the linear scaling of the entanglement entropy become more prominent as temperature decreases.) Another thing to consider is that the infinite temperature eigenstate $|\psi\rangle_{\beta=0}$ is completely random and contains no information about the Hamiltonian. In a finite size system, states near infinite temperature will also contain little information about the Hamiltonian and will therefore be unable to predict properties of the system at other energy densities. As a result of these finite size considerations, we typically study values of β between 0.2 and 0.5 in the remainder of this chapter.

2.5 Von Neumann and Rényi entropy of eigenstates at finite T

2.5.1 ETH prediction for von Neumann and Rényi entropies

Let us consider the Rényi Entropy $S_\alpha = -\frac{1}{\alpha-1}\ln(\mathrm{Tr}\ \rho_A^\alpha(|\psi\rangle_\beta))$ corresponding to an eigenstate $|\psi\rangle_\beta$ at inverse temperature β. Assuming that ETH, as encoded in Eq. 2a,

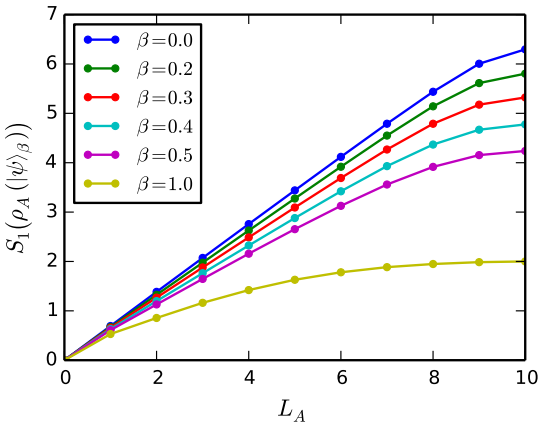

Figure 2.3: Scaling of the von Neumann entanglement entropy S_1 with subsystem size for the $L = 20$ system given in Eq. 2.30. Up to $\beta = 0.5$, the scaling is linear for small L_A, suggesting that the states are volume-law and are thus likely to satisfy ETH. The $\beta = 1.0$ eigenstate, on the other hand, is clearly not linear, and is too close to the ground state at this system size to exhibit ETH.

holds, S_α may be reexpressed as:

$$S_\alpha = -\frac{1}{\alpha - 1} \ln \left(\frac{Z(A, \alpha, \beta)}{Z(1, \beta)^\alpha} \right) \tag{2.32}$$

where $Z(A, \alpha, \beta)$ is the partition function of the system on an α-sheeted Riemann surface, such that subsystem A has an effective temperature $(\alpha\beta)^{-1}$ while subsystem $\overline{A}$ has an effective temperature β^{-1}. $Z(1, \beta)$ is the regular partition function of the system [43, 51, 52]. Therefore, keeping terms *only to the leading order in the subsystem size*, the above expression leads to Eq. 2.3 advertised in the Introduction,

$$S_\alpha = -\frac{1}{\alpha - 1} \ln \left(\frac{e^{-\alpha\beta V_A f(\alpha\beta) - \alpha\beta V_{\overline{A}} f(\beta)}}{e^{-\alpha\beta V_A f(\beta) - \alpha\beta V_{\overline{A}} f(\beta)}} \right) \tag{2.33}$$

$$= \frac{\alpha}{\alpha - 1} V_A \beta \left(f(\alpha\beta) - f(\beta) \right) \tag{2.34}$$

where f is the free energy density. Therefore, the wavefunction at temperature β^{-1} can be used to calculate the free energy at temperature $(\alpha\beta)^{-1}$. Indeed, the same result also follows using the approximate form in Eq. 2b. Taking the limit $\alpha \to 1$ leads to the conclusion that the von Neumann entanglement entropy S_1 satisfies

$$S_1 = V_A s_{\text{th}}(\beta) \tag{2.35}$$

where $s_{\text{th}}(\beta) = S_1(\rho_{A,\text{th}}(\beta))/L_A$ is the thermal entropy density at temperature β^{-1}.

2.5.2 Numerical Results for von Neumann and Rényi entropies

Figure 2.3 shows the scaling of von Neumann entropy S_1 as a function of subsystem size L_A for the eigenstates $|\psi\rangle_\beta$ of our model (Eq. 2.30). As discussed in Section 2.2.3, we expect Eq. 2.35 to hold as long as $V_A < V_{\overline{A}}$, in the limit $V_A, V_{\overline{A}} \to \infty$. This implies that in the thermodynamic limit, the function $S_1(V_A)$ is expected to form an inverted triangle shape, similar to the behavior of a random pure state (Eq. 2.6). However, in a finite total system at any non-infinite temperature, S_1 is an analytic function of the ratio V_A/V with a negative sign for $\frac{d^2 S_1}{dV_A^2}$, as shown in Figure 2.3 (note that the sign of the curvature is fixed by the strong subadditivity of entanglement). However, even in finite system, the volume law does hold to a good accuracy when $V_A \lesssim V/2$, and the finite size scaling, discussed below, indicates that the inverted triangle shape is recovered in the thermodynamic limit.

Figure 2.4 shows the comparison of S_1, S_2, S_3, and S_4 calculated for each individual

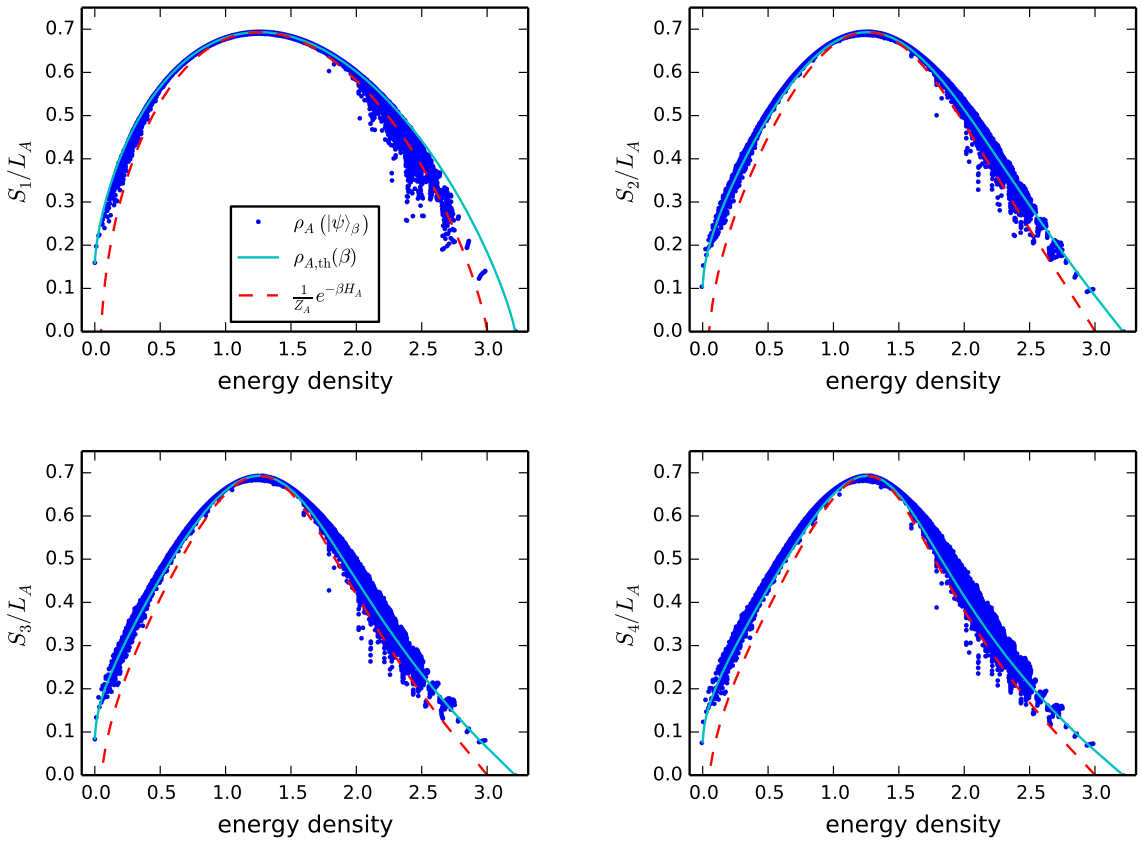

Figure 2.4: The von Neumann entropy S_1 and Rényi entropies S_2, S_3, and S_4 for the system given in Eq. 2.30 with $L = 21$ and $L_A = 4$. Here, $Z_A = \mathrm{Tr}_A(e^{-\beta H_A})$. The entropies of the reduced density matrix at each energy density agree remarkably with the the entropies calculated from the canonical ensemble, given by Eqs. 2a and 2b.

eigenstate for a subsystem size $L_A = 4$ in a $L = 21$ system, with their ETH predicted canonical counterparts, Eqs. 2.35 and 2.3. We use two different canonical counterparts corresponding to Eqs. 2a and 2b, the latter version being susceptible to boundary errors, which nevertheless are expected to vanish as $V_A, V_{\overline{A}} \to \infty$. The agreement for each entropy is remarkable. It is worth re-iterating that the Rényi entropies for an eigenstate $|\psi\rangle_\beta$ encode the free energy densities at temperatures different than β^{-1} (Eq. 2.3), and these results provide an instance of non-local Class II operators satisfying ETH. Also

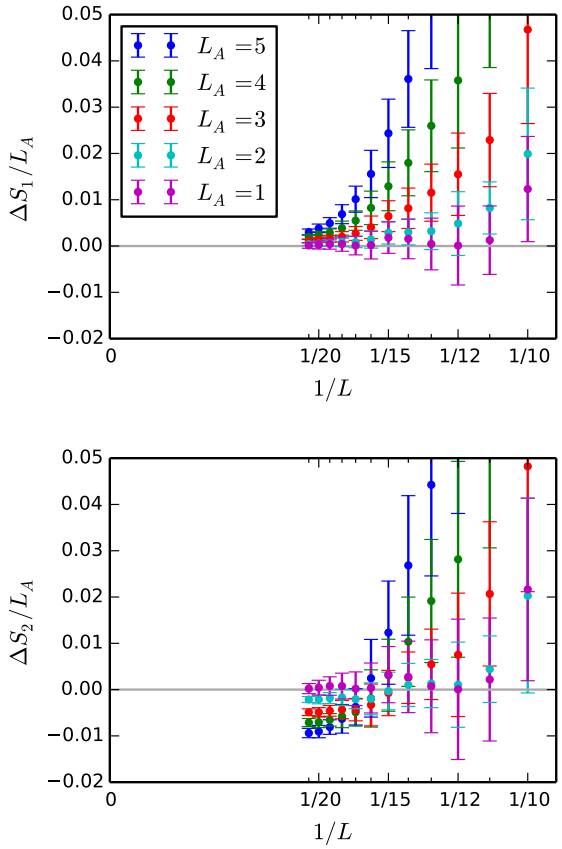

Figure 2.5: Scaling of the entropy deviation $\Delta S_\alpha \equiv S_\alpha(\rho_{A,\mathrm{th}}(\beta)) - S_\alpha(\rho_A(|\psi\rangle_\beta))$ with $1/L$ for constant L_A averaged over all eigenstates in the range $0.28 < \beta < 0.32$, for S_1 (top panel) and S_2 (bottom panel). The error bars represent one standard deviation away from the mean. For S_1 this deviation is strictly non-negative, but for higher Rényi entropies it can oscillate and become negative before tending to zero as $L \to \infty$.

note that as α becomes larger, finite size effects become more pronounced because S_α probes the system at lower temperatures $(\alpha\beta)^{-1}$.

We also studied finite-size scaling of the von Neumann entropy and Rényi entropies by keeping L_A constant and varying the total system size. The top panel of Figure 2.5 shows the deviation $\frac{\Delta S_1}{L_A} = \frac{S_1(|\psi\rangle_\beta)}{L_A} - s_{\mathrm{th}}(\beta)$ for eigenstates in a range of temperatures. The difference $\Delta S_1/L_A$ seemingly goes to zero faster than any inverse power of L, and

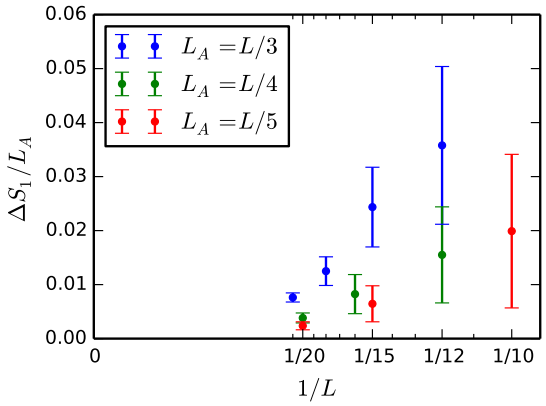

Figure 2.6: Scaling of the von Neumann entropy deviation ΔS_1 with $1/L$ for constant ratio L_A/L averaged over all eigenstates in the range $0.28 < \beta < 0.32$. As in Figure 2.5, the error bars represent one standard deviation away from the mean. Even though this plot considers the case where the subsystem size L_A becomes infinite as $L \to \infty$, the entropy deviations are going to zero rapidly as L becomes larger.

is consistent with an exponential dependence $\Delta S_1/L_A \sim e^{-L}$, or at the very least, a power-law decay $\Delta S_1/L_A \sim 1/L^x$ with $x \gg 1$ (although we should caution that inferring the precise asymptotic finite size scaling behavior using exact diagonalization studies is an inherently difficult task). The bottom panel shows a similar plot for the deviation of Rényi entropy S_2 from its ETH predicted value, Eq. 2.3. The finite size scaling of ΔS_2 is relatively difficult because unlike S_1, S_2 shows oscillations as a function of L_A (see e.g. [135, 156]). Despite this, ΔS_2 is less than a few percent of S_2 itself.

Figure 2.6 plots the entropy deviation $\Delta S_1/L_A$ for constant ratio L_A/L at all available system sizes. Although it is difficult to do a detailed scaling analysis with so few points, the data strongly suggests that $\Delta S_1/L_A$ vanishes in the thermodynamic limit.

The finite size scaling of Rényi entropies at constant ratio L_A/L is less conclusive, as can be seen in Figure 2.7. The analytical argument for the particle number conserving

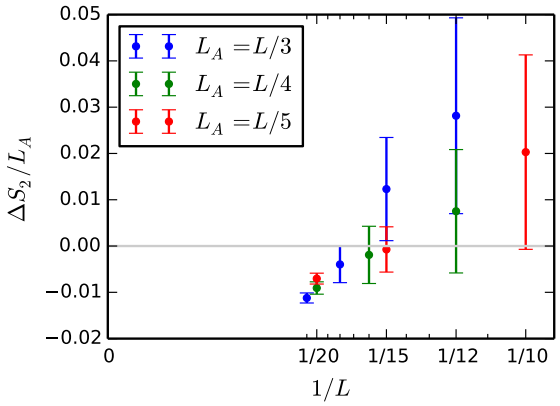

Figure 2.7: Scaling of the Rényi entropy deviation ΔS_2 with $1/L$ for constant ratio L_A/L averaged over all eigenstates in the range $0.28 < \beta < 0.32$. As in Figure 2.5, the error bars represent one standard deviation away from the mean.

model suggests that the Rényi entropies S_α for $\alpha \neq 1$ do not match their canonical counterparts when V_A/V is held fixed. Ref. [157] arrived at similar conclusions using a different approach.

2.6 Extracting the Hamiltonian from a single eigenstate

In this section we will present numerical results that substantiate our conjecture that ETH is valid for all Class I and Class II operators when $V_A \ll V$ as $V \to \infty$. Our numerical results consider the case where V_A is held constant as $V \to \infty$. We expect that all results in this section also hold true when the limits are taken such that $f \equiv V_A/V \to 0$ as $V_A, V \to \infty$. In Section 2.7 we will explore more carefully the case when $f < \frac{1}{2}$ is finite.

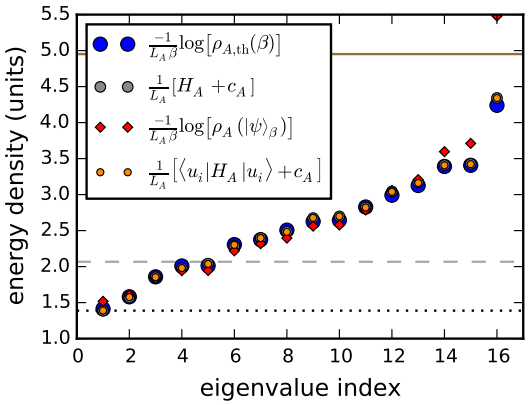

Figure 2.8: Comparison of the four quantities defined in the inset for an $L_A = 4$ subsystem at $L = 21$ and $\beta = 0.3$. Each quantity has been normalized so that the y-axis has units of energy density. The blue markers show the spectrum of the canonical (i.e. thermal) reduced density matrix while the red diamond markers correspond to the eigenvalues of a reduced density matrix $\rho_A(|\psi\rangle_\beta)$ for a *single* eigenstate at temperature β; the grey markers show the eigenvalues of H_A with a shift $c_A \equiv \frac{1}{\beta}\ln Z_A = \frac{1}{\beta}\ln \mathrm{Tr}_A(e^{-\beta H_A})$ so that it can be directly compared with $-\frac{1}{\beta}\ln[\rho_A(|\psi\rangle_\beta)]$ in accordance with Eq. 2b (note also that the combination $H_A + c_A$ is independent of the shift of the spectrum of H_A by an arbitrary uniform constant). Finally, the orange markers represent the expectation value of H_A, again with a shift c_A, with respect to the Schmidt eigenvector $|u_i\rangle$ of $\rho_A(|\psi\rangle_\beta)$. In each case, the eigenvalues/eigenvectors are ordered from smallest to largest energy density. The horizontal lines plot the energy density e (dashed, grey) and the critical energy density $e^* = \frac{eL}{L_A}$ (solid, brown) of the original eigenstate $|\psi\rangle_\beta$, with respect to the ground state energy density of $H_A + c_A$ (dotted, black).

We begin by probing in detail the entanglement spectra of individual eigenstates as well as the corresponding Schmidt states. Specifically, we compare four different quantities, as shown in Figure 2.8, which test the validity of Eqs. 2a and 2b. The agreement of the spectrum of $\frac{-1}{\beta}\ln[\rho_A(|\psi\rangle_\beta)]$ with that of $\frac{-1}{\beta}\ln[\rho_{A,\mathrm{th}}(\beta)]$ as well as with the actual Hamiltonian H_A in region A implies that essentially, the Schmidt eigenvalues λ_i satisfy $\lambda_i \propto e^{-\beta E_{A,i}}$ where $E_{A,i}$ are the eigenvalues of H_A. Similarly, the agreement with the expectation value $\langle u_i|H_A|u_i\rangle$ shows that the Schmidt eigenvectors $|u_i\rangle$ have the same character as the eigenvectors of the thermal density matrix.

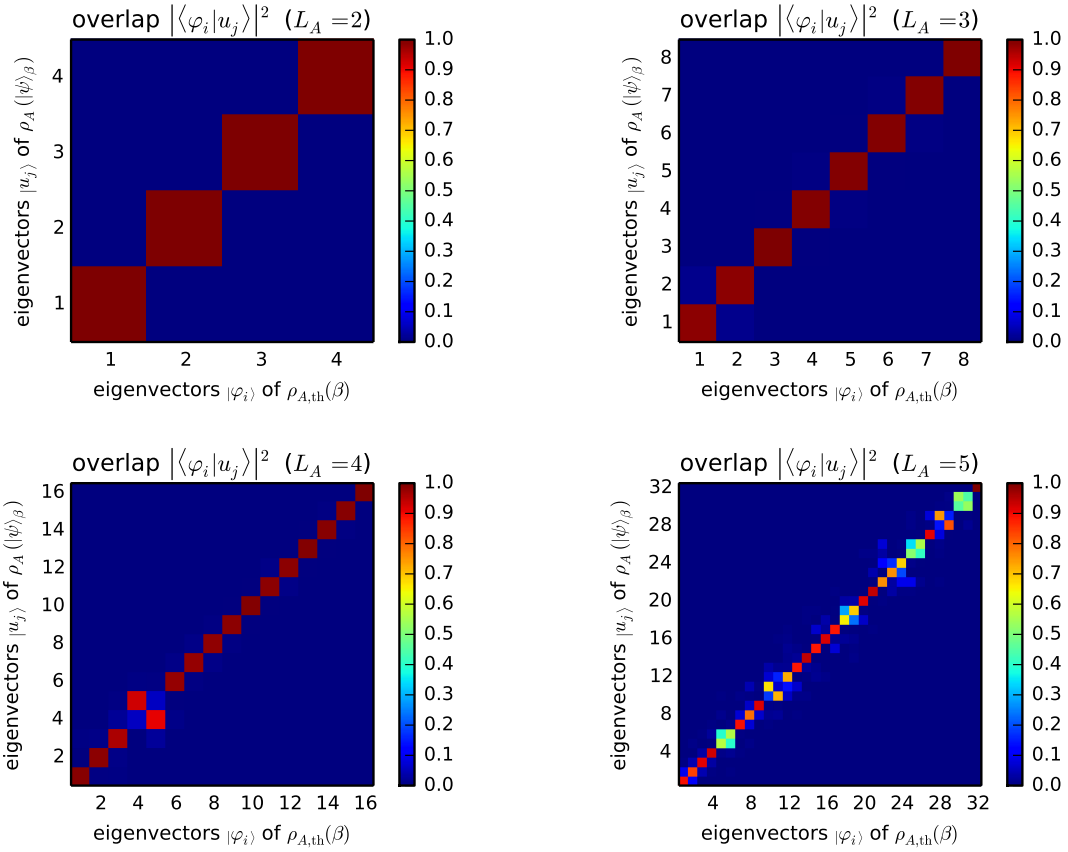

Figure 2.9: Overlap between the Schmidt eigenvectors $|u_j\rangle$ and the eigenvectors $|\varphi_i\rangle$ of the canonical density matrix, for an $L = 21$ system with $\beta = 0.3$, and subsystem sizes $L_A = 2, 3, 4, 5$. In each case, the eigenvectors are ordered from most significant (largest eigenvalue) to least significant (smallest eigenvalue).

To probe the Schmidt eigenvectors further, we directly calculated the overlaps between the eigenvectors of the reduced density matrix $\rho_A(|\psi\rangle_\beta)$ and the eigenvectors of the thermal density matrix $\rho_{A,\text{th}}(\beta)$ (see Figure 2.9). Again, we find excellent agreement.

To quantify the extent to which Eq. 2a is valid, we calculate the trace norm distance $||\rho_A(|\psi\rangle_\beta) - \rho_{A,\text{th}}(\beta)||_1$ between the reduced and canonical density matrices at various system sizes. The trace norm distance, defined as

$$||\rho_A(|\psi\rangle_\beta) - \rho_{A,\text{th}}(\beta)||_1 \equiv \frac{1}{2}\,\text{Tr}\left[\sqrt{(\rho_A(|\psi\rangle_\beta) - \rho_{A,\text{th}}(\beta))^2}\right] \tag{2.36}$$

places an upper bound on the probability difference that could result from any quantum measurement on the two density matrices [158]. As such, it provides an excellent measure of how distinguishable the two density matrices are. If the trace norm distance between two finite sized density matrices is zero, they are equal to each other element by element.

If ETH holds for all operators in subsystem A, then the results of Ref. [75] imply that the trace norm distance should go to zero as $1/L$. The suggestion that the trace norm distance between the pure state and thermal reduced density matrices with fixed subsystem size would tend to zero was also made in Ref. [159]. We restrict ourselves to states in a β range given by $0.28 < \beta < 0.32$. In the left panel of Figure 2.10, we plot the trace norm distance of every eigenstate in this β range at $L_A = 5$ for a few select system sizes. For each system size, the distribution of the trace norm distance is nearly constant throughout the given β range. The right panel then takes this data for each pair of L and L_A and plots the mean and standard deviation of the trace norm distance against

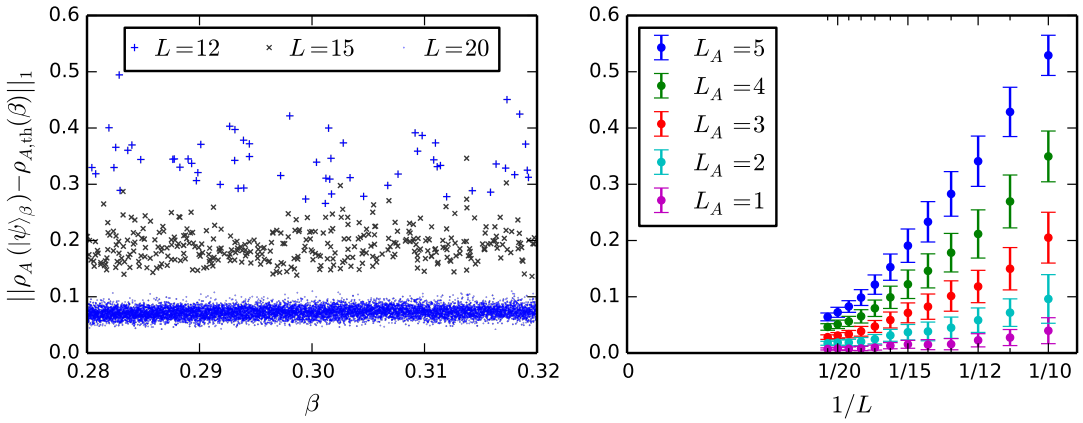

Figure 2.10: Trace norm distance between the canonical density matrix $\rho_{A,\mathrm{th}}(\beta)$ and the reduced density matrix $\rho_A(|\psi\rangle_\beta)$ for all eigenstates $|\psi\rangle_\beta$ in the range $0.28 < \beta < 0.32$. The left panel plots the trace norm distance for all such eigenstates with system sizes $L = 12$, 15, and 20, and subsystem size $L_A = 5$. The right panel plots the mean and standard deviation of the trace norm distance in this β range for values of L up to 21 and L_A up to 5.

$1/L$. The trace norm distance is tending toward zero at least linearly with $1/L$, perhaps even faster.

These results, taken together, strongly support the conjecture that ETH, as given by Eq. 2.1 holds for all operators when $V_A \ll V$. The Schmidt eigenvalues and eigenvectors match at all energy densities, not just the energy density of the eigenstate. Our results also imply that when $V_A \ll V$, ETH as specified by Eq. 2a holds. One consequence of this is that if V_A is held fixed, the density matrices $\rho_A(|\psi\rangle_\beta)$ and $\rho_{A,\mathrm{th}}(\beta)$ become elementwise equal in any basis as $V \to \infty$.

2.7 ETH with finite ratio V_A/V

In this section we will consider to what extent ETH is valid when the ratio $f \equiv V_A/V < \frac{1}{2}$ is held fixed and finite as $V_A, V \to \infty$. As demonstrated in Section 2.5.2, the von Neumann entropy of $\rho_A(|\psi\rangle_\beta)$ matches the thermal entropy in the thermodynamic limit even for finite $f < \frac{1}{2}$. In the current section we consider the extent to which other quantities match between a single eigenstate and the canonical ensemble.

There is one notable Class I operator for which ETH (in the sense of Eq. 2.1) fails when f is finite. As mentioned in Section 2.2.3 (see Eq. 2.7), the subsystem energy variance taken from a single eigenstate is suppressed by a factor of $(1-f)$ compared with its value in the canonical ensemble. To understand this, consider first the expectation value of the operator $H_A^2 - \langle H_A\rangle^2$ with respect to the thermal density matrix. This will be given by [140]:

$$\langle H_A^2 - \langle H_A\rangle^2\rangle_{\rho_{A,\mathrm{th}}(\beta)} = \frac{\int d(\delta E_A)\ (\delta E_A)^2\, e^{\frac{-\delta E_A^2}{cV_A}}}{\int d(\delta E_A)\ e^{\frac{-\delta E_A^2}{cV_A}}} \tag{2.37}$$

where c is the specific heat. Note that the probability distribution is Gaussian because it is obtained by expanding the Boltzmann factor around its maximum. On the other hand, in an *eigenstate*, the probability distribution will acquire an extra multiplicative factor of $e^{\frac{-\delta E_A^2}{cV_A}}$ because a fluctuation δE_A of energy in region A is necessarily accompanied by a fluctuation $-\delta E_A$ in the region $\overline{A}$ since for an eigenstate, there are no fluctuations of energy in the total system. Thus the expectation value of $H_A^2 - \langle H_A\rangle^2$ with respect to

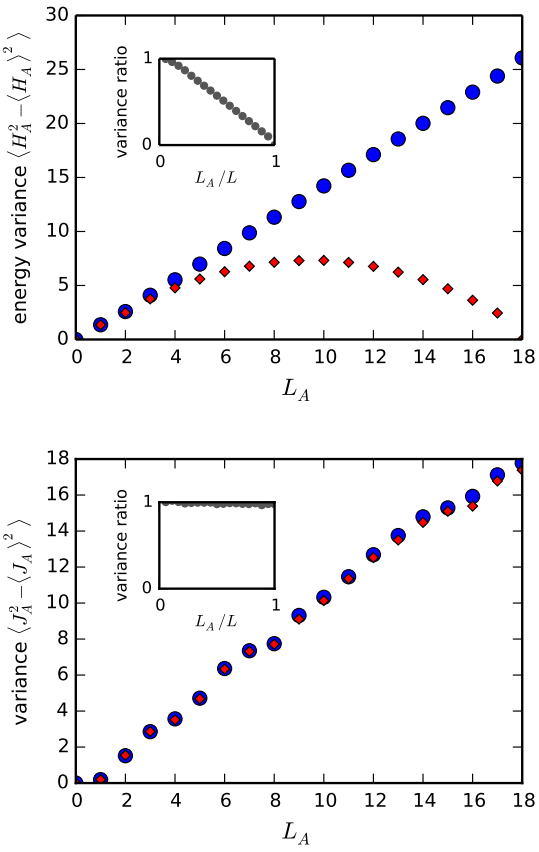

Figure 2.11: (Top panel) Subsystem energy variance with respect to subsystem size L_A for both the canonical ensemble (blue circular markers) and a single eigenstate $|\psi\rangle_\beta$ (red diamond markers), at $L = 18$ and $\beta = 0.3$. The inset shows the ratio between the energy variances at each subsystem size, which is expected to fit $1 - L_A/L$ in the thermodynamic limit (Eq. 2.7). (Bottom panel) The variance of an operator $J_A \equiv \sum_{i=1}^{L_A}(h_x^{(i)}\sigma_i^x + h_z^{(i)}\sigma_i^z) + \sum_{i=1}^{L_A-1} J_z^{(i)}\sigma_i^z\sigma_{i+1}^z$, which includes the same terms as H_A but does not relate to energy conservation, is plotted for comparison. Here, the quantities $h_x^{(i)}$, $h_x^{(i)}$, and $J_z^{(i)}$ are each taken from the uniform distribution $[-1, 1]$.

eigenstate $|\psi\rangle_\beta$ is given by:

$$\langle H_A^2 - \langle H_A\rangle^2\rangle_{\rho_A(|\psi\rangle_\beta)} = \frac{\int d(\delta E_A)\ (\delta E_A)^2\, e^{\frac{-\delta E_A^2}{cV_A}} e^{\frac{-\delta E_A^2}{cV_{\bar{A}}}}}{\int d(\delta E_A)\ e^{\frac{-\delta E_A^2}{cV_A}} e^{\frac{-\delta E_A^2}{cV_{\bar{A}}}}} \tag{2.38}$$

Eqs. 2.37 and 2.38 imply

$$\frac{\langle H_A^2 - \langle H_A\rangle^2\rangle_{\rho_A(|\psi\rangle_\beta)}}{\langle H_A^2 - \langle H_A\rangle^2\rangle_{\rho_{A,\mathrm{th}}(\beta)}} = 1 - V_A/V \tag{2.39}$$

To demonstrate this relationship, the top panel of Figure 2.11 shows scaling of the subsystem energy variance with subsystem size L_A for both a single eigenstate and the canonical ensemble. While the energy variance grows linearly for $L_A \ll L$ in both cases, the single eigenstate energy variance has an additional term that is negative and quadratic in the subsystem size, and which precisely matches the result in Eq. 2.39.

The bottom panel of Figure 2.11 shows, for comparison, the variance of a different operator J_A between a single eigenstate and the canonical ensemble. The operator J_A (defined in the figure's caption) is chosen to span the length of subsystem A and to include the same terms as H_A; however, the coefficient of each term is different. The fact that the variance of J_A matches between a single eigenstate and the thermal ensemble strongly suggests that all Class I operators that do not explicitly involve energy conservation will satisfy ETH in the sense of Eq. 2.1, even when V_A/V is finite.

Let us now consider an implication of the difference in subsystem energy variance between $\rho_A(|\psi\rangle_\beta)$ and $\rho_{A,\mathrm{th}}(\beta)$. This difference, which occurs only when f is finite,

suggests that the trace norm distance between the two density matrices vanishes only when $f \to 0$. To explore this more carefully, note that the trace norm distance places a bound on the difference in expectation value of *any* operator Λ that is bounded between zero and one as

$$|\mathrm{Tr}(\rho\Lambda) - \mathrm{Tr}(\sigma\Lambda)| \leq ||\rho - \sigma||_1. \tag{2.40}$$

In order to calculate a lower bound on trace norm distance due to the variance difference, we must write the energy variance as a bounded operator that maximally differs between the two density matrices. Naively one might be tempted to consider the operator $\mathcal{O}_{A,\beta}/\Delta^2 \equiv (H_A - \langle H_A \rangle_\beta)^2/\Delta^2$, where for the operator to be bounded, Δ must be chosen to be the largest energy available to the system. Since both $\mathcal{O}_{A,\beta}$ and Δ scale linearly with V, the expectation value of this operator is actually zero in the thermodynamic limit for both $\rho_A(|\psi\rangle_\beta)$ and $\rho_{A,\mathrm{th}}(\beta)$. Thus, no bound can be placed on the trace norm distance due to this particular operator.

Let us instead now consider a modified energy variance operator,

$$\Lambda_{A,\beta,\Delta} \equiv P_{A,\beta,\Delta} \frac{\mathcal{O}_{A,\beta}}{\Delta^2} P_{A,\beta,\Delta}, \tag{2.41}$$

where Δ is an arbitrary energy scale and $P_{A,\beta,\Delta}$ projects onto the subspace where $\mathcal{O}_{A,\beta}/\Delta^2$ has eigenvalues in the range $[0, 1]$, thus making $\Lambda_{A,\beta,\Delta}$ a bounded operator. This operator considers the energy variance within a restricted window of width 2Δ about the mean energy.

To arrive at an approximate bound due to this operator, let us assume that the energy histograms of $\rho_{A,\mathrm{th}}(\beta)$ and $\rho_A(|\psi\rangle_\beta)$ are given by normal distributions with variance σ^2_{th} and $\sigma^2_\psi = (1-f)\sigma^2_{\mathrm{th}}$, respectively. Since both distributions have the same mean, the difference in expectation values is expected to be

$$\begin{aligned} D &\equiv \mathrm{Tr}[\rho_{A,\mathrm{th}}(\beta)\Lambda_{A,\beta,\Delta}] - \mathrm{Tr}[\rho_A(|\psi\rangle_\beta)\Lambda_{A,\beta,\Delta}] \\ &= \frac{1}{\Delta^2}\int_{-\Delta}^{\Delta}\left[\frac{e^{-E^2/2\sigma^2_{\mathrm{th}}}}{\sigma_{\mathrm{th}}\sqrt{2\pi}} - \frac{e^{-E^2/2\sigma^2_\psi}}{\sigma_\psi\sqrt{2\pi}}\right]E^2\,dE. \end{aligned} \tag{2.42}$$

Given σ_{th} and f, it is possible to find Δ numerically such that D is maximized. Although Δ is proportional to $\sqrt{V}$, the value of D itself is independent of V as $V \to \infty$, since σ_{th} also scales with $\sqrt{V}$. The maximum quantity D then provides a lower bound on the trace norm distance between $\rho_{A,\mathrm{th}}(\beta)$ and $\rho_A(|\psi\rangle_\beta)$ in the thermodynamic limit [2].

Let us now turn to our results on the scaling of trace norm distance with system size when the ratio $f = L_A/L$ is held fixed as $L, L_A \to \infty$, which are shown in Figure 2.12. Although there are few points available for each ratio, the trend is clearly for the trace norm distance to decrease as L increases. The horizontal, dotted lines denote the theoretical minimum each trace norm distance can taken, given by Eq. 2.42. Remarkably, for each subsystem ratio, the trace norm distance rapidly approaches this lower bound, suggesting that the bound may actually provide the result in the thermodynamic limit. This in turn implies that other operators which do not involve energy conservation are likely

[2] One could also consider bounds on the trace norm distance due to higher moments $\langle(H_A - \langle H_A\rangle)^n angle$, but the most stringent bound comes from $n = 2$.

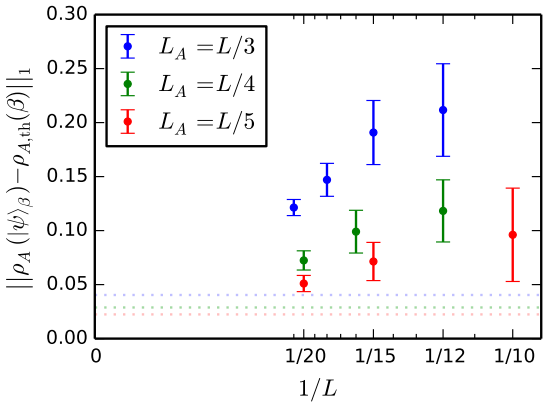

Figure 2.12: Trace norm distance between the canonical density matrix and reduced density matrix for constant ratio L_A/L and $0.28 < \beta < 0.32$. As in Figure 2.10, the error bars represent one standard deviation away from the mean. The horizontal lines indicate the approximate theoretical minimum each trace norm distance can take, based on the suppressed energy variance given by maximizing Eq. 2.42.

to have equal expectation values for a single eigenstate and for the canonical ensemble.

We now turn to results on the entanglement spectrum when f is a significant fraction of the total system size. As discussed in Section 2.2.3, if the constraint in Eq. 2.20 is violated, the entanglement spectrum cannot match above a critical energy density $e^* = e/f$ (see Eq. 2.19), where e is the energy density of the state $|\psi\rangle_\beta$. Figure 2.13 shows the comparison of spectra of four different quantities considered in Section 2.6 for several different energy densities of the reference state $|\psi\rangle_\beta$ with $f = 1/3$, at four different values of β. With $f = 1/3$, the energy constraint Eq. 2.20 is violated, and therefore we expect that the entanglement spectrum should deviate from the actual spectrum of the Hamiltonian at least beyond the critical energy density $e^* = e/f$. We find for each value of β that significant deviation starts to occur essentially right at this critical energy density.

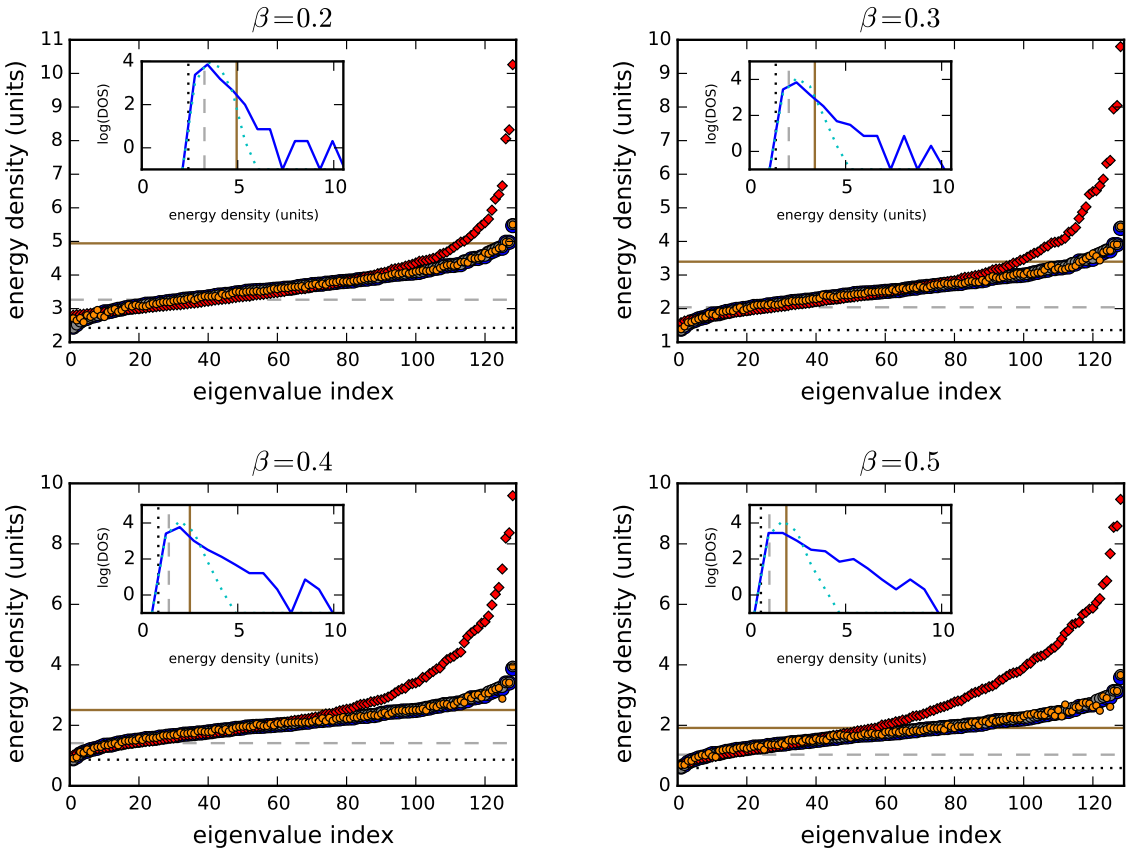

Figure 2.13: Comparison of the four quantities defined in the inset of Figure 2.8 for eigenstates of an $L = 21$ system with $L_A = 7$ at $\beta = 0.2$, 0.3, 0.4, and 0.5. Each inset plots a 12-bin histogram of the log of the density of states versus the energy density: the solid blue curve from a single eigenstate $\rho_A(|\psi\rangle_\beta)$ and the dotted cyan curve from the canonical ensemble $\rho_{A,\mathrm{th}}(\beta)$. We notice that in each of the four plots, the eigenvalues of the reduced density matrix corresponding to a single eigenstate (red diamond markers) begin to deviate significantly from the other markers (in particular, the eigenvalues of the thermal reduced density matrix i.e. the blue markers), as the energy density reaches the critical value e^* (denoted by the solid brown line), indicating breakdown of ETH beyond e^*.

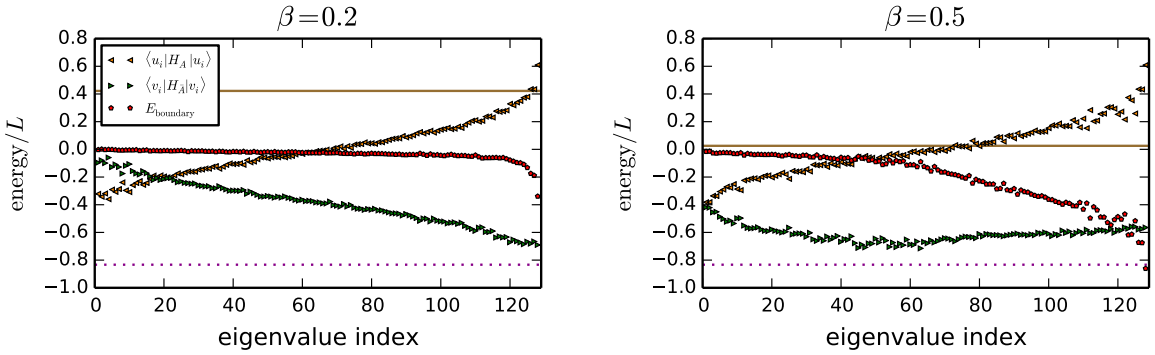

Figure 2.14: Decomposition of the energy density corresponding to an eigenstate amongst the three terms in Eq. 2.17 for $\beta = 0.2$ (left panel) and $\beta = 0.5$ (right panel) at $L = 21$ and $L_A = 7$. The dotted magenta line marks the ground state of $H_{\overline{A}}$. As in Figure 2.8, the solid brown line denotes the critical energy density e^* for subsystem A.

Surprisingly, even though the entanglement spectrum does not match the actual spectrum beyond the energy density e^*, the expectation values $\langle u_i|H_A|u_i\rangle/L_A$ continue to match the energy eigenvalues of the actual Hamiltonian! To understand this phenomenon better, we analyze the different terms in Eq. 2.17. As argued in Section 2.2.3, the only way $\langle u_i|H_A|u_i\rangle$ can exceed the total energy E of the eigenstate is, if the E_{boundary} term,

$$E_{\text{boundary}} \equiv \sum_j \sqrt{\frac{\lambda_j}{\lambda_{i0}}} \langle u_{i0}| \otimes \langle v_{i0}|H_{A\overline{A}}|u_j\rangle \otimes |v_j\rangle, \tag{2.43}$$

scales with the total system size. We find that this is indeed the case, as shown in Figure 2.14. In agreement with the general considerations in Section 2.2.3, the Schmidt eigenvalues deviate from their ETH predicted values beyond e^* (Figure 2.13) and become considerably smaller.

To summarize the results of this section, we provided evidence that ETH holds for all Class I operators not related to energy conservation. For Class II operators, there is

a critical energy density e^* beyond which ETH definitely fails, even though, surprisingly, the eigenvectors still seem to be correct. (We leave the understanding of this result for future studies.)

2.8 An application: equal-time correlators as a function of temperature from a single eigenstate

In the previous sections we provided evidence that a single eigenstate encodes the full Hamiltonian. As an application of this result, we now calculate correlation functions at arbitrary temperatures using a *single eigenstate* $|\psi\rangle_\beta$. The basic idea is similar to the relation between the Rényi entropies and the free energy densities (Eq. 2.3).

In particular, consider the correlation function,

$$\langle O(x)O(y)\rangle_{\beta,n} = \frac{\mathrm{Tr}_A\left(\rho_A^n(|\psi\rangle_\beta)O(x)O(y)\right)}{\mathrm{Tr}_A\left(\rho_A^n(|\psi\rangle_\beta)\right)} \tag{2.44}$$

where x, y are located in subsystem A, away from the boundary. Using Eqs. 2a, 2b to leading order in the subsystem size, $\langle O(x)O(y)\rangle_{\beta,n}$ equals the expectation value of the operator $O(x)O(y)$ at a temperature $(n\beta)^{-1}$.

Figure 2.15 shows the expectation values of local operators within subsystem A as a function of β, as predicted from a single eigenstate at inverse temperature β_0 (indicated by a yellow dot on the red curve). We choose operators that are as far away from the subsystem boundary as possible so as to minimize the finite size corrections. Even though

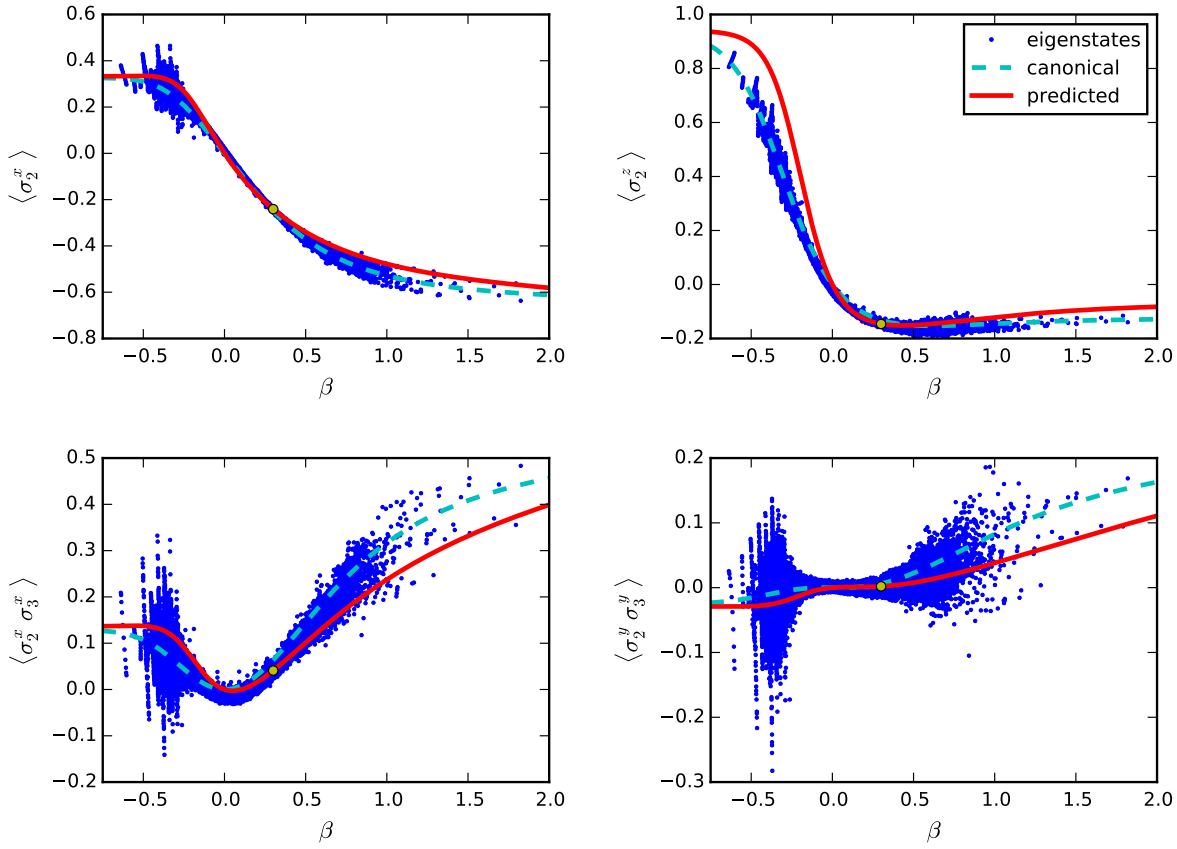

Figure 2.15: Equal time correlators for an $L = 21$ system plotted against inverse temperature β. The blue dots denote the expectation value with respect to each eigenstate, the dashed cyan curve plots the expectation value in the canonical ensemble, and the red curve plots the expectation value predicted from a single eigenstate at $\beta_0 = 0.3$ (yellow dot) by raising the $L_A = 4$ density matrix to the power β/β_0 and rescaling it to have unit trace.

the agreement with the canonical ensemble is not perfect, the qualitative trends and the numerical values match incredibly well, given the modest total system sizes to which we are restricted. These predicted correlators also undoubtedly suffer from corrections expected due to the conical singularity at the boundary of A in Eq. 2.44.

2.9 Summary and discussion

In this chapter, we analyzed the structure of reduced density matrices corresponding to the eigenstates of generic, non-integrable quantum systems. We argued that given an eigenstate $|\psi\rangle_\beta$ with energy density e and a corresponding temperature β^{-1}, the reduced density matrix for a subsystem A is given by

$$\rho_A(|\psi\rangle_\beta) = \rho_{A,\text{th}}(\beta)$$

where

$$\rho_{A,\text{th}}(\beta) = \frac{\text{Tr}_{\overline{A}}\left(e^{-\beta H}\right)}{\text{Tr}\left(e^{-\beta H}\right)}$$

if the condition $V_A \ll V$ is satisfied. This means that for a fixed eigenstate $|\psi\rangle_\beta$, one can always extract the properties of the corresponding Hamiltonian at arbitrary energy densities by taking $V_A/V \to 0$ as the limits $V_A, V \to \infty$ are taken. Remarkably, even when V_A/V ($< 1/2$) is taken to be fixed and finite, one can still access many properties of the underlying Hamiltonian for a range of energy densities in the interval described in

Eq. 2.19.

We also introduced the notion of "equithermal" (Class I) and "non-equithermal" (Class II) operators. In a canonical ensemble at temperature T, the expectation value of Class I operators depends only on the properties of the underlying Hamiltonian at temperature T, while the same is not true for Class II operators. Our results strongly suggest that all Class I operators not involving energy conservation satisfy Eq. 2.1 as long as $V_A < V/2$. For Class II operators not related to energy conservation, Eq. 2.1 is seemingly again satisfied as long as the constraint in Eq. 2.20 holds.

We also provided analytical results for the Rényi and von Neumann entropies of infinite temperature eigenstates of a particle number conserving model. These results substantiate our numerical results for the energy-only conserving model. In particular, we find that the von Neumann entanglement entropy for a subsystem of size V_A equals the thermal entropy for that subsystem as long as $V_A < V/2$, and therefore follows the so called 'Page curve' [42, 148–150] at all non-zero temperatures, thus generalizing the original work of Page and others [42, 148–150], and in agreement with the recent work on large central charge CFTs [143–145].

In this chapter we only considered contiguous subsystems. It seems reasonable to conjecture that Eq. 2a continues to hold as long as the support of operator O can be chosen to lie in a subsystem which is not necessarily contiguous and whose volume satisfies $V_A \ll V$. This encompasses the expectation values of local operators such as $\langle O(\vec{x})O(0)\rangle$, where $O(\vec{x})$ is localized at point $\vec{x}$ and $|\vec{x}|$ can be greater than $L/2$ (where L is the linear

dimension of the total system).

Let us mention some of the practical implications of our results. Firstly, the fact that a single eigenstate encodes properties of the full Hamiltonian could potentially be a useful numerical tool. For example, one could imagine targeting a finite energy density eigenstate of a Hamiltonian H by variationally minimizing the energy of the Hamiltonian $(H-E)^2$ with respect to trial wavefunctions. The techniques in this chapter would then allow one to access thermal properties of the Hamiltonian without directly calculating the partition function, which could be extremely helpful for Hamiltonians that suffer from the sign problem.

Secondly, owing to the recent progress in single atom imaging techniques in cold atomic systems [66], one can now access non-local operators experimentally [64, 65, 96, 160]. This potentially allows one to check some of our predictions pertaining to the violation of ETH in cold atomic systems. For example, one can perform a quantum quench on a low entanglement state which would at sufficiently long times lead to a thermal state in the same sense as Eq. 2a. This in principle allows one to determine the underlying Hamiltonian of a cold atomic system by performing tomography on a small subsystem to obtain the corresponding reduced density matrix, and then taking its logarithm.

We conclude by posing a few questions and future directions.

In this chapter we extracted equal-time correlators at different temperatures using a single eigenstate. It will be interesting to see if a similar method also works for unequal

time correlators at arbitrary temperatures. The main difference is that this requires calculating expressions such as Eq. 2.44 at an *imaginary* exponent, and estimating the effects due to the conical singularity in this case requires further study.

As mentioned above, we expect that all our discussion carries over to time-evolved states as well since such states are expected to also have thermal behavior at long times in the same sense as a single finite energy density eigenstate. If so, does the time scale for thermalization for a given operator (i.e. the time it takes for the expectation value of the operator to become equal to its canonical expectation value) depend on whether the operator is Class I (equithermal) or Class II (non-equithermal)?

Another question concerns the subleading corrections to the entanglement entropy. One expects that there always exist subleading area-law contributions to the entanglement entropy (either von Neumann or Rényi) of a single eigenstate. Are these contributions also captured correctly in the entanglement entropies calculated via a thermal reduced density matrix? Perhaps a more interesting question is whether the mutual information of two disjoint intervals (which cancels out both the volume law contribution and the area law contribution) takes the same value for a single eigenstate and its canonical counterpart.

The research in this chapter was performed in collaboration with Tarun Grover and is based on Ref. [78]. We are grateful to Leon Balents, John Cardy, Matthew Fisher, Tom Hartman, Patrick Hayden, Pavan Hosur, Max Metlitski, Olexei Motrunich, Chetan Nayak, Anatoli Polkovnikov, Marcos Rigol, Lea Santos, Brian Swingle, and especially

David Huse and Xiaoliang Qi for conversations about this work. This research was supported in part by the National Science Foundation, under Grant No. DMR-14-04230 (JRG), by the Caltech Institute of Quantum Information and Matter, an NSF Physics Frontiers Center with support of the Gordon and Betty Moore Foundation (JRG), and by the Gordon and Betty Moore Foundations' EPiQS Initiative through Grant GBMF4304 (TG). This research was also supported in part by the National Science Foundation under Grant No. NSF PHY11-25915. We also acknowledge support from the Center for Scientific Computing at the CNSI and MRL: an NSF MRSEC (DMR-1121053) and NSF CNS-0960316.

Chapter 3

Partial breakdown of quantum thermalization in a Hubbard-like model

3.1 Introduction

In recent years, physicists have made great strides toward better understanding the equilibration and thermalization of isolated, many-body quantum systems. Already, two distinct phases are well known: there exist systems that thermalize completely, such that for an arbitrary initial pure state any sufficiently small subregion will eventually approach the Gibbs ensemble; and, by contrast, there are systems that exhibit many-body localization (MBL) due to a strong disorder potential, failing to thermalize at any

time despite weak interactions.

In a system that does approach thermal equilibrium, energy, particles, and other conserved quantities propagate throughout such that the system acts as its own bath. After equilibration, any sufficiently small subregion will approximate the thermal density matrix (Gibbs ensemble), and all observables within any small subregion will match their values in the canonical ensemble. One of the most important steps toward understanding quantum thermalization occurred in the early 1990s, when Deutsch and Srednicki independently proposed that thermalization, when it occurs, happens at the level of each individual eigenstate of finite energy density [72, 73]. This result is generally known as the "eigenstate thermalization hypothesis" (ETH) [74–76, 161]. Within the framework of ETH, the ultimate fate of a system can be determined by examining the properties of its finite energy density eigenstates, without needing to consider the detailed quantum dynamics. In fact, a single eigenstate of such a system directly reproduces the thermal ensemble in an arbitrarily-large subregion A as long as the ratio of the subsystem to system size V_A/V approaches zero as $V \to \infty$, as was demonstrated in Chapter 2. Also, the von Neumann entanglement entropy S_A within the subsystem will match the thermal entropy, scaling as the volume of the subsystem, $S_A \sim L_A^d$ as long as $V_A < V/2$. This is in contrast with typical ground states, which scale as an "area law," $S_A \sim L_A^{d-1}$. In fact, the mechanism of thermalization can be thought of as the spreading of entanglement: each subsystem becomes maximally entangled with the remainder of the system over time, to the extent allowed by conservation laws (such as the conservation of energy).

One well-known counterexample to quantum thermalization is given by integrable systems, such as the one-dimensional Hubbard model (which is solvable via Bethe ansatz [162, 163]). Integrable systems typically have an infinite number of conserved quantities, which scales with total system size. While these conserved quantities can (in some cases) permit analytic solution, they also prohibit full thermalization. Instead of relaxing to a Gibbs ensemble, these systems relax to a "generalized Gibbs ensemble," which takes into account the additional conservation laws [83, 85]. It is perhaps surprising that integrable systems exhibit a "weak" form of ETH: nearly all states appear locally thermal, but there exist rare, non-thermal states which are responsible for the breakdown of thermalization [81]. While integrable systems are interesting examples of systems that do not fully thermalize, they are tuned to special (solvable) points in parameter space, and are therefore non-generic.

As mentioned above, there also exist *non-integrable*, interacting many-body quantum systems which do not thermalize and instead exhibit many-body localization (MBL) [89–93, 102, 122]. These systems have a strong disorder potential and sufficiently weak interactions, and are characterized by zero DC conductivity and partial memory of the initial state at all times. Remarkably, the strong disorder potential leads to an "emergent" integrability, with resulting local integrals of motion [100–102]. Due to these additional conservation laws, eigenstates in an energy window ΔE are very different from one another, and there are no avoided crossings between neighboring eigenstates when a parameter in the Hamiltonian is varied. This results in energy-level spacings obeying

Poisson statistics, in contrast to Wigner-Dyson statistics in a thermal system [91]. Additionally, the finite energy density eigenstates of these systems typically exhibit area law scaling of entanglement entropy ($S_A \sim L_A^{d-1}$), similar to a quantum ground state but in contrast to thermal systems (which instead exhibit volume law scaling) [93]. Recently, MBL has been demonstrated in experiments on cold atomic gases [95–97], thus putting a vast amount of theoretical and numerical work on an experimental footing. Conceptually, the existence of many-body localization provides an example of a system with a complete breakdown of thermalization, thus calling into question the general validity of quantum statistical mechanics.

It is tempting to wonder whether a phase of matter could exist between the extremes of full thermalization and MBL in a generic (i.e. non-integrable), isolated, many-body quantum system. Many-body localization can be viewed as a situation in which infinitely massive (i.e. stationary) particles cause a classical disorder potential. Given this line of thinking, one might be tempted to ask: what if the particles are quantum mechanical, allowed to move with a very large (but finite) mass? Could a phase similar to MBL exist in such a translationally invariant, fully quantum mechanical system? Guided by this question, Ref. [105] proposed a new phase of matter in multi-component liquids with two species of indistinguishable particles with a large mass ratio. This phase, the "quantum disentangled liquid" (QDL), is characterized by heavy particles which are fully thermalized, but light particles which have not thermalized independently of the heavy particles. Other work has also considered the possibility that thermalization can break

down in translationally invariant systems [123–132, 164–166].

In addition to proposing the QDL phase, Ref. [105] provided a qualitative diagnostic to identify eigenstates in the phase. This diagnostic can be phrased in terms of entanglement entropy after a partial measurement. As mentioned above, systems that fully thermalize exhibit volume law scaling for their entanglement entropy, while many-body localized systems exhibit an area law. The QDL phase, like the fully ergodic phase, is characterized by eigenstates that are in an overall volume law for the entanglement entropy. However, after a partial measurement of the locations of the heavy particles, the resulting wavefunction of the light particles is instead characterized by an area law in the QDL phase. This suggests that the light particles are "localized" by the heavy particles, and is in contrast to a fully ergodic system, where the entanglement entropy of the light particles would scale as a volume law even after the measurement of the heavy particles' positions. The phase is called a "quantum disentangled liquid" because a partial measurement results in a "disentangled" wavefunction, a smoking gun for the breakdown of full thermalization.

The diagnostic given in Ref. [105] is very general and can be applied to any multi-component system. In this chapter, we will focus on 1D itinerant electron models with two species of fermions (spin-up and spin-down) on a lattice, specifically the Hubbard model with an additional nearest-neighbor repulsion term, which breaks integrability. Instead of considering light and heavy particles, we will consider to what degree the spin and charge degrees of freedom thermalize independently from one another.

The chapter is organized as follows. In Section 3.2, we introduce the QDL diagnostic for a lattice system with spin-half particles. In Section 3.3, we introduce the Hubbard model with an additional nearest-neighbor repulsion term, which forms the basis for the remainder of the chapter. Section 3.4 describes in detail our method for performing numerical exact diagonalization on this model. In Section 3.5, we study each eigenstate's average doublon occupation, an observable which appears to violate ETH in the large-U limit of the non-integrable model. In Section 3.6, we study the entanglement entropy properties of eigenstates, both before and after a partial measurement on each site. In Section 3.7, we discuss implications for cold atom experiment and for the foundations of quantum statistical mechanics.

3.2 Entanglement entropy diagnostic

In this section we review and expound the diagnostic introduced in Ref. [105] for identifying quantum disentangled eigenstates, which is applicable to multi-component quantum systems on a lattice or in the continuum. While Ref. [105] focused on systems with mass-imbalanced particles, here we will instead consider lattice systems with two species of fermions (spin-up and spin-down), with both spin and charge degrees of freedom. The single-site Hilbert space consists of empty, spin-up, spin-down, and doubly-occupied states, which are denoted by $|-\rangle$, $|\uparrow\rangle$, $|\downarrow\rangle$, and $|\uparrow\downarrow\rangle$ respectively.

Let us first review the standard formulation of entanglement entropy. Given a pure state $|\psi\rangle$ and a spatial subregion A of size L_A^d (where d is the number of dimensions),

the reduced density matrix in region A is given by $\rho_A(|\psi\rangle) = \mathrm{Tr}_{\overline{A}} |\psi\rangle \langle\psi|$, where $\overline{A}$ is the spatial complement of region A. The von Neumann entanglement entropy in subregion A is then given by $S_A(|\psi\rangle) = -\mathrm{Tr}_A [\rho_A(|\psi\rangle) \ln \rho_A(|\psi\rangle)]$. In a thermal system this quantity scales extensively with the subsystem size ($S(|\psi\rangle) \sim L_A^d$), but in a many-body localized system it scales as the size of its boundary, $S(|\psi\rangle) \sim L_A^{d-1}$. These two possibilities are commonly known as "volume law" and "area law," respectively. The scaling of the overall entanglement entropy thus provides insight into whether a system is localized or not [93].

The goal of the QDL diagnostic is to identify volume law states in which spin and charge have not thermalized independently of each other, despite the degrees of freedom having entangled with one another. Guided by this intuition, the diagnostic considers the entanglement entropy after a *partial measurement*, e.g. of the spin on each site. If performing the partial measurement transforms a state from a volume law to an area law state, then the remaining degrees of freedom in the wavefunction have not thermalized independently of the measured degrees of freedom. The remainder of this section explains this diagnostic in detail.

Consider a finite energy density eigenstate $|\psi\rangle$ of a system with overall volume law scaling of the entanglement entropy ($S_A \sim L_A^d$). Given $|\psi\rangle$, we can perform a partial projective (von Neumann) measurement to determine the spin on each site along the z-axis, which results in a collapsed wavefunction

$$|\phi_{\{\sigma\}}\rangle = \frac{P_{\{\sigma\}} |\psi\rangle}{\sqrt{\langle\psi| P_{\{\sigma\}} |\psi\rangle}} \tag{3.1}$$

corresponding to some overall spin configuration $\{\sigma\}$. Here, $P_{\{\sigma\}}$ is the projector onto the subspace consistent with the measurement outcome $\{\sigma\}$, and the probability of outcome $\{\sigma\}$ is given by the Born rule: $\text{Prob}(\{\sigma\}) = \langle\psi| P_{\{\sigma\}} |\psi\rangle$. Note that in our notation $|\phi_{\{\sigma\}}\rangle$ has been rescaled to have unit norm.

The state $|\phi_{\{\sigma\}}\rangle$ after the spin measurement is a wavefunction in which only charge degrees of freedom remain. If a site has spin $+\frac{1}{2}$ or $-\frac{1}{2}$ along the z-axis, the charge on that site is one; however, if a site has overall spin zero, then it is possible that the site has either charge 0 or charge 2. The wavefunction $|\phi_{\{\sigma\}}\rangle$ is thus a partially-collapsed state in which sites with spin zero can be in a superposition of two different charge states. As a concrete example, let us consider a wavefunction $|\psi\rangle$ on a system with length $L = 4$ and $N_\uparrow = N_\downarrow = 2$. Say, for instance, that a partial measurement of the spins along the z-axis gives $[0, -\frac{1}{2}, 0, +\frac{1}{2}]$. Then the charge on sites 2 and 4 is known, but sites 1 and 3 can be in a superposition of charge 0 and 2. The resulting wavefunction is thus $|\phi_{\{\sigma\}}\rangle = \alpha\left(|-\rangle \otimes |\downarrow\rangle \otimes |\uparrow\downarrow\rangle \otimes |\uparrow\rangle\right) + \beta\left(|\uparrow\downarrow\rangle \otimes |\downarrow\rangle \otimes |-\rangle \otimes |\uparrow\rangle\right)$, where the values α and β can be calculated given full knowledge of the original state $|\psi\rangle$.

In order to quantify the remaining amount of entanglement in the partially-collapsed state $|\phi_{\{\sigma\}}\rangle$, we consider the scaling of its entanglement entropy. Given a subsystem A of size L_A^d and a measurement outcome $\{\sigma\}$, the reduced density matrix in region A is given by $\rho_A(|\phi_{\{\sigma\}}\rangle) = \text{Tr}_{\overline{A}} |\phi_{\{\sigma\}}\rangle \langle\phi_{\{\sigma\}}|$ and the entanglement entropy is $S_A(|\phi_{\{\sigma\}}\rangle) = -\text{Tr}_A\left[\rho_A(|\phi_{\{\sigma\}}\rangle) \ln \rho_A(|\phi_{\{\sigma\}}\rangle)\right]$. By averaging over all possible measurement outcomes with their associated Born-rule probabilities, we can calculate the average post-measurement

entanglement entropy,

$$S_A^{c/s} \equiv \sum_{\{\sigma\}} \text{Prob}(\{\sigma\})\, S_A(|\phi_{\{\sigma\}}\rangle), \tag{3.2}$$

where c/s denotes the entropy of the resulting charge wavefunction after a measurement of the spin on each site. It is instructive to consider the scaling of this entanglement entropy taken after the partial measurement. In a fully ergodic system, it should scale as a volume law for any partial measurement which does not fully collapse the wavefunction. If the post-measurement entanglement entropy instead scales as an area law, then the charge has not thermalized independently of the spin, and the system is non-ergodic.

It is also possible to consider a diagnostic which reverses the roles of spin and charge (i.e. a partial measurement of the charge, with a resulting spin wavefunction). We will denote this quantity as $S_A^{s/c}$. If an eigenstate $|\psi\rangle$ is in an area law after the partial measurement of either the spin or the charge on each site, then we refer to $|\psi\rangle$ as a "quantum disentangled eigenstate."

Let us now summarize the procedure for performing the diagnostic. Given a subregion A and a finite energy density eigenstate $|\psi\rangle$ (which we assume exhibits an overall volume law for the entanglement entropy), the QDL diagnostic is as follows. (i) Perform a partial measurement of the system, by measuring the spin on each site, which gives some spin configuration $\{\sigma\}$. (ii) Consider the post-measurement wavefunction, $|\phi_{\{\sigma\}}\rangle$. (iii) Calculate the post-measurement entanglement entropy, $S_A(|\phi_{\{\sigma\}}\rangle)$. (iv) Average this quantity over all possible measurement outcomes, weighted by their Born rule probabilities, to obtain $S_A^{c/s}$. (v) Consider the scaling of $S_A^{c/s}$ with subsystem size L_A^d to identify

whether it scales with the boundary size or the volume of region A. If it scales with the boundary, then $|\psi\rangle$ is a quantum disentangled eigenstate.

The partial measurements considered can be implemented in experiments on cold atomic gases, and it has recently become possible to measure the Rényi entanglement entropy (a close cousin of the von Neumann entropy) in cold atomic systems [63–65]. We will further discuss these connections in Section 3.7.

Having introduced the entanglement entropy diagnostic for quantum disentangled eigenstates, we now turn to the model on which we will focus for the remainder of the chapter.

3.3 Model

We consider the 1D Hubbard chain with an additional nearest-neighbor repulsion term:

$$H = H_{\text{Hubbard}} + H_V \tag{3.3}$$

$$H_{\text{Hubbard}} = -t \sum_{\langle ij \rangle \, \sigma} \left(c^\dagger_{i\sigma} c_{j\sigma} + \text{H.c.} \right) + U \sum_i n_{i\uparrow} n_{i\downarrow}$$

$$H_V = V \sum_{\langle ij \rangle} n_i n_j$$

where $n_{i\sigma} = c^\dagger_{i\sigma} c_{i\sigma}$, $n_i = n_{i\uparrow} + n_{i\downarrow}$, and $\sum_{\langle ij \rangle}$ denotes a sum over nearest neighbors. The spin label σ takes the values $\{\uparrow, \downarrow\}$. The 1D Hubbard chain is solvable exactly by Bethe ansatz and is therefore not expected to exhibit eigenstate thermalization due

to its integrability. Hence we add the nearest-neighbor repulsion term, which breaks integrability when $V \neq 0$. We will consider periodic boundary conditions throughout. We choose an overall energy scale by setting $t = 1$.

The model in Eq. 3.3 has a number of symmetries. It conserves total particle number $N \equiv N_\uparrow + N_\downarrow$, where $N_\sigma \equiv \sum_i n_\sigma$. Momentum is conserved due to translation invariance. The system also conserves total $S^z \equiv \sum_i S_i^z$ and total spin $\sum_{ij} \mathbf{S}_i \cdot \mathbf{S}_j$.

If the lattice is bipartite (in 1D, if the number of sites L is even), there is an additional symmetry in the Hubbard model, which can be seen by considering a particle-hole transformation on the down spin species: $c_{j\downarrow} \to (-)^j c_{j\downarrow}^\dagger$. This transformation leaves the kinetic term invariant but maps the U term to $-U$ in H_{Hubbard}. It also implements the transformation $n_j \to \sigma_j^z + 1$ and $\sigma_j^z \to n_j - 1$, thus mapping the spin sector to charge sector and vice-versa. Because of this duality, it is apparent that the Hubbard model has a "hidden" charge SU(2) symmetry in addition to its spin SU(2) symmetry, resulting in an enlarged symmetry group, SO(4) [167, 168]. This transformation also maps the nearest-neighbor repulsion term H_V to a nearest-neighbor spin term, $4V \sum_{\langle ij \rangle} S_i^z S_j^z$. As a result, the V term breaks the charge SU(2) symmetry.

In this chapter we will focus on the above Hamiltonian with positive U, and consider the entanglement entropy after a partial measurement of the spin. Because of the above duality transformation, this is equivalent to considering a negative-U Hubbard model with a nearest-neighbor $S_i^z S_j^z$ exchange term, and the entanglement entropy after a partial measurement of the charge degrees of freedom. Although we will focus on the positive-U

model, we will not hesitate to discuss the equivalent physics in negative-U model when doing so can guide intuition.

3.4 Numerical details

To investigate the properties of eigenstates of the Hamiltonian (Eq. 3.3), we perform numerical exact diagonalization calculations. When performing exact diagonalization, it is advantageous to represent the Hamiltonian in block-diagonal form, taking advantage of as many symmetries as possible. This allows one to perform the numerical diagonalization separately in each symmetry sector, each of which has a reduced basis size. The model conserves both spin-up and spin-down particle number separately. We focus on half filling ($N_\uparrow = N_\downarrow = L/2$), in which case the model also has spin-flip and particle-hole symmetries. Due to periodic boundary conditions, the model also conserves momentum, allowing the physics to be considered in each momentum sector independently. We exploit each of these abelian symmetries.

The non-abelian $SU(2)$ spin symmetry of the model leads to additional conserved quantities. Because it is it much more difficult to take advantage of non-abelian symmetries in exact diagonalization, we explicitly break the degeneracy due to the $SU(2)$ spin symmetry by adding a total spin term $\sum_{ij} \mathbf{S}_i \cdot \mathbf{S}_j$ to the Hamiltonian with large, irrational coefficient. This does not change the physics in any given sector, but does allow us to obtain eigenstates of the Hamiltonian that are also eigenstates of the $SU(2)$ total spin operator. As discussed in Section 3.3, the pure Hubbard model ($V = 0$) on a bipartite

lattice has a second $SU(2)$ "pseudo-spin" symmetry, which is due to the symmetry between the charge and spin sectors. For this reason, we also add a total pseudo-spin term to the model when $V = 0$ to break the degeneracies arising from this symmetry.

At system sizes where computational resources permit, we perform a full diagonalization of the system in each momentum sector independently. For larger system sizes, we use ARPACK [106] to obtain several hundred eigenvalue/eigenvector pairs that are lowest in energy. In each case, we study the system at half filling and focus on total spin singlets.

3.5 Doublon expectation value results

In this section we examine the expectation value of the doublon density $\langle n_{i\uparrow} n_{i\downarrow} \rangle$ for each eigenstate in the many-body spectrum. (Because the system is translationally invariant, this quantity is independent of site i.)

3.5.1 Large U

Let us begin by considering each eigenstate of the large-U Hubbard model ($V = 0$), as shown in Figure 3.1a. As mentioned in Section 3.3, the highest excited state of this model is the ground state of the model with $U \to -U$, due to the duality resulting from the particle-hole transformation on the down spin species. This symmetry is apparent in the plot, as it is symmetric under a combined horizontal and vertical reflection. (Note that under this duality, total spin singlets are mapped to states with total pseudo-spin

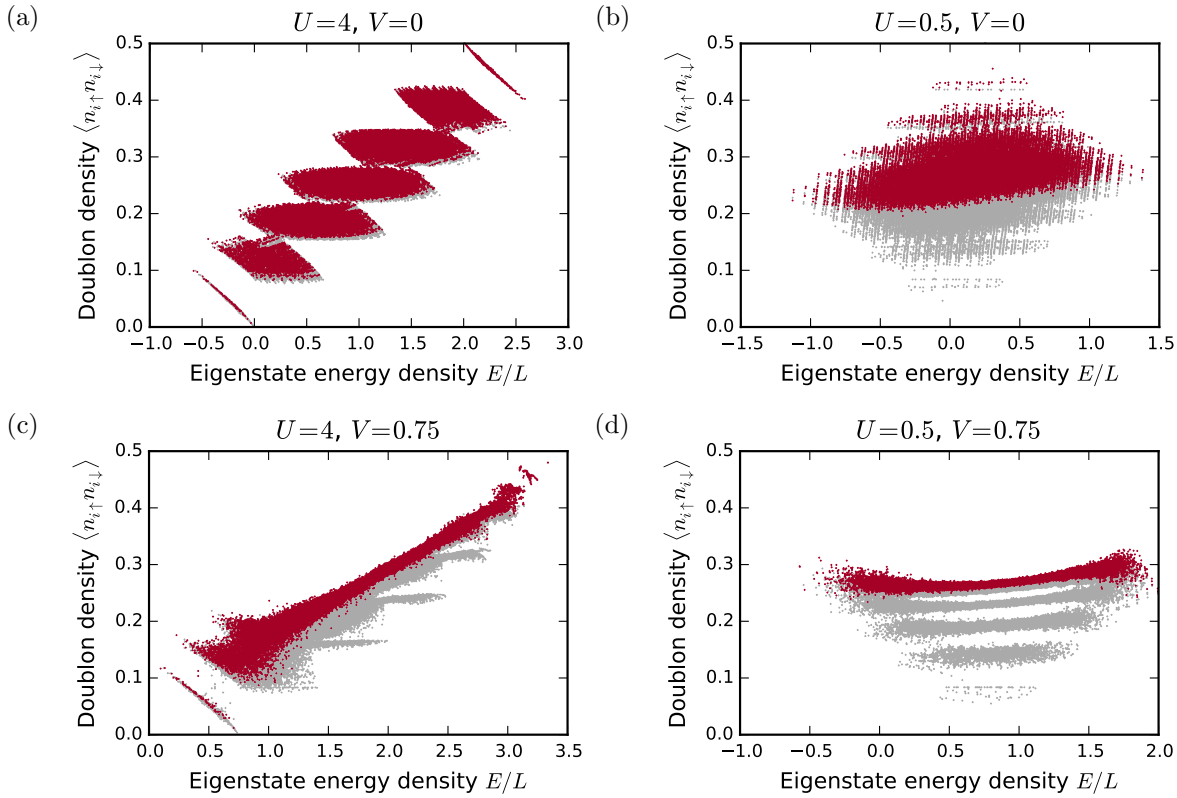

Figure 3.1: Doublon occupancy of the itinerant electron model (Eq. 3.3) obtained from exact diagonalization at system size $L = 12$. Plotted are all eigenstates at half-filling ($N_\uparrow = N_\downarrow = L/2$), with total spin singlets emphasized in red. The top panels show the pure Hubbard model ($V = 0$), while the bottoms panels show the model with an additional nearest-neighbor repulsion term ($V = 3/4$), which breaks integrability. The left panels show a "large" value of U, while the right panels show results for "small" U.

zero, which need not be spin singlets.)

At a given finite energy density in the pure Hubbard model, there exist eigenstates with a range of doublon expectation values. This is expected for an integrable model, as the plot of a generic expectation value with respect to energy density should fill an area in the thermodynamic limit. (By contrast, a system which obeys ETH must take a unique expectation value at each energy density.) In Figure 3.1a, it is clear that the results are for a finite size system, as one can easily recognize the bands due to each overall possible

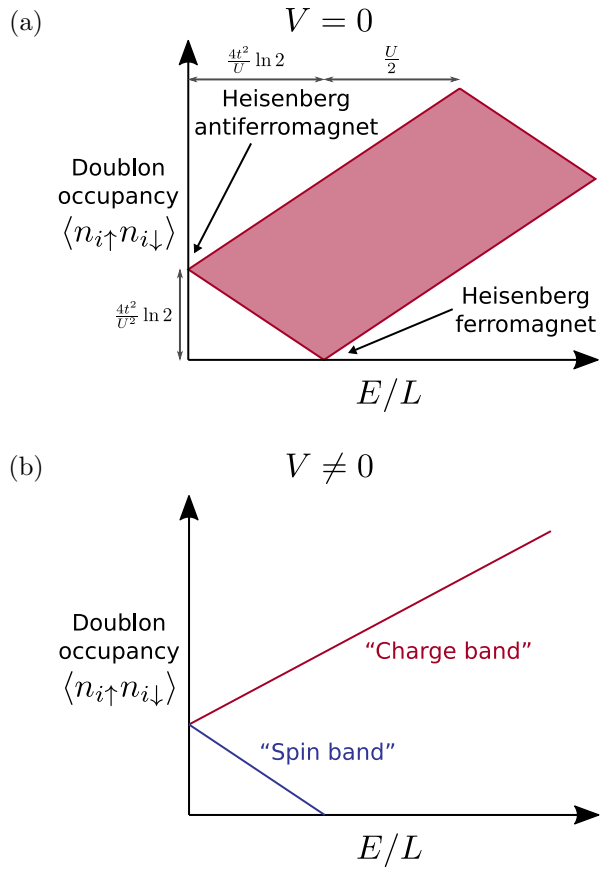

Figure 3.2: Putative sketch of the doublon occupancy versus eigenstate energy density for large U, for both (a) the Hubbard model ($V = 0$) and (b) the non-integrable model ($V \neq 0$). In each case, eigenstates at half-filling which are total spin singlets are considered.

doublon count (from 0 to $L/2$), each offset in energy density by approximately U/L. The band lowest in energy density includes states with low charge fluctuations, the spectrum of which is governed entirely by spin excitations. In fact, there are $\binom{L}{L/2}$ states in this "spin band," each of which maps to a state in the Heisenberg model restricted to $S_z = 0$. In the thermodynamic limit, the bands will become indistinguishable, resulting in the eigenstates filling a large area of the plot in the shape of a parallelogram. A sketch of this plot in the thermodynamic limit is given in Figure 3.2a.

The plot's area is bordered on the bottom left by the states in the Heisenberg spin band. These states can be identified by performing a canonical transformation in powers of t/U [16, 169], resulting in the effective spin-only Hamiltonian

$$H^{(2)}_{\text{spin}} = \frac{4t^2}{U} \sum_{\langle ij \rangle} \left(\mathbf{S}_i \cdot \mathbf{S}_j - \frac{1}{4} \right), \tag{3.4}$$

which is equivalent to the Heisenberg model with $J = 4t^2/U$. From Bethe ansatz, the 1D ground state is known to have $\langle \mathbf{S}_i \cdot \mathbf{S}_{i+1} \rangle = \frac{1}{4} - \ln 2$; thus, the ground state energy density is $-(4t^2/U)\ln 2$ up to corrections of order t^3/U^2. The ground state doublon expectation value in the anti-ferromagnetic ground state can also be determined to be

$$\begin{aligned} \langle n_{i\uparrow} n_{i\downarrow} \rangle &= \frac{1}{L} \frac{\partial}{\partial U} \langle H^{(2)}_{\text{spin}} \rangle \\ &= 4 \ln 2 \left(\frac{t}{U} \right)^2, \end{aligned} \tag{3.5}$$

up to corrections of order $(t/U)^3$.

The Heisenberg ferromagnet, which consists in the $S_z = 0$ sector of all spins pointing in the x-direction, has doublon expectation value and energy density of precisely zero. The Heisenberg ferromagnet is itself not a singlet, but it is clear from Figure 3.1a that there are overall spin singlet states arbitrarily close to this point. Note that under the spin-charge duality introduced in Section 3.3, the Heisenberg ferromagnet maps to the "η-paired" state (first introduced in Ref. [167]), which itself has doublon occupancy $\frac{1}{2}$.

Let us now break integrability by setting $V = 3/4$. Here, common wisdom dictates

that full thermalization ought to occur, since the system is non-integrable and contains no disorder. Figure 3.1c shows the doublon expectation value results for large U in this model. Remarkably, the "spin band" of states corresponding to the Heisenberg model remains distinct from the remaining states (which we dub the "charge band"), even though they overlap in energy density. In this range of energy densities, the doublon expectation value takes two distinct values, an apparent violation of ETH. The highest excited state in the spin band is the Heisenberg ferromagnetic, which remains an eigenstate when $V \neq 0$. This state appears to play a special role, "pinning" Heisenberg-like states into the spin band. Figure 3.2b provides a putative sketch of this plot in the thermodynamic limit. We will provide evidence in Section 3.6 that the states in the spin band are *quantum disentangled eigenstates* according to the definition in Section 3.2.

The spin band remains intact for all system sizes accessible to our numerics. Figure 3.3a shows the doublon expectation value for $L = 14$ calculated using ARPACK's iterative eigensolver in the range of energy densities where the spin and charge bands overlap. Note that both this figure and Figure 3.1a show avoided crossings between the spin and charge bands; these are expected at any finite system size. The ultimate question is whether these bands remain distinct in the thermodynamic limit. Figure 3.3b shows a 2D histogram of the same quantity, plotted on a logarithmic scale. Although there are many states in the charge band with which the spin band states could mix, the spin band appears to remain robustly distinct from the charge band, thus supporting the claim that this model violates ETH.

It is important to note that the regime we are considering in numerics ($U = 4$, $V = 3/4$, and $t = 1$) consists of all parameters of order unity. Finite size effects are most relevant when the ratio of parameters is of order (or greater than) the total system size [132]. In the case considered here, the ratio of any two parameters is significantly less than the largest accessible system size, $L = 14$. This suggests that the apparent ETH violation may indeed be robust in the thermodynamic limit.

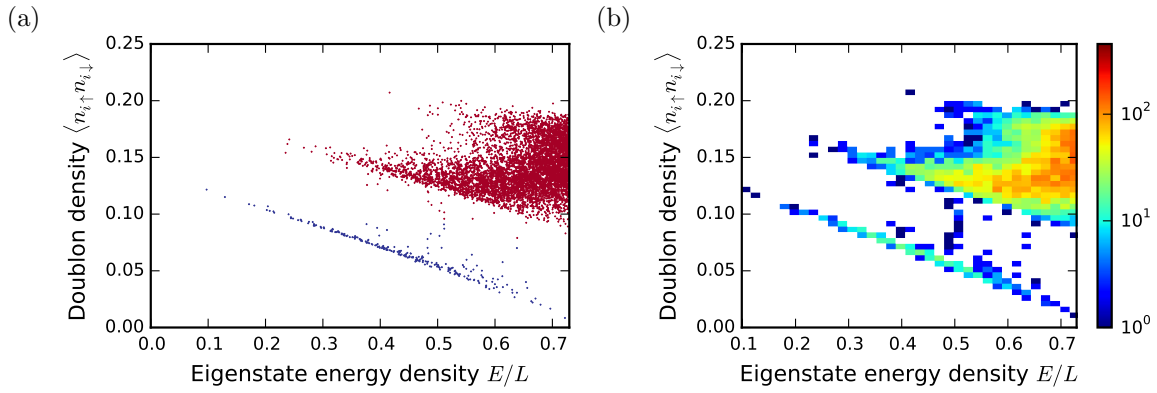

Figure 3.3: (a) Doublon occupancy for $U = 4$, $V = 3/4$ at system size $L = 14$, as calculated using ARPACK's iterative eigensolver, which returns a portion of the spectrum. Included are all eigenstates that are total spin singlets at half filling. The "spin band" states are emphasized in blue. States in all momentum, spin-flip, and particle-hole sectors are combined in this plot. (b) Logarithmic histogram plot of same quantity.

Counting both singlets and non-singlets, there are $[\binom{L}{L/2}]^2$ total states in the half-filled sector we are considering. Of these states, $\binom{L}{L/2}$ are in the spin band. The number of states in the spin band is exponential in system size; however, there are *exponentially more* states in the charge band. The continued existence of the spin band is therefore a violation of the strongest form of ETH, where non-thermal states vanish in the thermodynamic limit [81]. Such a violation was previously only expected in integrable models.

In principle, the existence of states for which ETH fails implies that there exist initial states that will fail to thermalize at any time [77].

3.5.2 Transition to small U

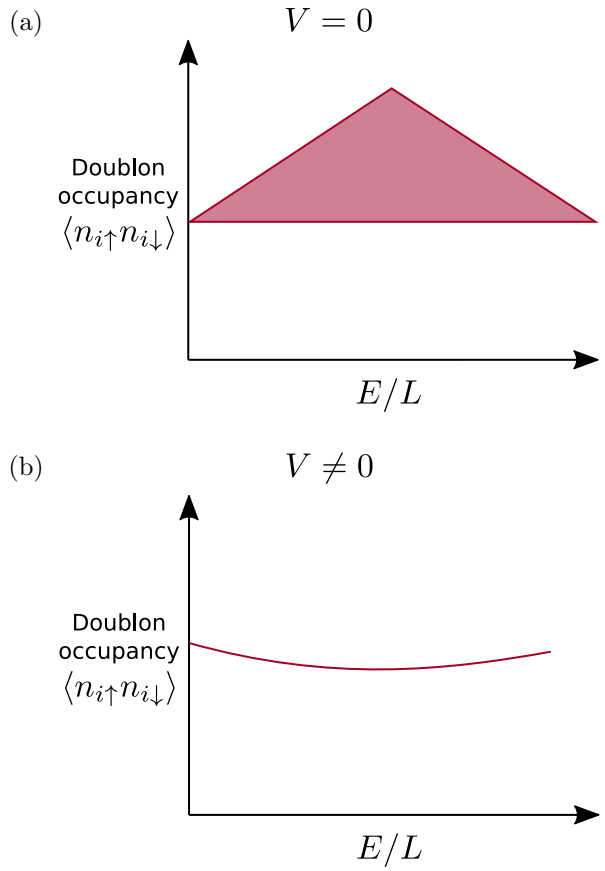

Figure 3.4: Putative sketch of the doublon occupancy versus eigenstate energy density for small U, for both (a) the Hubbard model ($V = 0$) and (b) the non-integrable model ($V \neq 0$). In each case, eigenstates at half-filling which are total spin singlets are considered.

Let us now turn to the physics for small U, as shown in the right panels of Figure 3.1. We start with the pure Hubbard model (Figure 3.1b). As expected for an integrable model, the eigenstates in this plot fill an area in the doublon–energy-density plane. One

particularly striking feature of this plot is that there no longer exist total spin singlet states which are arbitrarily close to the Heisenberg ferromagnet. As one decreases U, the singlet states appear to "lift off" the x-axis around $U/t \simeq 1$, regardless of system size. A proposed sketch of the resulting plot for singlets is shown in Figure 3.4a. It is an interesting open question whether there exists a critical U_c, below which there are no longer singlet states arbitrarily close to the Heisenberg ferromagnet. The question of whether such an eigenstate phase transition exists in the Hubbard model is expected to be analytically tractable using Bethe ansatz, and we leave this for future work.

Figure 3.1d shows the doublon expectation value results for small U in the non-integrable model ($V \neq 0$). In this parameter regime, the model exhibits strong ETH, although each total spin sector thermalizes to a different value. Figure 3.4b sketches the expected shape of this plot for singlets only in the thermodynamic limit.

3.6 Entanglement entropy diagnostic results

Now that we have provided numerical evidence for the existence of two bands (a "charge band" and "spin band") in the large-U limit of the non-integrable model (as sketched in Figure 3.2b), we turn toward considering the entanglement entropy and QDL diagnostics, as introduced in Section 3.2.

Figure 3.5a plots the half-cut entanglement entropy density for each eigenstate that is a total spin singlet, with respect to its energy density. The states identified from Figure 3.1c to be in the spin band are colored in blue, while the remaining charge band

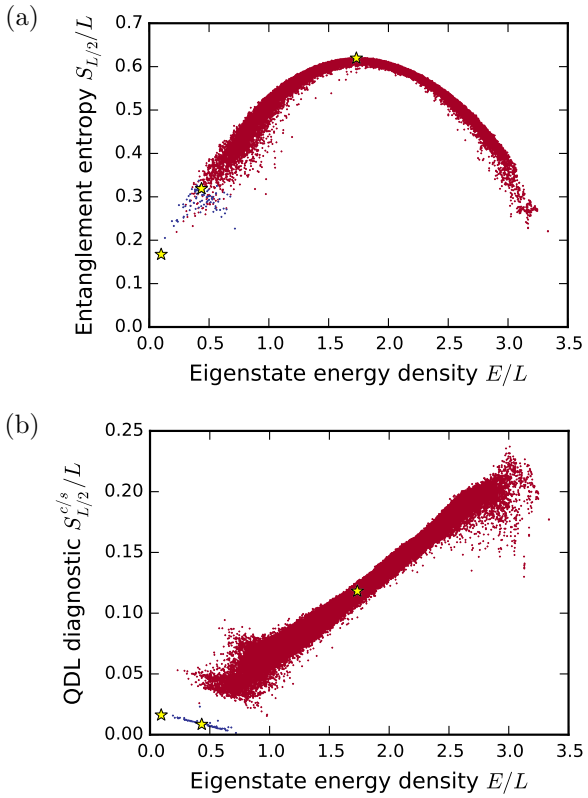

Figure 3.5: Numerical half-cut (a) entanglement entropy density $S_{L/2}/L$ and (b) QDL diagnostic density $S^{c/s}_{L/2}/L$ for the model in Eq. 3.3 at $L = 12$, $U = 4$, $V = 3/4$, and $t = 1$, the same non-integrable parameters as Figs. 3.1a and 3.3. Here, all eigenstates that are total spin singlets are plotted, and the states identified to be in the spin band are colored in blue, while charge band states are in red. The QDL diagnostic shown is the average entanglement entropy after a partial measurement of the spin on each site, as detailed in Section 3.2. Starred are three states that are explored in detail in Figure 3.8.

states are in red. It appears from this plot that the spin and charge bands form two distinct entropy curves, which overlap in energy density. In both cases, the entanglement entropy scales linearly with total system size for states with finite energy density, although the states in the spin band have a smaller volume-law coefficient. Figure 3.6a provides a proposed sketch of this plot in the thermodynamic limit. Results at $L = 14$ further support the existence of two overlapping entropy curves (see Figure 3.7).

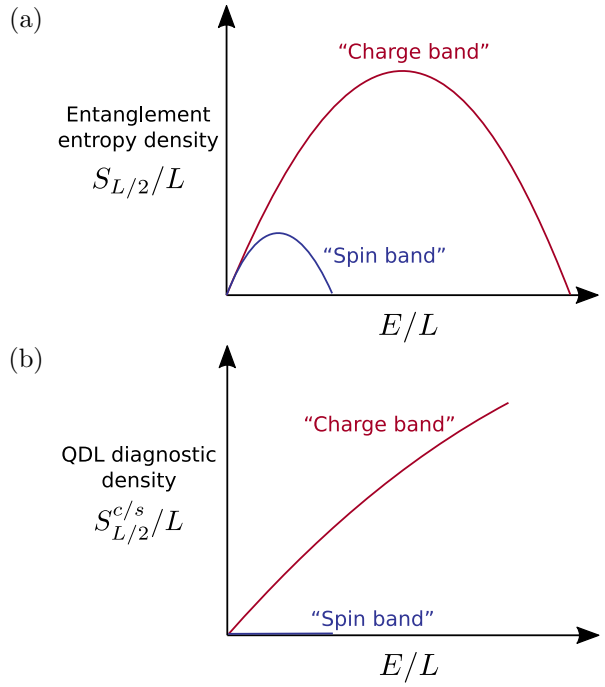

Figure 3.6: Proposed sketches of (a) the entanglement entropy density and (b) the QDL diagnostic density in the thermodynamic limit, for singlets in the large-U non-integrable model, as based on Figs. 3.5 and 3.8.

The apparent existence of two distinct, overlapping entropy curves calls into question the basic tenets of quantum statistical mechanics. Within the context of ETH, entanglement entropy is equal to thermal entropy, and it is possible to assign a "temperature" to an eigenstate by identifying $1/T$ to be the slope of the energy-entropy curve[1]. Thus, all states where the entropy has a positive slope are at positive temperatures, the states with maximum entropy are at infinite temperature, and the states where the entropy slope is negative are at negative temperatures. If we assume Figure 3.6a is correct in the thermodynamic limit, it implies that there are energy densities that contain "hot" spin-band states alongside much cooler charge-band states. If these states are indeed ro-

[1]In general, defining temperature this way will be equivalent to the temperature obtained by matching an eigenstate's energy density to the system's energy density in the canonical ensemble at some temperature.

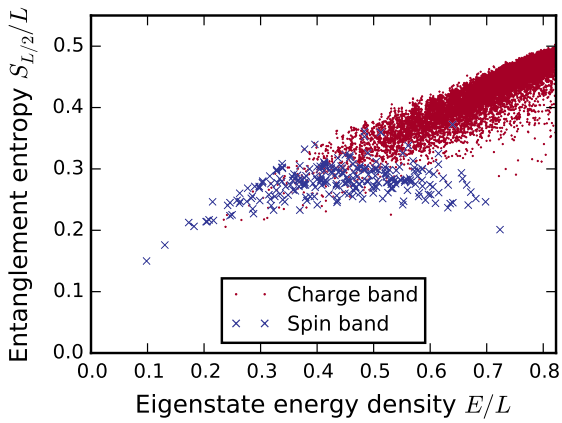

Figure 3.7: Numerical half-cut entanglement entropy density results for system size $L = 14$ at the non-integrable point $U = 4$, $V = 3/4$. The "spin band" states, as identified in Figure 3.3a, are plotted in blue.

bust as $L \to \infty$, an isolated quantum system governed by this model will not thermalize according to canonical statistical mechanics.

Let us now consider the QDL diagnostic after a partial measurement of the spin on each site, the half-cut of which is shown in Figure 3.5b. The spin-band states have greatly reduced entropy after such a partial measurement, as knowledge of the spin state provides nearly all information in these states with very little charge fluctuation. To further explore the entropy and QDL diagnostic properties of this system, we focus in detail on three states: (i) the ground state; (ii) a highly excited state in the charge band; and (iii) a highly excited state in the spin band. These three states are represented by stars in Figure 3.5, and are explored in detail in Figure 3.8. Plotted in this figure is the scaling of the entanglement entropy of each state, as well as the scaling of the QDL diagnostics after a partial measurement of the charge or spin on each site.

The scaling properties of the ground state are plotted in the top row of Figure 3.8

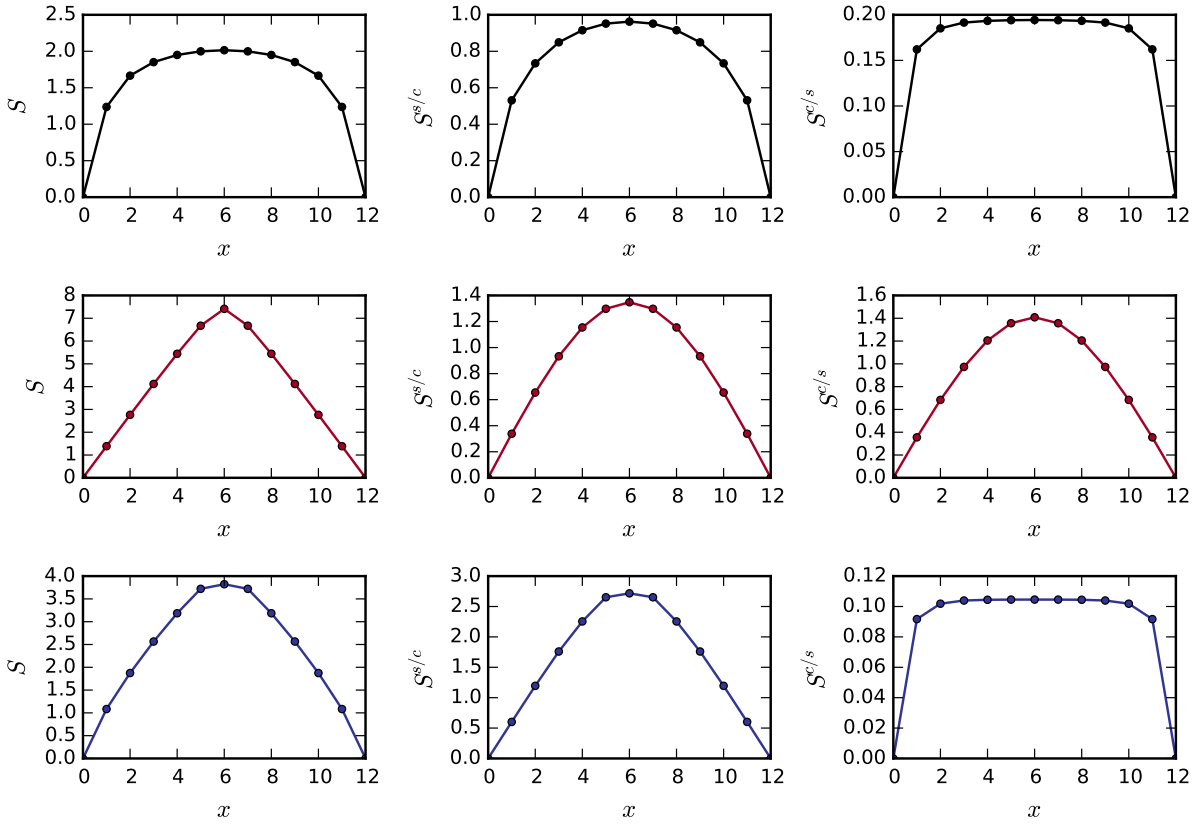

Figure 3.8: Scaling of the entanglement entropy and QDL diagnostics with subsystem cut size x, for the three starred states in Figure 3.5. The left column is the overall entanglement entropy. The middle and right columns plot the QDL diagnostic entanglement entropy after a partial measurement of the charge and spin on each site, respectively. The top row (in black) shows each quantity plotted for the ground state, each of which scales sub-thermally. The middle row (in red) shows the quantities for a highly excited state in the charge band, each of which appears to scale as a volume law. Finally, the bottom row (in blue) shows the three quantities for a highly excited state in the spin band. Here, S and $S^{s/c}$ both scale as a volume law, but the entanglement entropy after a spin measurement $S^{c/s}$ scales as an area law, thus fulfilling the criteria for a *quantum disentangled eigenstate* as defined in Section 3.2.

(in black). Because the model is gapless, the ground state's entanglement entropy scales as $\log x$ [43]. As expected, this sub-thermal entanglement scaling remains after a partial measurement of the charge or spin on each site, as can be seen in the center and right panels of the top row.

The middle row (in red) shows the scaling properties of a high entropy excited state from the charge band. As expected, the overall entanglement entropy of this state scales extensively with system size, which is consistent with the state being in a volume law. It remains in a volume law after a partial measurement of the charge or spin on each site (middle and right panels). As such, this highly excited state in the charge band appears to be fully ergodic.

In the bottom row, we examine the scaling properties of a high entropy state from the spin band (in blue). As can be seen in the left panel, the overall entanglement entropy of this state scales as a volume law, as is expected for a state with finite energy density. The middle panel considers the QDL diagnostic $S^{s/c}$ which measures the entropy remaining after a partial measurement of the charge on each site. Because spin-band states have little charge fluctuations, such a measurement obtains very little information about the state, and the post-measurement state is still in a highly-entangled, volume law state. The bottom right panel of Figure 3.8 shows the QDL diagnostic $S^{c/s}$, the entanglement entropy after a partial measurement of the spin on each site. Remarkably, this plot saturates to a constant and scales as an *area law*, thus fulfilling the criteria of a quantum disentangled liquid. The partial measurement of the spin degrees of freedom *disentangles*

the charge degrees of freedom in the state, transforming the wavefunction from a volume law to an area law. This result is consistent with the states breaking ergodicity.

Having established that the states in the spin band are in an area law for the QDL diagnostic $S^{c/s}$, we can form a sketch of the half-cut QDL diagnostic density, which is provided in Figure 3.6b. The QDL diagnostic for the charge band states scales extensively with system size, so this quantity takes a finite value at each finite energy density in the thermodynamic limit. On the other hand, the spin band states have vanishing QDL diagnostic density in the thermodynamic limit since $S^{c/s}$ scales only with the size of the *boundary* between subregions.

The QDL diagnostic thus acts as a tool for identifying the breakdown of full thermalization. It provides a qualitative distinction between states in the charge band and those in the spin band—in other words, volume law states which are fully thermal and those which are not.

3.7 Discussion

In this chapter, we have provided numerical evidence for the violation of ETH in a non-integrable system without disorder. The model, given by Eq. 3.3, supports two qualitatively distinct bands of eigenstates which overlap in energy density, thus calling into question the general validity of quantum statistical mechanics in translationally invariant systems.

While the model has exponentially many "spin band" states, they are nonetheless

exponentially rare compared with the more common "charge band" states. This is reminiscent of an integrable system, where ETH is satisfied for all but a vanishing fraction of eigenstates [81, 170]. In both cases, the existence of non-thermal eigenstates implies that there exist initial states that will fail to thermalize. In principle, any initial state that has non-vanishing overlap with the spin band will never reach thermal equilibrium. It will be interesting to identify experimentally preparable states that fall in this class. Could an initial product state—for instance with one fermion of arbitrary spin per site—be sufficient in demonstrating the failure of thermalization? Other initial states to consider include quenched states, or states that result from adding a finite density of spin excitations to the quantum ground state of Eq. 3.3.

Once non-thermalizing initial states have been identified, it will be fascinating to study the system's time evolution from these states numerically. What observables fail to relax at long times? Can this provide any additional clues to the mechanism behind the breakdown of ETH? It would also be particularly interesting to attempt to realize a quantum disentangled liquid experimentally by implementing the model in a cold atomic gas of fermions, similar to recent experiments on many-body localization [95–97]. While a nearest-neighbor repulsion term is beyond the reach of current technology, an alternative method would involve realizing the S^zS^z term in the equivalent dual model, which was discussed in Section 3.3. In any case, an experiment in an optical lattice should allow access to much larger system sizes than can be simulated numerically.

The definitive distinguishing feature of the putative QDL phase is the area law scal-

ing of the entanglement entropy after a partial measurement of the spin on each site, as introduced in Section 3.2. Remarkably, a recent experiment has measured the Rényi entanglement entropy S_2 in a cold atomic gas of bosons by performing controlled interference between identical copies of the system [63–65]. In principle, it is also possible to measure Rényi entanglement entropies in cold fermionic gases [67–70]. Suppose we have a reliable experimental protocol for preparing a state in the QDL phase. We could then identically prepare two copies of the system and perform a partial measurement on each. Unfortunately, it is very unlikely that the two copies would exhibit the same measurement outcome, and it follows that the quantum states of the two systems will almost certainly be different. Because the Rényi measurement protocol relies on identical copies of a state, it thus cannot be implemented after a partial measurement. In the end, measuring the average post-measurement entanglement entropy may require performing full quantum tomography on the state resulting after each possible measurement outcome, which is a daunting task. Let us emphasize that while this diagnostic is unlikely to be implemented in experiment, the mere demonstration of the breakdown of thermalization is likely to be a much easier task. Along these lines, existing experiments on realizing MBL phases have focused on observables that fail to thermalize, not on demonstrating the area-law scaling of entanglement entropy.

It is worth considering what role symmetries play in the breakdown of ETH in a translationally invariant system. In this chapter we considered the itinerant fermion model only at half filling, but it would be interesting to investigate whether QDL states

exist at other filling fractions as well. Likewise, to what degree is the observed ETH violation *dependent* on symmetries? The spin band states only exist in certain sectors of total spin, particle-hole parity, and spin-flip parity. What is special about these sectors which harbor QDL behavior? Interestingly, breaking *both* the charge and spin SU(2) symmetries seems to eliminate the spin band. One is tempted to wonder: is a non-abelian symmetry necessary for realizing the QDL phase?

On the other hand, with so many symmetries one must be wary of finite size effects, as each sector contains fewer states with which to mix. In Ref. [77] it was found that sectors with additional symmetries typically have more pronounced outlier states at a given system size. Still, each sector we consider has a Hilbert space size comparable to, if not larger than, the best ETH studies to date. As we have shown above, numerical results up to system sizes of $L = 14$ support the existence of the spin band and thus the violation of ETH. The ultimate question, of course, is whether the spin band continues to exist in the thermodynamic limit. One method for determining the fate of the spin band is to examine the level spacing statistics between the spin band and charge band as the system size is increased, similar to studies of MBL [91]. Unfortunately, because there is no disorder over which to average, it is very difficult to get good statistics. Even if one averages over all possible twists of boundary conditions, the energy level spacings are still highly correlated with each other among samples.

The spin band states exist only in the large-U limit of Eq. 3.3, and another interesting task would involve constructing a canonical transformation in powers of t/U, transform-

ing Heisenberg eigenstates into eigenstates of Eq. 3.3 in the spirit of Refs. [16] and [169]. This would in principle allow access to larger system sizes, and such a transformation may provide insight into (or a technique for perturbatively proving) the breakdown of thermalization.

Finally, it should be emphasized that ETH violation in a translationally invariant system has implications beyond condensed matter physics. In particular, it was recently argued that ETH is itself analogous to the "no-hair theorem" for classical black holes [107]. In other words, the statement of ETH parallels the idea that the metric is completely determined by the energy density of a black hole. The existence of a featureless model that violates ETH may thus have implications for quantum gravity.

In conclusion, using state-of-the-art numerics we have provided evidence for the violation of ETH in a non-integrable model of itinerant electrons. Our results suggest that this model realizes two distinct bands of energy eigenstates, which overlap in energy density and can be distinguished by a universal, qualitative diagnostic based on the entanglement entropy after a partial measurement. Because the number of ETH-violating states scales extensively with the system size, there exist initial states that will never reach thermal equilibrium, thus calling into question the validity of quantum statistical mechanics.

The research in this chapter was performed in collaboration with Ryan V. Mishmash and Matthew P. A. Fisher. We are grateful to Leon Balents, Bela Bauer, Erez Berg, Dominic Else, Fabian Essler, Keith Fratus, Steven Girvin, Tarun Grover, Katharine Hyatt, Robert Konik, Cheng-Ju Lin, Lesik Motrunich, Markus Müller, Chetan Nayak, Gil

Refael, Sid Parameswaran, Neil Robinson, Mauro Schiulaz, Thomas Veness, and David Weld for enlightening discussions regarding this work. This research was supported in part by the National Science Foundation, under Grant No. DMR-14-04230 (JRG and MPAF), by the Walter Burke Institute for Theoretical Physics at Caltech (RVM), and by the Caltech Institute of Quantum Information and Matter, an NSF Physics Frontiers Center with support of the Gordon and Betty Moore Foundation (JRG and MPAF). We acknowledge support from the Center for Scientific Computing at the CNSI and MRL: an NSF MRSEC (DMR-1121053) and NSF CNS-0960316.

Chapter 4

Concluding remarks

The phenomenon of quantum thermalization can be understood in terms of the Eigenstate Thermalization Hypothesis (ETH), which posits that an arbitrary initial state of an isolated, interacting, many-body quantum system will eventually reach thermal equilibrium, provided the eigenstates of the Hamiltonian themselves appear thermal. In Chapter 2, we provided numerical evidence for a strong form of ETH where in the thermodynamic limit, the reduced density matrix due to a single eigenstate precisely matches the corresponding density matrix in the canonical ensemble, as long as the subsystem considered is a vanishing fraction of the total system size. This statement has the remarkable implication that the Hamiltonian itself is encoded in a single finite energy density eigenstate. Using this fact, we predicted approximate correlation functions at all temperatures from a single eigenstate of a finite system. Additionally, we considered operators than span a finite fraction of the system, and found that many (but not all) of these operators satisfy

ETH as well.

In addition to systems which satisfy ETH and thus thermalize at long times, there also exist interacting, quantum systems which, due to a strong disorder potential, will never reach thermal equilibrium. This phenomenon goes by the name "many-body localization" (MBL). One open question is whether thermalization can break down (in a way similar to MBL) in a system lacking disorder and far from an integrable point. In Chapter 3, we provided numerical evidence for the breakdown of ETH in a non-integrable, Hubbard-like chain with both charge and spin degrees of freedom. We introduced a qualitative diagnostic, based on the scaling of entanglement entropy after a partial measurement, that can be used to identify eigenstates in this "Quantum Disentangled Liquid" (QDL) phase. The putative existence of this phase has wide-ranging implications; most notably, it calls into question the general validity of quantum statistical mechanics.

4.1 Outlook

Theoretical physicists are continually making progress toward better understanding quantum thermalization and its breakdown in isolated, many-body systems. It is an exciting time for the field, yet many interesting and fundamental questions remain. One of the most important questions is the one addressed in Chapter 3, namely whether thermalization can fail in a non-integrable system lacking disorder. Although we provide numerical evidence for such a breakdown of ETH, this dissertation is far from the final word on the subject. Indeed, the largest currently accessible system size ($L = 14$) is

still far from the thermodynamic limit, and it remains a mystery precisely what criteria must hold for ETH to fail given an arbitrary model. Ultimately, it would be wonderful to have a full theoretical framework for predicting when thermalization will occur (and when it will fail) in multi-component systems.

Our understanding of quantum thermalization will remain incomplete until we are able to conclusively identify what phases (if any) exist besides many-body localization and full ergodicity. The nature of the transition (as one decreases the disorder strength) from MBL to ergodic has received much attention, but there has been limited theoretical progress to date. One of the most important qualitative questions is whether there is a single transition, or whether there exist other, intermediate phases between MBL and full ergodicity. Similarly, if (as discussed in Section 3.1) we consider the "disorder" in a localized Hamiltonian to be caused by infinitely-massive, quantum particles, what additional phases exist when one allows the particles to have large but finite mass? Are there multiple, qualitatively distinct phases within the framework of QDL?

One broad observation is that the field of quantum thermalization is currently stymied by the lack of powerful theoretical and numerical methods. Much of the existing knowledge about ETH and MBL has relied on full numerical exact diagonalization studies, which are by their nature limited to small system sizes. There has been a fair amount of theoretical progress on the MBL side, but certain questions remain controversial, such as whether a many-body mobility edge can even exist [171]. Also, many of the theoretical techniques available for studying MBL are relevant only deep within the phase, and

provide no insight into the nature of the transition. Volume law phases, such as the fully ergodic phase or the QDL phase, are also beyond the reach of these techniques. Random matrix theory has provided some insight into the ergodic phase, but local Hamiltonians hardly qualify as "random" matrices. As can be seen in Chapter 2, exact diagonalization can teach us a great deal about ETH, but it is still desirable to find a method that will work well in dimensions greater than one, or is able to detect the presence or failure of ETH in multi-component systems. Perhaps experiments on cold atomic gases can help us simulate systems we would be unable to model on a computer (such as MBL in 2D [97], or the potential realization of a QDL). Still, the ability to realize such phases in experiment does not imply theoretical understanding of them.

In this dissertation, we focused mainly on the question of whether or not a system thermalizes by considering its eigenstates within the framework of ETH. Of course, knowledge of the properties of finite energy density eigenstates tells us only about the long-time behavior, and is completely blind to short and intermediate times. It will be interesting to investigate how the thermalization time for a given operator depends upon properties of the operator, of the system size, of the Hamiltonian, and of the initial state (such as whether the energy is uniformly distributed at $t = 0$). There exist "Lieb-Robinson" speed limits on the propagation of entanglement in quantum systems [172–174], as well as a recent bound on the scrambling time [175]. Can one explicitly construct a model that reaches thermal equilibrium so quickly that it saturates these bounds? If not, it should be possible to prove tighter bounds. Luckily, many questions about

thermalization time scales can be examined with further exact diagonalization studies.

On a practical level, it is worth considering how one might leverage the breakdown of thermalization in an effort toward building long-time quantum memories. Is it experimentally possible to control coherent qubits in a many-body localized system (following recent proposals [176,177]), or even in the QDL phase? Such technology would have clear applications to quantum computing.

Finally, an understanding of thermalization within the framework of the Schrödinger equation implies that unitary time evolution is sufficient for explaining thermal behavior in the world around us; we need not rely on an additional dynamical mechanism, such as the "collapse" of a wavefunction. Still, our understanding of thermal behavior does not explain the origin of the Born rule; it does not fully resolve the quantum measurement problem; and it provides few clues about how quantum mechanics and gravity fit together in a unified framework. Overall, it is an exciting time to be studying physics.

Appendix A

Exact diagonalization of lattice system with abelian symmetries

This appendix gives a brief introduction to performing numerical exact diagonalization in a way that exploits abelian symmetries. A complementary treatment of this subject can be found in Ref. [178].

In exact diagonalization, the goal is to numerically determine one or more eigenstates of the Hamiltonian $\hat{H}$. When $\hat{H}$ is translationally invariant, we can change basis such that $\hat{H}$ is diagonal in each momentum sector. This allows us then to diagonalize each sector independently, or to diagonalize only the sector(s) in which we are interested. As a result, eigenstates can be determined using both less processor time and less memory, allowing access to larger system sizes. As a bonus, the energy eigenstates returned will simultaneously be eigenstates of the symmetry operators, thus resolving degeneracies due

to symmetry in a predictable way.

A.1 Translationally invariant systems

Given a translationally invariant Hamiltonian $\hat{H}$, how can one diagonalize each momentum sector separately?

Let $\sum_{\mathbf{r}}$ denote a sum over all sites of the Bravais lattice. Consider the projection operator

$$\hat{P}_{\mathbf{k}} \equiv \frac{1}{N} \sum_{\mathbf{r}} e^{i\mathbf{k}\cdot\mathbf{r}} \prod_{i=1}^{d} \hat{T}_i^{r_i}, \tag{A.1}$$

where N is the number of sites, r_i is defined by $\mathbf{r} = \sum_{i=1}^{d} r_i \mathbf{a}_i$ ($\mathbf{a}_i$ are the primitive vectors of the lattice), $\hat{T}_i$ is the operator that translates by distance $\mathbf{a}_i$, and $\mathbf{k}$ is some allowed momentum of the system. (In a one dimensional spin-1/2 system of length L with periodic boundary conditions, the translation operator is defined such that $\hat{T}_1 |\sigma_1 \cdots \sigma_{L-1}\sigma_L\rangle = |\sigma_L\sigma_1 \cdots \sigma_{L-1}\rangle$, and $k = 2\pi k_{\text{idx}}/L$ where $k_{\text{idx}} \in \mathbb{Z}_L$.)

Since $[\hat{H}, \hat{T}_i] = 0$, it follows that $[\hat{H}, \hat{P}_{\mathbf{k}}] = 0$. It can also be shown that $\hat{P}_{\mathbf{k}}^\dagger = \hat{P}_{\mathbf{k}} = \hat{P}_{\mathbf{k}}^2$. In other words, $\hat{P}_{\mathbf{k}}$ is a Hermitian projection operator that commutes with the Hamiltonian.

We can use this operator to project an arbitrary "representative" state in the position basis $|r\rangle$ to a momentum state $\hat{P}_{\mathbf{k}} |r\rangle$. If $\hat{P}_{\mathbf{k}} |r\rangle = 0$, there is no state at momentum k

represented by $|r\rangle$. However, if $\hat{P}_{\mathbf{k}}|r\rangle \neq 0$, we can define a normalized state

$$|r_{\mathbf{k}}\rangle \equiv \frac{1}{\mathcal{N}_{r_{\mathbf{k}}}} \hat{P}_{\mathbf{k}}|r\rangle\,, \tag{A.2}$$

where $\mathcal{N}_{r_{\mathbf{k}}} \equiv \sqrt{\langle r|\hat{P}_{\mathbf{k}}|r\rangle}$ such that $\langle r_{\mathbf{k}}|r_{\mathbf{k}}\rangle = 1$. Note that $|r_{\mathbf{k}}\rangle$ is an eigenstate of $\hat{T}_j$ with eigenvalue e^{-ik_j}. Here, $\mathbf{k} = \sum_{i=1}^{d} k_i \mathbf{b}_i$, where $\mathbf{b}_i$ are the reciprocal vectors of the lattice, satisfying $\mathbf{a}_i \cdot \mathbf{b}_j = 2\pi\delta_{ij}$.

As a concrete example, consider a one dimensional system with length $L = 4$ and periodic boundary conditions. The representative state $|\uparrow\downarrow\downarrow\downarrow\rangle$ can exist at any available momentum in the system. For instance, at $k = \pi/2$, the corresponding momentum state is

$$|\uparrow\downarrow\downarrow\downarrow\ {}_{\pi/2}\rangle \equiv \frac{1}{2}\left[|\uparrow\downarrow\downarrow\downarrow\rangle + i\,|\downarrow\uparrow\downarrow\downarrow\rangle - |\downarrow\downarrow\uparrow\downarrow\rangle - i\,|\downarrow\downarrow\downarrow\uparrow\rangle\right]. \tag{A.3}$$

The representative state $|\uparrow\downarrow\uparrow\downarrow\rangle$, on the other hand, does not exist at momentum $\pi/2$, since $\hat{P}_{\pi/2}|\uparrow\downarrow\uparrow\downarrow\rangle = 0$. However, there are such states at momenta 0 and π:

$$|\uparrow\downarrow\uparrow\downarrow\ {}_{0}\rangle \equiv \frac{1}{\sqrt{2}}\left[|\uparrow\downarrow\uparrow\downarrow\rangle + |\downarrow\uparrow\downarrow\uparrow\rangle\right]; \tag{A.4a}$$

$$|\uparrow\downarrow\uparrow\downarrow\ {}_{\pi}\rangle \equiv \frac{1}{\sqrt{2}}\left[|\uparrow\downarrow\uparrow\downarrow\rangle - |\downarrow\uparrow\downarrow\uparrow\rangle\right]. \tag{A.4b}$$

With this in mind we generally act as follows. We choose a unique representative state $|r\rangle$ for each class of states that are connected to each other by translation. Then, given a momentum $\mathbf{k}$, we go through each representative state and calculate its normalization

$\mathcal{N}_{r_\mathbf{k}}$. We consider each state $|r_\mathbf{k}\rangle$ where $\mathcal{N}_{r_\mathbf{k}} \neq 0$ to be part of our basis in this momentum sector. We can then evaluate the matrix elements of the Hamiltonian in the momentum basis, given by

$$\langle r'_\mathbf{k}|\hat{H}|r_\mathbf{k}\rangle = \frac{1}{\mathcal{N}_{r'_\mathbf{k}}\mathcal{N}_{r_\mathbf{k}}} \langle r'|\hat{P}_\mathbf{k}\hat{H}\hat{P}_\mathbf{k}|r\rangle = \frac{1}{\mathcal{N}_{r'_\mathbf{k}}\mathcal{N}_{r_\mathbf{k}}} \langle r'|\hat{P}_\mathbf{k}\hat{H}|r\rangle\,, \tag{A.5}$$

where the final manipulation uses $[\hat{H}, \hat{P}_\mathbf{k}] = 0$ and $\hat{P}_\mathbf{k}^2 = \hat{P}_\mathbf{k}$. We then diagonalize the matrix given by elements $\langle r'_\mathbf{k}|\hat{H}|r_\mathbf{k}\rangle$. Given the eigenstates in this basis, we can recover our eigenstates in the original (position space) basis by evaluating $\langle s|r_\mathbf{k}\rangle$ using the definition of $|r_\mathbf{k}\rangle$ above.

Note that by taking advantage of translation invariance, one can reduce the Hilbert space size under consideration by approximately a factor of N.

A.2 Other abelian symmetries

It is possible to take advantage of abelian symmetries other than momentum, such as spin-flip or particle-hole symmetry. Each of these symmetries can be implemented following a procedure similar to the one in the previous section. Instead of T_i being a translation operator, let it be the operator that implements the relevant symmetry. Because spin-flip and particle-hole are each $\mathbb{Z}_2$ symmetries, the allowed "momenta" are then 0 and π, corresponding to even and odd under the given symmetry.

These additional symmetries can be considered simultaneously with momentum. The

Hamiltonian in Chapter 3 (Eq. 3.3) is invariant under spin-flip, particle-hole, and momentum symmetries at half-filling. When implemented together, these symmetries reduce the Hilbert space size in a given sector by a factor of $4L$, thus allowing access to a large portion of the spectrum even at $L = 14$. At this system size, the full Hilbert space in the half-filled Hubbard model is of size $[\binom{14}{7}]^2 = 11778624$. Storing a dense matrix of all eigenstates in this basis would require over a petabyte of data, clearly beyond the reach of any single machine. However, by taking advantage of the aforementioned abelian symmetries, the dense eigenstates can be represented in a few hundred gigabytes per sector, and diagonalization is feasible.

Bibliography

[1] D. ter Haar, *Collected Papers of L.D. Landau* (Elsevier Science, 2013).

[2] A. J. Leggett, "A theoretical description of the new phases of liquid ^{3}He," *Rev. Mod. Phys.* **47**, 331 (1975).

[3] D. Pines and P. Nozières, *The Theory of Quantum Liquids: Normal Fermi liquids* (W.A. Benjamin, 1966).

[4] "II. The Doctor's Dissertation (Text and Translation)," in *Early Work (1905–1911)*, edited by L. Rosenfeld and J. R. Nielsen, volume 1 of *Niels Bohr Collected Works*, pp. 163–393 (Elsevier, 1972).

[5] H.-J. Van Leeuwen, "Problèmes de la théorie électronique du magnétisme," *J. Phys. Radium* **2**, 361 (1921).

[6] J. Bardeen, L. N. Cooper, and J. R. Schrieffer, "Theory of Superconductivity," *Phys. Rev.* **108**, 1175 (1957).

[7] L. Balents, "Spin liquids in frustrated magnets," *Nature* **464**, 199 (2010).

[8] J. G. Bednorz and K. A. Müller, "Possible high T_c superconductivity in the Ba-La-Cu-O system," *Zeitschrift fur Physik B Condensed Matter* **64**, 189 (1986).

[9] Y. Kamihara, T. Watanabe, M. Hirano, and H. Hosono, "Iron-Based Layered Superconductor $La[O_{1-x}F_x]FeAs$ ($x = 0.05 - 0.12$) with $T_c = 26$ K," *Journal of the American Chemical Society* **130**, 3296 (2008).

[10] G. R. Stewart, "Non-Fermi-liquid behavior in d- and f-electron metals," *Rev. Mod. Phys.* **73**, 797 (2001).

[11] R. B. Laughlin, "Anomalous Quantum Hall Effect: An Incompressible Quantum Fluid with Fractionally Charged Excitations," *Phys. Rev. Lett.* **50**, 1395 (1983).

[12] M. Z. Hasan and C. L. Kane, "Colloquium: Topological insulators," *Reviews of Modern Physics* **82**, 3045 (2010) 1002.3895.

[13] X.-L. Qi and S.-C. Zhang, "Topological insulators and superconductors," *Reviews of Modern Physics* **83**, 1057 (2011) 1008.2026.

[14] J. Hubbard, "Electron Correlations in Narrow Energy Bands," *Proceedings of the Royal Society of London A: Mathematical, Physical and Engineering Sciences* **276**, 238 (1963).

[15] P. A. Lee, N. Nagaosa, and X.-G. Wen, "Doping a Mott insulator: Physics of high-temperature superconductivity," *Rev. Mod. Phys.* **78**, 17 (2006).

[16] A. H. MacDonald, S. M. Girvin, and D. Yoshioka, "$\frac{t}{U}$ expansion for the Hubbard model," *Phys. Rev. B* **37**, 9753 (1988).

[17] R. Coldea, D. A. Tennant, E. M. Wheeler, E. Wawrzynska, D. Prabhakaran, M. Telling, K. Habicht, P. Smeibidl, and K. Kiefer, "Quantum Criticality in an Ising Chain: Experimental Evidence for Emergent E_8 Symmetry," *Science* **327**, 177 (2010) 1103.3694.

[18] K. G. Wilson, "The renormalization group: Critical phenomena and the Kondo problem," *Rev. Mod. Phys.* **47**, 773 (1975).

[19] D. Jaksch and P. Zoller, "The cold atom Hubbard toolbox," *Annals of Physics* **315**, 52 (2005) cond-mat/0410614.

[20] I. Bloch, J. Dalibard, and W. Zwerger, "Many-body physics with ultracold gases," *Reviews of Modern Physics* **80**, 885 (2008) 0704.3011.

[21] S. Inouye, M. R. Andrews, J. Stenger, H.-J. Miesner, D. M. Stamper-Kurn, and W. Ketterle, "Observation of Feshbach resonances in a Bose-Einstein condensate," *Nature* **392**, 151 (1998).

[22] P. Courteille, R. S. Freeland, D. J. Heinzen, F. A. van Abeelen, and B. J. Verhaar, "Observation of a Feshbach Resonance in Cold Atom Scattering," *Phys. Rev. Lett.* **81**, 69 (1998).

[23] M. P. A. Fisher, P. B. Weichman, G. Grinstein, and D. S. Fisher, "Boson localization and the superfluid-insulator transition," *Phys. Rev. B* **40**, 546 (1989).

[24] D. Jaksch, C. Bruder, J. I. Cirac, C. W. Gardiner, and P. Zoller, "Cold Bosonic Atoms in Optical Lattices," *Phys. Rev. Lett.* **81**, 3108 (1998) cond-mat/9805329.

[25] M. Greiner, O. Mandel, T. Esslinger, T. W. Hansch, and I. Bloch, "Quantum phase transition from a superfluid to a Mott insulator in a gas of ultracold atoms," *Nature* **415**, 39 (2002).

[26] R. Jördens, N. Strohmaier, K. Günter, H. Moritz, and T. Esslinger, "A Mott insulator of fermionic atoms in an optical lattice," *Nature* **455**, 204 (2008) 0804.4009.

[27] H. P. Büchler, M. Hermele, S. D. Huber, M. P. A. Fisher, and P. Zoller, "Atomic Quantum Simulator for Lattice Gauge Theories and Ring Exchange Models," *Phys. Rev. Lett.* **95**, 040402 (2005) cond-mat/0503254.

[28] A. Einstein, B. Podolsky, and N. Rosen, "Can Quantum-Mechanical Description of Physical Reality Be Considered Complete?" *Phys. Rev.* **47**, 777 (1935).

[29] J. S. Bell, "On the Einstein-Podolsky-Rosen paradox," *Physics* **1**, 195 (1964).

[30] A. Aspect, P. Grangier, and G. Roger, "Experimental Tests of Realistic Local Theories via Bell's Theorem," *Phys. Rev. Lett.* **47**, 460 (1981).

[31] A. Aspect, P. Grangier, and G. Roger, "Experimental Realization of Einstein-

Podolsky-Rosen-Bohm *Gedankenexperiment*: A New Violation of Bell's Inequalities," *Phys. Rev. Lett.* **49**, 91 (1982).

[32] A. Aspect, J. Dalibard, and G. Roger, "Experimental Test of Bell's Inequalities Using Time-Varying Analyzers," *Phys. Rev. Lett.* **49**, 1804 (1982).

[33] D. M. Greenberger, M. A. Horne, and A. Zeilinger, "Going Beyond Bell's Theorem," *ArXiv e-prints* (2007) 0712.0921.

[34] J.-W. Pan, D. Bouwmeester, M. Daniell, H. Weinfurter, and A. Zeilinger, "Experimental test of quantum nonlocality in three-photon Greenberger-Horne-Zeilinger entanglement," *Nature* **403**, 515 (2000).

[35] B. Hensen, H. Bernien, A. E. Dréau, A. Reiserer, N. Kalb, M. S. Blok, J. Ruitenberg, R. F. L. Vermeulen, R. N. Schouten, C. Abellán, W. Amaya, V. Pruneri, M. W. Mitchell, M. Markham, D. J. Twitchen, D. Elkouss, S. Wehner, T. H. Taminiau, and R. Hanson, "Experimental loophole-free violation of a Bell inequality using entangled electron spins separated by 1.3 km," *ArXiv e-prints* (2015) 1508.05949.

[36] L. K. Shalm, E. Meyer-Scott, B. G. Christensen, P. Bierhorst, M. A. Wayne, M. J. Stevens, T. Gerrits, S. Glancy, D. R. Hamel, M. S. Allman, K. J. Coakley, S. D. Dyer, C. Hodge, A. E. Lita, V. B. Verma, C. Lambrocco, E. Tortorici, A. L. Migdall, Y. Zhang, D. R. Kumor, W. H. Farr, F. Marsili, M. D. Shaw, J. A. Stern, C. Abellán, W. Amaya, V. Pruneri, T. Jennewein, M. W. Mitchell, P. G. Kwiat,

J. C. Bienfang, R. P. Mirin, E. Knill, and S. W. Nam, "Strong Loophole-Free Test of Local Realism," *Phys. Rev. Lett.* **115**, 250402 (2015) 1511.03189.

[37] M. Giustina, M. A. M. Versteegh, S. Wengerowsky, J. Handsteiner, A. Hochrainer, K. Phelan, F. Steinlechner, J. Kofler, J.-Å. Larsson, C. Abellán, W. Amaya, V. Pruneri, M. W. Mitchell, J. Beyer, T. Gerrits, A. E. Lita, L. K. Shalm, S. W. Nam, T. Scheidl, R. Ursin, B. Wittmann, and A. Zeilinger, "Significant-Loophole-Free Test of Bell's Theorem with Entangled Photons," *Phys. Rev. Lett.* **115**, 250401 (2015) 1511.03190.

[38] J. Eisert, M. Cramer, and M. B. Plenio, "Colloquium: Area laws for the entanglement entropy," *Reviews of Modern Physics* **82**, 277 (2010) 0808.3773.

[39] M. Srednicki, "Entropy and area," *Phys. Rev. Lett.* **71**, 666 (1993).

[40] M. B. Hastings, "An area law for one-dimensional quantum systems," *Journal of Statistical Mechanics: Theory and Experiment* **8**, 24 (2007) 0705.2024.

[41] S. Popescu, A. J. Short, and A. Winter, "Entanglement and the foundations of statistical mechanics," *Nat Phys* **2**, 754 (2006).

[42] D. N. Page, "Average entropy of a subsystem," *Phys. Rev. Lett.* **71**, 1291 (1993) gr-qc/9305007.

[43] P. Calabrese and J. Cardy, "Entanglement entropy and quantum field the-

ory," *Journal of Statistical Mechanics: Theory and Experiment* **6**, 2 (2004) hep-th/0405152.

[44] B. Swingle, "Entanglement Entropy and the Fermi Surface," *Phys. Rev. Lett.* **105**, 050502 (2010) 0908.1724.

[45] A. Kitaev and J. Preskill, "Topological Entanglement Entropy," *Phys. Rev. Lett.* **96**, 110404 (2006) hep-th/0510092.

[46] M. Levin and X.-G. Wen, "Detecting Topological Order in a Ground State Wave Function," *Phys. Rev. Lett.* **96**, 110405 (2006) cond-mat/0510613.

[47] Y. Zhang, T. Grover, A. Turner, M. Oshikawa, and A. Vishwanath, "Quasiparticle statistics and braiding from ground-state entanglement," *Phys. Rev. B* **85**, 235151 (2012) 1111.2342.

[48] H. Li and F. D. M. Haldane, "Entanglement Spectrum as a Generalization of Entanglement Entropy: Identification of Topological Order in Non-Abelian Fractional Quantum Hall Effect States," *Phys. Rev. Lett.* **101**, 010504 (2008) 0805.0332.

[49] T. H. Hsieh and L. Fu, "Bulk Entanglement Spectrum Reveals Quantum Criticality within a Topological State," *Phys. Rev. Lett.* **113**, 106801 (2014) 1305.1949.

[50] K. Zyczkowski, "Renyi extrapolation of Shannon entropy," *ArXiv e-prints* (2003) quant-ph/0305062.

[51] C. Holzhey, F. Larsen, and F. Wilczek, "Geometric and renormalized entropy in conformal field theory," *Nuclear Physics B* **424**, 443 (1994) hep-th/9403108.

[52] C. Callan and F. Wilczek, "On geometric entropy," *Physics Letters B* **333**, 55 (1994).

[53] M. Headrick, "Entanglement Rényi entropies in holographic theories," *Phys. Rev. D* **82**, 126010 (2010) 1006.0047.

[54] M. B. Hastings, I. González, A. B. Kallin, and R. G. Melko, "Measuring Renyi Entanglement Entropy in Quantum Monte Carlo Simulations," *Phys. Rev. Lett.* **104**, 157201 (2010).

[55] Y. Zhang, T. Grover, and A. Vishwanath, "Entanglement Entropy of Critical Spin Liquids," *Phys. Rev. Lett.* **107**, 067202 (2011).

[56] T. Grover, "Entanglement of Interacting Fermions in Quantum Monte Carlo Calculations," *Phys. Rev. Lett.* **111**, 130402 (2013) 1307.1486.

[57] P. Broecker and S. Trebst, "Rényi entropies of interacting fermions from determinantal quantum Monte Carlo simulations," *Journal of Statistical Mechanics: Theory and Experiment* **8**, 08015 (2014) 1404.3027.

[58] M. Horodecki, P. Horodecki, and R. Horodecki, "Separability of mixed states: necessary and sufficient conditions," *Physics Letters A* **223**, 1 (1996) quant-ph/9605038.

[59] B. M. Terhal, "Bell inequalities and the separability criterion," *Physics Letters A* **271**, 319 (2000) quant-ph/9911057.

[60] O. Gühne and G. Tóth, "Entanglement detection," *Physics Reports* **474**, 1 (2009).

[61] R. Horodecki, P. Horodecki, M. Horodecki, and K. Horodecki, "Quantum entanglement," *Reviews of Modern Physics* **81**, 865 (2009) quant-ph/0702225.

[62] A. K. Ekert, C. M. Alves, D. K. L. Oi, M. Horodecki, P. Horodecki, and L. C. Kwek, "Direct Estimations of Linear and Nonlinear Functionals of a Quantum State," *Phys. Rev. Lett.* **88**, 217901 (2002).

[63] C. Moura Alves and D. Jaksch, "Multipartite Entanglement Detection in Bosons," *Phys. Rev. Lett.* **93**, 110501 (2004) quant-ph/0409036.

[64] A. J. Daley, H. Pichler, J. Schachenmayer, and P. Zoller, "Measuring Entanglement Growth in Quench Dynamics of Bosons in an Optical Lattice," *Phys. Rev. Lett.* **109**, 020505 (2012) 1205.1521.

[65] R. Islam, R. Ma, P. M. Preiss, M. Eric Tai, A. Lukin, M. Rispoli, and M. Greiner, "Measuring entanglement entropy in a quantum many-body system," *Nature* **528**, 77 (2015) 1509.01160.

[66] W. S. Bakr, J. I. Gillen, A. Peng, S. Fölling, and M. Greiner, "A quantum gas microscope for detecting single atoms in a Hubbard-regime optical lattice," *Nature* **462**, 74 (2009) 0908.0174.

[67] H. Pichler, L. Bonnes, A. J. Daley, A. M. Läuchli, and P. Zoller, "Thermal versus entanglement entropy: a measurement protocol for fermionic atoms with a quantum gas microscope," *New Journal of Physics* **15**, 063003 (2013) 1302.1187.

[68] L. W. Cheuk, M. A. Nichols, M. Okan, T. Gersdorf, V. V. Ramasesh, W. S. Bakr, T. Lompe, and M. W. Zwierlein, "A Quantum Gas Microscope for Fermionic Atoms," *ArXiv e-prints* (2015) 1503.02648.

[69] M. F. Parsons, F. Huber, A. Mazurenko, C. S. Chiu, W. Setiawan, K. Wooley-Brown, S. Blatt, and M. Greiner, "Site-resolved Imaging of Fermionic Lithium-6 in an Optical Lattice," *ArXiv e-prints* (2015) 1504.04397.

[70] D. Greif, M. F. Parsons, A. Mazurenko, C. S. Chiu, S. Blatt, F. Huber, G. Ji, and M. Greiner, "Site-resolved imaging of a fermionic Mott insulator," *Science* **351**, 953 (2016) 1511.06366.

[71] R. Nandkishore and D. A. Huse, "Many-Body Localization and Thermalization in Quantum Statistical Mechanics," *Annual Review of Condensed Matter Physics* **6**, 15 (2015) 1404.0686.

[72] J. M. Deutsch, "Quantum statistical mechanics in a closed system," *Phys. Rev. A* **43**, 2046 (1991).

[73] M. Srednicki, "Chaos and quantum thermalization," *Phys. Rev. E* **50**, 888 (1994).

[74] M. Srednicki, "Thermal fluctuations in quantized chaotic systems," *Journal of Physics A: Mathematical and General* **29**, L75 (1996).

[75] M. Srednicki, "The approach to thermal equilibrium in quantized chaotic systems," *Journal of Physics A: Mathematical and General* **32**, 1163 (1999) cond-mat/9809360.

[76] M. Rigol, V. Dunjko, and M. Olshanii, "Thermalization and its mechanism for generic isolated quantum systems," *Nature* **452**, 854 (2008) 0708.1324.

[77] H. Kim, T. N. Ikeda, and D. A. Huse, "Testing whether all eigenstates obey the eigenstate thermalization hypothesis," *Phys. Rev. E* **90**, 052105 (2014) 1408.0535.

[78] J. R. Garrison and T. Grover, "Does a single eigenstate encode the full Hamiltonian?" *ArXiv e-prints* (2015) 1503.00729.

[79] K. R. Fratus and M. Srednicki, "Eigenstate thermalization in systems with spontaneously broken symmetry," *Phys. Rev. E* **92**, 040103 (2015) 1505.04206.

[80] R. Mondaini, K. R. Fratus, M. Srednicki, and M. Rigol, "Eigenstate thermalization in the two-dimensional transverse field Ising model," *Phys. Rev. E* **93**, 032104 (2016) 1512.04947.

[81] G. Biroli, C. Kollath, and A. M. Läuchli, "Effect of Rare Fluctuations on the Thermalization of Isolated Quantum Systems," *Phys. Rev. Lett.* **105**, 250401 (2010) 0907.3731.

[82] M. Rigol and M. Srednicki, "Alternatives to Eigenstate Thermalization," *Phys. Rev. Lett.* **108**, 110601 (2012) 1108.0928.

[83] M. Rigol, V. Dunjko, V. Yurovsky, and M. Olshanii, "Relaxation in a Completely Integrable Many-Body Quantum System: An Ab Initio Study of the Dynamics of the Highly Excited States of 1D Lattice Hard-Core Bosons," *Phys. Rev. Lett.* **98**, 050405 (2007) cond-mat/0604476.

[84] A. C. Cassidy, C. W. Clark, and M. Rigol, "Generalized Thermalization in an Integrable Lattice System," *Phys. Rev. Lett.* **106**, 140405 (2011) 1008.4794.

[85] P. Calabrese, F. H. L. Essler, and M. Fagotti, "Quantum Quench in the Transverse-Field Ising Chain," *Phys. Rev. Lett.* **106**, 227203 (2011) 1104.0154.

[86] J.-S. Caux and F. H. L. Essler, "Time Evolution of Local Observables After Quenching to an Integrable Model," *Phys. Rev. Lett.* **110**, 257203 (2013) 1301.3806.

[87] T. Kinoshita, T. Wenger, and D. S. Weiss, "A quantum Newton's cradle," *Nature* **440**, 900 (2006).

[88] E. H. Lieb and W. Liniger, "Exact Analysis of an Interacting Bose Gas. I. The General Solution and the Ground State," *Phys. Rev.* **130**, 1605 (1963).

[89] P. W. Anderson, "Absence of Diffusion in Certain Random Lattices," *Physical Review* **109**, 1492 (1958).

[90] D. M. Basko, I. L. Aleiner, and B. L. Altshuler, "Metal insulator transition in a weakly interacting many-electron system with localized single-particle states," *Annals of Physics* **321**, 1126 (2006) cond-mat/0506617.

[91] V. Oganesyan and D. A. Huse, "Localization of interacting fermions at high temperature," *Phys. Rev. B* **75**, 155111 (2007) cond-mat/0610854.

[92] A. Pal and D. A. Huse, "Many-body localization phase transition," *Phys. Rev. B* **82**, 174411 (2010) 1010.1992.

[93] B. Bauer and C. Nayak, "Area laws in a many-body localized state and its implications for topological order," *Journal of Statistical Mechanics: Theory and Experiment* **9**, 5 (2013) 1306.5753.

[94] D. J. Luitz, N. Laflorencie, and F. Alet, "Many-body localization edge in the random-field Heisenberg chain," *Phys. Rev. B* **91**, 081103 (2015) 1411.0660.

[95] S. S. Kondov, W. R. McGehee, W. Xu, and B. DeMarco, "Disorder-Induced Localization in a Strongly Correlated Atomic Hubbard Gas," *Phys. Rev. Lett.* **114**, 083002 (2015) 1305.6072.

[96] M. Schreiber, S. S. Hodgman, P. Bordia, H. P. Lüschen, M. H. Fischer, R. Vosk, E. Altman, U. Schneider, and I. Bloch, "Observation of many-body localization of interacting fermions in a quasirandom optical lattice," *Science* **349**, 842 (2015) 1501.05661.

[97] J.-y. Choi, S. Hild, J. Zeiher, P. Schauß, A. Rubio-Abadal, T. Yefsah, V. Khemani, D. A. Huse, I. Bloch, and C. Gross, "Exploring the many-body localization transition in two dimensions," *ArXiv e-prints* (2016) 1604.04178.

[98] J. Smith, A. Lee, P. Richerme, B. Neyenhuis, P. W. Hess, P. Hauke, M. Heyl, D. A. Huse, and C. Monroe, "Many-body localization in a quantum simulator with programmable random disorder," *ArXiv e-prints* (2015) 1508.07026.

[99] J. H. Bardarson, F. Pollmann, and J. E. Moore, "Unbounded Growth of Entanglement in Models of Many-Body Localization," *Phys. Rev. Lett.* **109**, 017202 (2012) 1202.5532.

[100] M. Serbyn, Z. Papić, and D. A. Abanin, "Local Conservation Laws and the Structure of the Many-Body Localized States," *Phys. Rev. Lett.* **111**, 127201 (2013) 1305.5554.

[101] D. A. Huse, R. Nandkishore, and V. Oganesyan, "Phenomenology of fully many-body-localized systems," *Phys. Rev. B* **90**, 174202 (2014) 1305.4915.

[102] J. Z. Imbrie, "On Many-Body Localization for Quantum Spin Chains," *Journal of Statistical Physics* **163**, 998 (2016) 1403.7837.

[103] A. Chandran, I. H. Kim, G. Vidal, and D. A. Abanin, "Constructing local integrals of motion in the many-body localized phase," *Phys. Rev. B* **91**, 085425 (2015) 1407.8480.

[104] V. Ros, M. Müller, and A. Scardicchio, "Integrals of motion in the many-body localized phase," *Nuclear Physics B* **891**, 420 (2015) 1406.2175.

[105] T. Grover and M. P. A. Fisher, "Quantum disentangled liquids," *Journal of Statistical Mechanics: Theory and Experiment* **10**, 10 (2014) 1307.2288.

[106] R. B. Lehoucq, D. C. Sorensen, and C. Yang, "ARPACK Users Guide: Solution of Large Scale Eigenvalue Problems by Implicitly Restarted Arnoldi Methods" (1997).

[107] S. Khlebnikov and M. Kruczenski, "Thermalization of isolated quantum systems," *ArXiv e-prints* (2013) 1312.4612.

[108] S. R. White, "Density matrix formulation for quantum renormalization groups," *Phys. Rev. Lett.* **69**, 2863 (1992).

[109] U. Schollwöck, "The density-matrix renormalization group," *Reviews of Modern Physics* **77**, 259 (2005) cond-mat/0409292.

[110] S. Östlund and S. Rommer, "Thermodynamic Limit of Density Matrix Renormalization," *Phys. Rev. Lett.* **75**, 3537 (1995) cond-mat/9503107.

[111] U. Schollwöck, "The density-matrix renormalization group in the age of matrix product states," *Annals of Physics* **326**, 96 (2011) 1008.3477.

[112] A. Chandran, J. Carrasquilla, I. H. Kim, D. A. Abanin, and G. Vidal, "Spectral tensor networks for many-body localization," *Phys. Rev. B* **92**, 024201 (2015) 1410.0687.

[113] D. Pekker and B. K. Clark, "Encoding the structure of many-body localization with matrix product operators," *ArXiv e-prints* (2014) 1410.2224.

[114] V. Khemani, F. Pollmann, and S. L. Sondhi, "Obtaining highly-excited eigenstates of many-body localized Hamiltonians by the density matrix renormalization group," *ArXiv e-prints* (2015) 1509.00483.

[115] X. Yu, D. Pekker, and B. K. Clark, "Finding matrix product state representations of highly-excited eigenstates of many-body localized Hamiltonians," *ArXiv e-prints* (2015) 1509.01244.

[116] J. J. Bisognano and E. H. Wichmann, "On the duality condition for quantum fields," *Journal of Mathematical Physics* **17**, 303 (1976).

[117] J. J. Bisognano and E. H. Wichmann, "On the duality condition for a Hermitian scalar field," *Journal of Mathematical Physics* **16**, 985 (1975).

[118] L. Susskind and J. Lindesay, *An Introduction to Black Holes, Information and the String Theory Revolution: The Holographic Universe* (World Scientific, 2005).

[119] H. Casini, M. Huerta, and R. C. Myers, "Towards a derivation of holographic entanglement entropy," *Journal of High Energy Physics* **5**, 36 (2011) 1102.0440.

[120] L. Bombelli, R. K. Koul, J. Lee, and R. D. Sorkin, "Quantum source of entropy for black holes," *Phys. Rev. D* **34**, 373 (1986).

[121] B. L. Altshuler, Y. Gefen, A. Kamenev, and L. S. Levitov, "Quasiparticle Lifetime in a Finite System: A Nonperturbative Approach," *Phys. Rev. Lett.* **78**, 2803 (1997) cond-mat/9609132.

[122] I. V. Gornyi, A. D. Mirlin, and D. G. Polyakov, "Interacting Electrons in Disordered Wires: Anderson Localization and Low-T Transport," *Phys. Rev. Lett.* **95**, 206603 (2005) cond-mat/0506411.

[123] Y. Kagan and M. I. Klinger, "Theory of quantum diffusion of atoms in crystals," *Journal of Physics C: Solid State Physics* **7**, 2791 (1974).

[124] Y. Kagan and L. A. Maksimov, "Localization in a system of interacting particles diffusing in a regular crystal," *Zh. Eksp. Teor. Fiz.* **87**, 348 (1984).

[125] M. Schiulaz and M. Müller, "Ideal quantum glass transitions: Many-body localization without quenched disorder," in *American Institute of Physics Conference Series*, volume 1610, pp. 11–23 (2014) 1309.1082.

[126] M. Schiulaz, A. Silva, and M. Müller, "Dynamics in many-body localized quantum systems without disorder," *Phys. Rev. B* **91**, 184202 (2015) 1410.4690.

[127] J. M. Hickey, S. Genway, and J. P. Garrahan, "Signatures of many-body localisation in a system without disorder and the relation to a glass transition," *ArXiv e-prints* (2014) 1405.5780.

[128] N. Y. Yao, C. R. Laumann, J. I. Cirac, M. D. Lukin, and J. E. Moore, "Quasi

Many-body Localization in Translation Invariant Systems," *ArXiv e-prints* (2014) 1410.7407.

[129] W. De Roeck and F. Huveneers, "Asymptotic Quantum Many-Body Localization from Thermal Disorder," *Communications in Mathematical Physics* **332**, 1017 (2014) 1308.6263.

[130] W. De Roeck and F. Huveneers, "Scenario for delocalization in translation-invariant systems," *Phys. Rev. B* **90**, 165137 (2014) 1405.3279.

[131] W. De Roeck and F. Huveneers, *From Particle Systems to Partial Differential Equations II: Particle Systems and PDEs II, Braga, Portugal, December 2013*, pp. 173–192 (Springer International Publishing, 2015) 1409.8054.

[132] Z. Papić, E. M. Stoudenmire, and D. A. Abanin, "Many-body localization in disorder-free systems: The importance of finite-size constraints," *Annals of Physics* **362**, 714 (2015) 1501.00477.

[133] P. Hosur and X.-L. Qi, "Characterizing eigenstate thermalization via measures in the Fock space of operators," *ArXiv e-prints* (2015) 1507.04003.

[134] J. M. Deutsch, "Thermodynamic entropy of a many-body energy eigenstate," *New Journal of Physics* **12**, 075021 (2010) 0911.0056.

[135] L. Bonnes, H. Pichler, and A. M. Läuchli, "Entropy perspective on the thermal crossover in a fermionic Hubbard chain," *Phys. Rev. B* **88**, 155103 (2013) 1304.5340.

[136] R. R. P. Singh, M. B. Hastings, A. B. Kallin, and R. G. Melko, "Finite-Temperature Critical Behavior of Mutual Information," *Phys. Rev. Lett.* **106**, 135701 (2011) 1101.0430.

[137] L. F. Santos, A. Polkovnikov, and M. Rigol, "Weak and strong typicality in quantum systems," *Phys. Rev. E* **86**, 010102 (2012) 1202.4764.

[138] M. Storms and R. R. P. Singh, "Entanglement in ground and excited states of gapped free-fermion systems and their relationship with Fermi surface and thermodynamic equilibrium properties," *Phys. Rev. E* **89**, 012125 (2014) 1308.6257.

[139] H.-H. Lai and K. Yang, "Entanglement entropy scaling laws and eigenstate typicality in free fermion systems," *Phys. Rev. B* **91**, 081110 (2015) 1409.1224.

[140] R. Pathria and P. Beale, *Statistical Mechanics* (Elsevier Science, 1996).

[141] J. C. Baez, "Renyi Entropy and Free Energy," *ArXiv e-prints* (2011) 1102.2098.

[142] J. Cardy, "Thermalization and Revivals after a Quantum Quench in Conformal Field Theory," *Phys. Rev. Lett.* **112**, 220401 (2014) 1403.3040.

[143] C. T. Asplund, A. Bernamonti, F. Galli, and T. Hartman, "Holographic entanglement entropy from 2d CFT: heavy states and local quenches," *Journal of High Energy Physics* **2**, 171 (2015) 1410.1392.

[144] P. Caputa, J. Simón, A. Štikonas, and T. Takayanagi, "Quantum entanglement of

localized excited states at finite temperature," *Journal of High Energy Physics* **1**, 102 (2015) 1410.2287.

[145] A. L. Fitzpatrick, J. Kaplan, and M. T. Walters, "Virasoro conformal blocks and thermality from classical background fields," *Journal of High Energy Physics* **11**, 200 (2015) 1501.05315.

[146] E. Lubkin, "Entropy of an n-system from its correlation with a k-reservoir," *Journal of Mathematical Physics* **19**, 1028 (1978).

[147] S. Lloyd and H. Pagels, "Complexity as thermodynamic depth," *Annals of Physics* **188**, 186 (1988).

[148] S. K. Foong and S. Kanno, "Proof of Page's conjecture on the average entropy of a subsystem," *Phys. Rev. Lett.* **72**, 1148 (1994).

[149] J. Sánchez-Ruiz, "Simple proof of Page's conjecture on the average entropy of a subsystem," *Phys. Rev. E* **52**, 5653 (1995).

[150] S. Sen, "Average Entropy of a Quantum Subsystem," *Phys. Rev. Lett.* **77**, 1 (1996) hep-th/9601132.

[151] M. Rigol, "Quantum Quenches in the Thermodynamic Limit," *Phys. Rev. Lett.* **112**, 170601 (2014) 1401.2160.

[152] H. Tasaki, "From Quantum Dynamics to the Canonical Distribution: General Picture and a Rigorous Example," *Phys. Rev. Lett.* **80**, 1373 (1998) cond-mat/9707253.

[153] S. Goldstein, J. L. Lebowitz, R. Tumulka, and N. Zanghì, "Canonical Typicality," *Phys. Rev. Lett.* **96**, 050403 (2006) cond-mat/0511091.

[154] L. F. Santos and M. Rigol, "Onset of quantum chaos in one-dimensional bosonic and fermionic systems and its relation to thermalization," *Phys. Rev. E* **81**, 036206 (2010) 0910.2985.

[155] J. M. Deutsch, H. Li, and A. Sharma, "Microscopic origin of thermodynamic entropy in isolated systems," *Phys. Rev. E* **87**, 042135 (2013) 1202.2403.

[156] P. Calabrese, M. Campostrini, F. Essler, and B. Nienhuis, "Parity Effects in the Scaling of Block Entanglement in Gapless Spin Chains," *Phys. Rev. Lett.* **104**, 095701 (2010).

[157] A. Dymarsky and H. Liu, "Canonical Typicality of Energy Eigenstates of an Isolated Quantum System," *ArXiv e-prints* (2015) 1511.06680.

[158] M. M. Wilde, "From Classical to Quantum Shannon Theory," *ArXiv e-prints* (2011) 1106.1445.

[159] B. Swingle and I. H. Kim, "Reconstructing Quantum States from Local Data," *Phys. Rev. Lett.* **113**, 260501 (2014) 1407.2658.

[160] M. Endres, M. Cheneau, T. Fukuhara, C. Weitenberg, P. Schauß, C. Gross, L. Mazza, M. C. Bañuls, L. Pollet, I. Bloch, and S. Kuhr, "Observation of Corre-

lated Particle-Hole Pairs and String Order in Low-Dimensional Mott Insulators," *Science* **334**, 200 (2011) 1108.3317.

[161] G. De Palma, A. Serafini, V. Giovannetti, and M. Cramer, "Necessity of Eigenstate Thermalization," *Phys. Rev. Lett.* **115**, 220401 (2015) 1506.07265.

[162] E. H. Lieb and F. Y. Wu, "Absence of Mott Transition in an Exact Solution of the Short-Range, One-Band Model in One Dimension," *Phys. Rev. Lett.* **21**, 192 (1968).

[163] F. H. L. Essler, H. Frahm, F. Göhmann, A. Klümper, and V. E. Korepin, *The One-Dimensional Hubbard Model* (Cambridge University Press, 2005).

[164] G. Carleo, F. Becca, M. Schiró, and M. Fabrizio, "Localization and Glassy Dynamics of Many-Body Quantum Systems," *Scientific Reports* **2**, 243 (2012) 1109.2516.

[165] M. van Horssen, E. Levi, and J. P. Garrahan, "Dynamics of many-body localisation in a translation invariant quantum glass model," *ArXiv e-prints* (2015) 1505.07089.

[166] R.-Q. He and Z.-Y. Weng, "Emergent flat bands and many-body localization in a doped Mott insulator," *ArXiv e-prints* (2015) 1512.07599.

[167] C. N. Yang, "η pairing and off-diagonal long-range order in a Hubbard model," *Phys. Rev. Lett.* **63**, 2144 (1989).

[168] C. N. Yang and S. Zhang, "SO4 Symmetry in a Hubbard Model," *Modern Physics Letters B* **04**, 759 (1990).

[169] J.-Y. P. Delannoy, M. J. Gingras, P. C. Holdsworth, and A.-M. S. Tremblay, "Néel order, ring exchange, and charge fluctuations in the half-filled Hubbard model," *Phys. Rev. B* **72**, 115114 (2005) cond-mat/0412033.

[170] V. Alba, "Eigenstate thermalization hypothesis and integrability in quantum spin chains," *Phys. Rev. B* **91**, 155123 (2015) 1409.6096.

[171] W. De Roeck, F. Huveneers, M. Müller, and M. Schiulaz, "Absence of many-body mobility edges," *Phys. Rev. B* **93**, 014203 (2016) 1506.01505.

[172] E. H. Lieb and D. W. Robinson, "The finite group velocity of quantum spin systems," *Comm. Math. Phys.* **28**, 251 (1972).

[173] M. B. Hastings and T. Koma, "Spectral Gap and Exponential Decay of Correlations," *Communications in Mathematical Physics* **265**, 781 (2006) math-ph/0507008.

[174] M. Foss-Feig, Z.-X. Gong, C. W. Clark, and A. V. Gorshkov, "Nearly Linear Light Cones in Long-Range Interacting Quantum Systems," *Phys. Rev. Lett.* **114**, 157201 (2015) 1410.3466.

[175] J. Maldacena, S. H. Shenker, and D. Stanford, "A bound on chaos," *ArXiv e-prints* (2015) 1503.01409.

[176] S. Choi, N. Y. Yao, S. Gopalakrishnan, and M. D. Lukin, "Quantum Control of Many-body Localized States," *ArXiv e-prints* (2015) 1508.06992.

[177] N. Y. Yao, C. R. Laumann, and A. Vishwanath, "Many-body localization protected quantum state transfer," *ArXiv e-prints* (2015) 1508.06995.

[178] A. Weiße and H. Fehske, "Exact Diagonalization Techniques," in *Computational Many-Particle Physics*, edited by H. Fehske, R. Schneider, and A. Weiße, volume 739 of *Lecture Notes in Physics*, pp. 529–544 (Springer, 2008).